2012

Controlling atomistic processes on Pb films via quantum size effects and lattice rotation

Steven Michael Binz
Iowa State University

Controlling atomistic processes on Pb films via quantum size effects and lattice rotation

by

Steven Michael Binz

A dissertation submitted to the graduate faculty

in partial fulfillment of the requirements for the degree of

DOCTOR OF PHILOSOPHY

Major: Condensed Matter Physics

Program of Study Committee:

Michael C. Tringides, Major Professor

Bruce N. Harmon

Charles R. Kerton

Robert J. McQueeney

Patricia A. Thiel

Iowa State University

Ames, Iowa

2012

TABLE OF CONTENTS

LIST OF TABLES

LIST OF FIGURES

ACKNOWLEDGEMENTS

It is hard to believe that I am actually submitting this dissertation. It has been a long road since I started as a computer science undergrad at Bradley University. My first thanks must therefore go to Dr. Kevin Kimberlin, whose course in Introductory Physics was both fun and interesting, catalyzing my decision to add physics as a major. Dr. Kimberlin also taught me the basics of surface science, which went a long way towards preparing me for my graduate work. Of course, I can't discuss my undergraduate career without mentioning Erika Crandall, who worked with me on most of my undergraduate math and physics assignments, providing help, support, and motivation that was integral to my success.

Moving onto my graduate career, I want to thank Dr. Michael C. Tringides for accepting me as his graduate student and guiding me through the long process of carrying out research and completing my dissertation. Dr. Tringides spent countless hours helping me prepare papers, suggesting ideas on how to explain my data, preparing me for my Oral Prelim and Final Defense, and much more. As a result I am secondary author on three other published papers. Thanks also to my other group members, Dr. Myron Hupalo for his guidance on STM and various condensed matter topics, Michael Yakes and Jizhou Chen for teaching me how to use SPA-LEED, and Matt Hershberger for listening to excerpts from my dissertation and helping me with my job applications and related presentations. I want to thank Dr. Craig Ogilvie, my Preparing Future Faculty mentor, and Dr. Joanne Olson, my Curriculum and Instruction teacher, for helping me develop not only as a future professor but also as a future teacher. I must also thank Dr. Tringides, Dr. Ogilvie, and Dr. Olson for their endurance in writing upwards of 20 recommendation letters during my job hunt. I also want to thank Steven Hahn and Stella Kim for being my first (and generally last) stops whenever I had a question about a condensed matter topic. Special thanks also go to Stella for helping me with hobbies I probably did not have time for and sharing food which definitely improved my diet, as well

as her support in listening to my problems and frustrations. Thank you to Dr. Tringides, Dr. Hupalo, Matt, Steven, Stella, Emily Hellerich, and Chelsea Berns for listening to my final defense presentation and helping me improve it. Chelsea also provided much comfort and support in 9 months leading up to my graduation, especially during my job interviews and final defense. Her notes of support gave me the confidence to succeed just when I needed it most.

Finally, there are a few people whose contributions to my success defy the boundaries of the various eras of my education. First, and most obviously, I thank my family members, especially my parents, Carl and Barbara Binz. I owe them gratitude for such a bewilderingly large and ever-growing number of things that any attempt to list them would be a full-time occupation, as well as require a much larger hard drive. Alas, I must hope that it is sufficient, if grossly understated, to say that I owe them everything and really appreciate the love and support they have provided me the last 29 years. I also want to thank my sisters, Sara and Laura, for providing love, support, luxurious vacation spots, and other distractions - I couldn't ask for better sisters. Without our frequent conversations about cats, kids, plants, and other staples of daily life to keep me grounded in reality, I might have descended into insanity long before finishing my dissertation. Last, I'd like to thank Andrew Crawley, the only non-family member to earn a spot in this paragraph, who was a fantastic roommate at Bradley and has been a great friend ever since. Among his many contributions, he's administered servers for me, fielded many a frantic tech support call after some computer-related mishap, provided confidence that I could do all that I planned to, and did way more than his fair share of our undergrad computer science group projects. More recently, Andrew has listened to my frustrations, provided advice on topics ranging from software architecture to the suitability of solid-platinum sofas as currency, and proofread hundreds of pages of my dissertation and job applications. Any wording or grammatical errors that remain are mine alone!

Unfortunately, the limits of my memory and the space available here mean that some deserving individuals have no doubt been unfairly left out. To all who have assisted me along the path that has led me here, I offer my most heartfelt thanks.

This work was performed at the Ames Laboratory under contract number DE-AC02-07CH11358 with the U.S. Department of Energy. The document number assigned to this dissertation is IS-T 3036.

CHAPTER 1. Introduction to Quantum Size Effects, Reactivity, and Surface Processes

1.1 Introduction

In our everyday lives the objects and materials we use are pretty well understood. We know how their atoms are arranged, what their electronic structure is, what their conductivity is and so on. In essence, we know their bulk properties. However, even for common materials, like Pb, when some or all dimensions of a material are very short (on the order of 10^{-9} m), it starts to behave in very different ways. In the case of Pb, coverages of less than 4/3 of a ML on top of Si(111) results in a series of different 2D structures culminating in what is called the Devil's Staircase, under the right conditions. The Devil's Staircase is composed of a nearly limitless number of phases, arrangements of the Pb atoms that are composed of varying numbers of $\sqrt{3}$ x $\sqrt{3}$ and $\sqrt{7}$ x $\sqrt{3}$ unit cell rows. At 1.2 ML of coverage, the surface is entirely $\sqrt{7}$ x $\sqrt{3}$, and as more Pb is deposited the number of $\sqrt{3}$ rows increases until the ratio is 1 to 1 at 1.25 ML. As the coverage increases, the $\sqrt{7}$ rows become more infrequent, and the surface is completely $\sqrt{3}$ at a coverage of 4/3 ML. The Pb Devil's Staircase is not the exact same as the traditional Devil's Staircase because the two phases that it is composed of are off by 2 lattice constants instead of just 1, and while this does affect the math and stability of the various phases it does not change the overall effect.[1,2] At coverages that are higher, but still less than 7 ML, islands form that have a strongly preferred height of 7 layers and have nearly vertical sides.[3,4] The study of these phenomena focused on the physical dimensions, atomic arrangement, and the cause, but that is only a part of the story. The really exciting part is that each of these 2D phases, layer thickness, and nano-particle sizes have different electronic properties in the direction perpendicular to the surface. For example, the electronic band structure of different

height Pb films differs in that the electron density near the Fermi Level changes.[5] The reasons for this will be explained below, but the main point is that it creates a very large "knob" for us to turn as we search for the next material or interface to change the face of the world.

Electrons are the mediators of bonding, so the different electronic properties mean that the materials will have different reactivities, again, more on the details of this below. The most obvious application is the production of better catalysts for the chemical and power industries. Making chemical reactions easier and faster, and catalysts longer lasting would be a huge boon for the economy. Better catalysts would also be beneficial in making fuel cells, either in making them more efficient, longer lasting, or possibly even providing a cheaper substitute for the platinum commonly used.[6,7]

Increasing reactivity is not the only application of this. We often coat objects to protect them from their environments, and it might be possible to reduce the amount of material used in current processes, or produce materials that are better altogether. As an example of this, many tools are Zn plated to prevent them from oxidizing.

1.2 Quantum Size Effects

The unusual properties of materials that are short in at least one dimension are called Quantum Size Effects (QSE), and these effects are the reason that changing the thickness of a Pb film by a single atomic layer can change the electron density at the Fermi level so strongly. They are caused by the confinement of electrons in those dimensions. Electrons, as with all matter, are both particles and waves so they have a wavelength that depends upon, among other things, their energy. In a simplistic view of bulk metals, conduction electrons move about freely within the metal. However, in any direction in which the size of the crystal is on the order of the wavelength of the conduction electrons, the electrons are confined. This results in a situation very similar to the classic quantum well problem, where an electron is confined in a potential well with fixed width and depth. The width of the well is determined by the thickness of the material, and in the case of this dissertation, that means the height of the island or film. The depth of the well can be approximated several different ways. A section of Chapter 6 assumes a semi-infinite square well, with the interface with the Si(111) producing

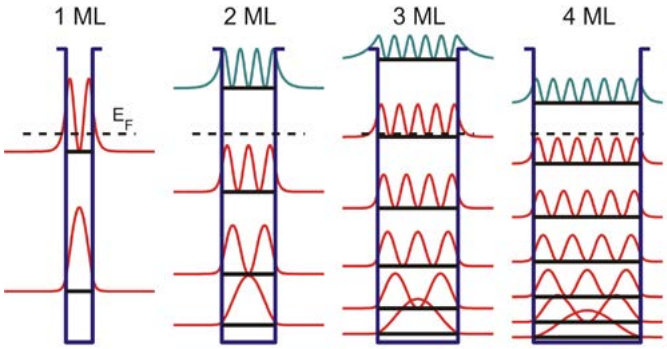

Figure 1.1 Shows the confined electron levels in different film thicknesses ranging from 1 to 4 atoms thick. In this example the 2- and 4-layer thick films are the most stable while the 1- and 3-layer thick films are the most reactive due to their high concentration of electrons near the Fermi Energy.

an infinite barrier, and the interface with the vacuum producing a barrier based on the depth of the conduction band plus the work function of the surface. Solving that problem results in an estimate for the energies of the confined electrons. This is similar to approximations done by Yeh et al.[8] and Zhang et al.[9] A more powerful and physically realistic model is called the Phase Accumulation Model (PAM). Instead of allowing the phase change at the interfaces to be estimated by the barriers, the PAM proactively calculates them based on known equations for that specific interface. For example, the interface between d-band metals with inverted S-P gaps and vacuum can be approximated via the WKB approximation:

$$\frac{\phi_B}{\pi} = \left(\frac{3.4}{E_V - E}\right)^{\frac{1}{2}} - 1 \tag{1.1}$$

E_v is the vacuum level and E is the energy of the electron.[10] Other interfaces will require different approximations. Instead of assuming solutions as in the potential well problem above, PAM uses the condition that any confined electrons must have a total phase shift of 0 as it moves from one side to the other and back though a total phase shift of 0 is equivalent to saying that the total phase change of the path is a multiple of 2π.

$$\phi_c + 2kd + \phi_b = 2\pi n \tag{1.2}$$

ϕ_c and ϕ_b are the phase shifts at the two interfaces, k is the wave vector of the electrons, d is the film thickness, and n is a positive integer.

Since the electrons are quantized in the narrow directions of the material, the electron energy distribution is not uniform over the entire conduction band there are more electrons at energies allowed by the QSE. If k is not the same as $\pi/(layerheight)$, the highest allowed quantized level might be lower or higher than before with respect to the Fermi energy, which explains how adding a layer of atoms can change the density of electrons. The physical manifestation of this is that some film thicknesses are preferred over others because the total energy of the electrons is lower in films where the quantized electrons are forced to be far from the Fermi Energy. This effect is especially strong in the Pb on Si(111) system. As mentioned earlier, when less than 7 ML of Pb is deposited onto Si(111) 7 x 7 it preferentially forms 7-layer thick islands. This preference is so strong that is not uncommon to have difficulty finding another height.[3] Other systems exhibit QSE in a very similar fashion: Pb deposited on top of Si(111) covered by In 4 x 1 has a preference for growing 4-layer high islands, and as shown in this dissertation Pb also shows QSE height selection on In $\sqrt{31}$ x $\sqrt{31}$ as well as In $\sqrt{3}$ x $\sqrt{3}$. Pb is not the only material to show QSE; In deposited onto Pb α-phase on Si(111) has shown a strong preference for 4-layer thick islands,[11] Bi films have shown a preference for even layer heights on Si(111),[12] and Bi has also shown a preferred height of 4, or multiples thereof, on the quasi-crystal $Al_{63}Cu_{24}Fe_{13}$.[13] However, preferred thickness of films is not the only effect of QSE, which have also been shown to change the resistivity of films,[14] the transition temperature of thin film super conductors,[15] and much more, including an effect that is important to this research: the relationship between the Fermi Energy of the surface and the confined levels plays an important role in determining the reactivity of a surface. Aballe et al.[16] deposited Mg films on top of W(110) while watching them in real time with Low Energy Electron Microscopy (LEEM). Following the surface with LEEM allowed them to determine exactly how many layers of Mg were associated with each reflectivity. After creating the surface, it was exposed to O_2, and they found that different thicknesses of Mg had very different O_2 adsorption rates via the strong change in contrast some heights experienced. They then verified the LEEM result with X-ray Photoelectron Emission Microscopy by taking the ratio of the contribution of the Mg 2p O peak to the total Mg 2p peak. For exposures from 2 to 13 Langmuires the 7^{th} and 15^{th} layers showed distinctly higher O content than the 10-layer thick films. At lower exposures the

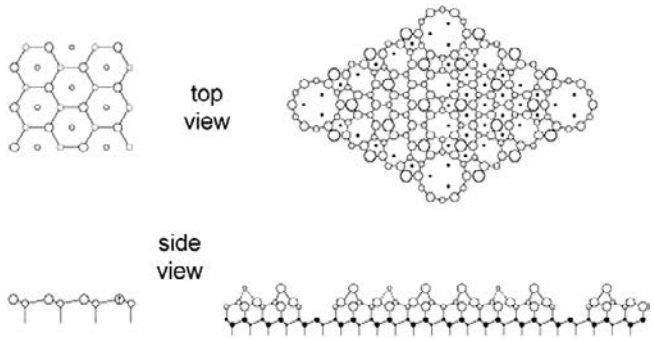

Figure 1.2 Si (111) 7 x 7 reconstruction, a very important surface in surface science and the semiconductor industry and the substrate used in all of the experiments presented in this dissertation. The atoms on the surface of the bulk terminated 1x1 surface reconstruct at temperatures above 670 K to create this more complicated, but lower energy surface.[18,19]

difference was more than a factor of 2, and at higher exposures it was closer to 15%. They attributed this to the fact that the QSE increased the density of electrons near the Fermi Energy in the films that had higher adsorption. The larger number of higher energy electrons made it more likely for them to interact with the O_2 atoms. This may not be the whole picture, as noted by Binggeli and Altarelli[17], but that will be addressed in further detail in Chapter 6.

The adsorption of a gas onto a substrate is only one part of catalytic activity. Once on the sample the atoms must diffuse, find the other species, react, and then desorb with that species. It is known that QSE have a strong effect on surface adsorption rates, so it stands to reason that other processes that involve interacting with the surface will also see a strong change. For example, diffusion and nucleation on the surface, both of which can be important factors in catalytic activity, should be affected. The first three results chapters of this dissertation study Pb films on top of Si(111) 7 x 7 (see Figure 1.2), because they are well known to have strong QSE.[3,4] Pb and In were deposited onto Pb films with thicknesses of 4 and 5 layers, heights chosen because QSE are strongest at lower heights. This does not reveal the true reactivity of the thicknesses since neither Pb nor In are gases, but it does serve as a proxy for how strongly the reactivity may depend upon layer thickness. To best understand the results, a quick introduction to how and why newly deposited atoms arrange themselves on surfaces is in order.

1.3 Nucleation Theory

As is true in all of physics, the only real factor in how the surface will be organized is energy. The surface will organize itself into the configuration that has the lowest free energy as long as it has enough energy to do so.

As stated above, Pb depositions onto Si(111) 7 x 7 leads to islands that are 7 layers thick. This is why, in the experiments, the surface was cooled immediately after deposition to keep the islands from shifting to their preferred height. The situation gets a lot more complicated when it comes to newly deposited atoms, because now the free energy plays a much smaller role and kinetics have to be taken into account. The atoms' ability to move around on a surface is limited by their energy and the potential wells on the surface and this plays a larger role in how the surface will turn out than the free energy of the resulting structures at lower temperatures. The definition of lower temperatures depends upon the materials being used as the substrate and adsorbate. For example, depositing Pb onto 5 layers of Pb at 40 K creates fractals, a classic case of edge diffusion limited growth, and they are not stable at 100 K.[20] On the other hand, Gd fractal islands can be grown on graphene at RT.[21] Atomic movement on the sample is accomplished through diffusion, which is where a single atom gains enough energy through crystal vibrations to hop over potential barriers on the surface to reach the next potential minimum.

The following discussion will be kept general but examples will be in the Pb on Si system prevalent in this dissertation. When an atom is deposited onto the surface, as long as it has enough energy to overcome the potential barriers on the surface it will move around on the surface until it finds a place with a low enough potential that it cannot readily move out of the well. This can be a step edge, another adatom, any number of other adatoms, a defect in the substrate or any other potential minimum. Assuming that the diffusion barrier in each direction is the same then the atom will move in a Random Walk, that is, the direction the atom travels next is not in any way related to the direction it moved last. There has been a lot of research done on random walks because they are applicable to many different physical systems, but for the purposes of this dissertation there are two important characteristics: first,

the direction of travel is completely random, and second, because travel is random it takes a relatively long time for an average atom to travel a large net distance, as described by this equation:

$$\left\langle \Delta r^2 \right\rangle = \nu a^2 t \tag{1.3}$$

Where Δr is the displacement, ν is the frequency with which the atom will hop to the next lattice site, a is the distance between lattice sites, and t is time. The hopping rate is simply:

$$\nu = \nu_0 e^{\frac{-E_d}{k_b T}} \tag{1.4}$$

Where ν_0 is the attempt frequency, generally estimated to be 10^{14} attempts/second, E_d is the diffusion barrier, k_b and T are Boltzmann's constant and the temperature. The diffusion barrier is the difference in potential energy between the bottom of the potential well the atom is in currently and the highest potential between the current well and the next site. This is generally located along a bridge – the area directly between two adjacent surface atoms.[22] This means that a Pb atom that lands on top of an existing Pb island will be on top of it for a fairly long time and that atoms that land in the middle of a large open terrace will likely stay there, especially if the diffusion rate is low.

Besides simply hopping, atoms on the surface can go up or down step edges, once again depending upon the associated barrier and the energy of the atom (temperature of the surface). There is an extra barrier associated with hopping across step edge barriers; it is called the step edge barrier or Ehrlich-Schoweobel barrier.[23] Large step edge barriers create surfaces with a lot of pyramid like structures on it, while small step edge barriers lead to layer-by-layer growth. An island with a large step edge barrier will cause the atoms that land on it to stay on top, leading to the nucleation of another layer on top of it. Also, as alluded to earlier, the atoms could get stuck at the bottom side of step edges as well as at defects. Once on a step edge the atoms may be able to diffuse along it or even detach from it completely, although detaching generally takes more energy and is therefore less likely. The diffusion along the step edge will continue until it meets a kink, a place where the step edge is not straight. If the atoms are unable to diffuse along the step edge of an island then a fractal will be created. They are not mathematically rigorous fractals but the resemblance is striking, see Chapters 4 and 5 for examples. Systems

where atoms are allowed to diffuse along island edges generally create compact islands, but the shape may not be the equilibrium shape of the species because of kinetic limitations, i.e., diffusion along certain island sides may be different.

Atoms on sufficiently large defect free terraces will eventually run into each other and, if the atoms do not have enough energy to break apart, will create a stable island. If it takes two atoms to create a stable island then the critical island size, i_c, is 1. If the atoms are unable to diffuse at all then $i_c = 0$; The word "stable" is used but that simply means that, generally speaking, once an island is $i_c + 1$ atoms in size it will continue to grow rather than completely dissociate, but it does not mean that no atom will ever disassociate from it. The atoms on the surface can be constantly in motion, with atoms joining and leaving both stable and unstable islands, as well as creating new ones. However, for the cases in this dissertation, it is assumed that once an atom hits a stable island it does not dissociate from it. Islands are capable of moving across the surface but the larger they are the less likely it is to happen. When atoms land on existing islands containing a sufficient number of atoms, they could nucleate a 2^{nd} layer or they could fall off. It comes down to the balance between diffusion rate, critical island size, and the step edge barrier, a relationship which will be discussed in much more detail in chapter 6. In addition, if an atom lands on the edge of an island it is likely to experience "downward funneling", which is where the newly deposited atom immediately goes down the step edge.[24] All of these possibilities are summed up in Figure 1.3.

After a certain amount of deposition, the island density is high enough that any further deposited atoms will almost certainly find an existing stable island before finding other adatom(s) to nucleate a new island. This is called the saturation island density, and is usually around 15% coverage of the surface for a critical island size of 1. As more atoms are deposited the islands will start to merge, and as the islands get bigger the chances of a 2^{nd} layer nucleating on top increases.[26] This also depends upon the flux rate, the rate at which new atoms arrive on the surface. When a Pb atom lands on the surface it will continue to move around until it either hits an existing island or meets other Pb atoms to form a new stable island. Therefore a slower diffusion rate or higher the flux rate will result in a higher saturation island density. The following is a mathematical model constructed based on the movement methods described

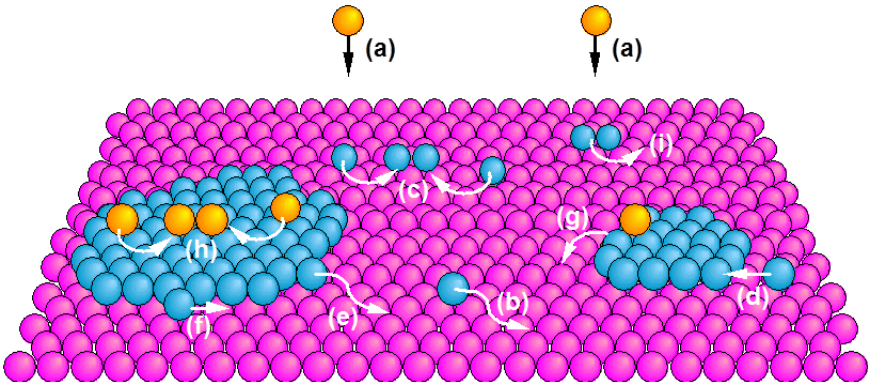

Figure 1.3 Summary of all of the basic processes during atomic deposition. (a) deposition, (b) diffusion, (c) nucleation, (d) attachment, (e) detachment, (f) edge diffusion, (g) downward funneling, diffusion down a step, (h) nucleation on top of existing islands, (i) dimer diffusion. After Caflisch [25].

so that values can be predicted.

The number of islands that nucleate, in the simple but powerful model being presented, depends upon critical island size, temperature, flux rate, and the diffusion barriers. A quick aside, upon thinking about the above descriptions you may realize that the temperature and flux rates are intertwined. The movement on the surface depends upon the temperature: at higher temperatures, atoms diffuse and reach stable locations more quickly. This lowers the monomer density, which can also be achieved by lowering the flux rate. It is for this reason that when simulations are done, the important factors are the diffusion barriers, critical island size, and the ratio of the temperature and flux rate.

Nucleation theory attempts to solidify the relationship between those four variables and the saturation island density. To do this, the first step is to write down the equations that

$$\frac{dn_1}{dt} = F - 2\sigma_1 \nu n_1^2 - \sigma_2 \nu n_1 n_x - \kappa_x F\left(Ft - n_1\right) - 2\kappa_1 F n_1 \tag{1.5}$$

$$\frac{dn_x}{dt} = \sigma_1 \nu n_1^2 + \kappa_1 F n_1 \tag{1.6}$$

describe the density of monomers, dimers, and so forth. For this example, i_c will be 1 but the higher critical island size equations are simple extensions of the first two equations. This simple model involves many approximations and they will not all be explicit. However, one notable approximation is that islands that are one larger than the critical size (2 atoms in this

case) are considered to be completely stable which means that once an island hits the stable island size, the atoms have no chance of disassociating from it. Let n_1 denote the monomer density and n_x denote all the density of all other island sizes. In equation 1.5, F is the flux adding to the number of monomers, the second term is the combining of two monomers to create a dimer, the third term represents monomers colliding with already existing islands, the fourth term is the rate at which newly deposited atoms land on existing islands, and the final term takes into account the occurrence of new atoms landing directly on monomers. The σ's represent the capture rates, which is based on the distribution of monomers on the surface. In the mean-field approximation the monomers are evenly distributed across the entire surface that does not yet have an island. ν is the diffusion rate. $(Ft - n_1)$ in the fourth term represents the total number of lattice sites that already have islands growing on them and the k_x term contains information that converts that to a percentage. Equation 1.6 is built very similarly, but since there are fewer possibilities for a group of atoms there are only two terms. The first is the creation of a dimer and the second is from the impingement of a newly deposited atom onto a monomer.[26]

In this simple model, the rate equations are fairly straight-forward, but solving them is not for the light hearted and is beyond the scope of this quick introduction. However, here is the solution to the more general problem that did not make assumptions about i_c.

$$n_x = \eta(\Theta, i)\left(\frac{1}{F}\frac{\nu_0 e^{\frac{-E_m}{k_b T}}}{2d}\right)^{\frac{-i}{i+2}} e^{\frac{E_i}{(i+2)k_b T}} \tag{1.7}$$

The η function has a rather complicated background but the appropriate value for some simple situations can be found in Venables et al.[27] E_i is the binding energy, a measure of the strength of the bond between an atom and an island and represents the change in free energy.[22,26]

There are a few things that can be pointed out in equation 1.7 that match the earlier discussion. The first is that the flux rate and the island density are directly related, so a higher flux rate means a higher saturation island density. The second is that the diffusion term, equation 1.4, is inversely related to the island density. Thus, if the diffusion rate is high, the newly arriving atoms can travel great distances to meet up with an existing island, preventing them from starting a new island.

1.4 Pb and In on Pb Films on Si(111)

The Pb island density on the 4-layer Pb films is up to 60 times higher than on the 5-layer films at 40 K, and the first explanation that comes to mind is that the diffusion rate is faster on the 5. However, previous research shows that the diffusion on the 4 is actually higher, so differences in diffusion barriers cannot be the cause.[28] The only other explanation is that the critical island size on the 5-layer films is much higher than that on the 4-layer films, perhaps as high as 10, while the critical island size on the 4-layer film is 1. This is also shown independently of the requirement that the diffusion rate on the 4-layer be higher than on the 5-layer. When the diffusion length of the atoms is several times that of the area they occupy, the island density is independent of the temperature, flux rate, and diffusion.[29–31] This occurs not only on separate islands but also on single islands with two separate heights and even on nearly flat islands that span a Si step edge, where the difference is seen right above the underlying step edge.

Impressively, the effect still exists when depositing In on the Pb films, producing a two times difference in island density, with the 5-layer film still having the lower density. While this is weaker than the Pb on Pb case, that is to be expected given the higher temperatures and heterogeneous system.

An effect was also seen when depositing Fe on top of Pb.[32] Ma et al.[32] deposited Fe atoms on top of large Pb films, 10 layers or taller, and noted that the island density on the odd film heights is consistently higher than on the even heights. This is due to the fact that the coverage of the odd height is 50% higher than on the even heights. For a more direct comparison to this work, the island densities were counted and the difference was a factor of 1.34, significantly lower than 60, and even the factor of 2 seen for In on Pb, as it should be based on the larger heights. This much smaller difference in island density is caused by differences in diffusion, not critical island size. Ma et al.[33] also reported differences in O adsorption on top of Pb islands 10 layers or taller, experiencing 60 Langmuirs of exposure at 100 K. They reported a difference in O_2 adsorption of as much as a factor of three difference between 10-layer and 11-layer thick films, with more adsorption happening on the 10-layer. Most other differences between adjacent layers were less than a factor of 2, but the large difference in the lower

heights, which feel QSE more strongly, is an indication that depositing O_2 on top of thinner Pb films could produce results similar in magnitude to those shown here. The differences in O_2 adsorption were attributed to changes in the local density of states caused by QSE. Hu et al.[34] performed density function theory (DFT) calculations on the adsorption energy of atomic O on top of Pb(111) films and found that the adsorption energy oscillated with a nearly bilayer period by as much as 0.05 eV when there is already 0.25 ML of O on the surface. This, too, indicates that QSE can affect O adsorption.

The effect seen for Pb and In on Pb films was also much stronger than the effect seen by Aballe et al.[16] for O_2 on Mg(0001). The largest effect they saw was a 10% difference in O_2 adsorption between 7- and 10-layer thick Mg films. This may indicate that Pb would show a stronger difference in adsorption. However, this comparison is not a fair one since we are comparing island densities of Pb to adsorption rates of O_2.

Both the Pb and In on Pb systems are quite interesting even past the first completed adlayer. The Pb depositions happened at 40 K and still had the mobility to grow layer-by-layer, confirming RHEED data that showed the film grows more uniformly at 18 K than it does at 70 K.[14] This is ascribed to the relatively low diffusion barriers and fractal-like morphology of the Pb islands at this temperature as opposed to a non-thermal diffusion mechanism. The 2^{nd} layer of In has very high diffusion and is relatively unlikely to form a 2^{nd} layer directly on top of the Pb islands. However, the In starts to congregate around the edges of the Pb islands, encasing them in In. Nucleation of higher layers on top of the all In sections of the islands is very quick, resulting in prominent 3D growths.

1.5 Pb on In $\sqrt{31}$ and In $\sqrt{3}$ and Lattice Rotations

The second part of this dissertation takes a step back from the possible applications of QSE and instead investigates QSE's structural effect on Pb deposition on two different 2D phases of In on Si(111) 7 x 7. However, QSE are not the only factor involved because the Pb crystal structure and that of the two In phases, $\sqrt{3}$ x $\sqrt{3}$ R30° (In $\sqrt{3}$) and $\sqrt{31}$ x $\sqrt{31}$ R8.7° (In $\sqrt{31}$), do not match. This is because the two crystal structures have different lattice constants, and, in the case of the In $\sqrt{31}$, the unit cells have different shapes. It is favorable to have a low energy

interface, and since stretching and compressing the atomic structure takes a lot of energy, it tends not to occur. The crystal structure can align itself along another direction, in which the lattice constants of two crystal structures lead to a closer match between non-primitive lattice vectors. While this possibility was postulated and confirmed quite some time ago for generic lattices,[35] it had not, until now, been seen in this specific system.

In addition to the myriad of effects already listed, QSE may also be able to affect the alignment of crystals. This is because, as stated earlier, the confinement of electrons costs energy, which raises the total energy of the island. This could cause the islands to align along different directions whose symmetry lattice matchup weakens or otherwise changes the electron boundary conditions with the substrate. This could cause the QSE to weaken and hence reduce the energy cost. With this possibility, there are two competing effects to determine which direction the islands will align. Based on what is known about QSE it is likely that it will have a much stronger effect at lower layer thicknesses where the confinement is more pronounced, while the lattice matching will have a constant effect per unit area and therefore dominate at higher coverages.

Recently, this was seen in a similar system to the one studied in this dissertation, Pb on Pb $\sqrt{3}$x$\sqrt{3}$ R30° on Ge(111) by Tang et al.[36] They saw two different crystal structures, both of which were regular Pb lattices, but one was aligned along the Ge [1$\bar{1}$0] direction at lower coverages while the other was aligned along [11$\bar{2}$] direction at higher coverages. The Pb aligned along the [11$\bar{2}$] direction can be thought of as Pb 2 x 2 R30°, it is the same as the normal Pb(111) 1 x 1 lattice, but now rotated 30° to match up with the Ge $\sqrt{3}$ x $\sqrt{3}$ R30° lattice. It takes 2 Pb lattice constants to match up with a single Ge (111) $\sqrt{3}$ x $\sqrt{3}$ R30° lattice constant; their respective values are 0.984 and 0.979 nm. They argued that while the $\sqrt{3}$ x $\sqrt{3}$ R30° configuration of the Pb, has a lower interface energy due to the better lattice constant matchup than the Pb aligned along Ge[1$\bar{1}$0] it dominates at lower coverages because it helps limit the energy cost associated with confining the free electrons in the film. The Pb aligned along Ge[1$\bar{1}$0] shares the same symmetry as the substrate, so even though the lattices are not commensurate Tang et al.[36] argues that the hybridization across the Pb-Ge interface allowed by the symmetry greatly reduces the energy cost associated with confining electrons. This

effect weakens as the thickness of the film increases, so the $\sqrt{3}$ x $\sqrt{3}$ R30° orientation of the Pb islands is favorable there because of the lattice matchup.

This work has some definite similarities with Pb growth on top of the two In phases (In $\sqrt{3}$ and In $\sqrt{31}$). Both substrates produce multiple Pb orientations that could be caused by a similar effect as that seen by Tang et al.[36] Similarly to Tang et al.[36] Pb growth along the Si[1$\bar{1}$0] direction on top of $\sqrt{3}$ is metastable, but since depositions up to 4.5 ML do not show any rotation of the islands, it appears to be thermally limited instead of limited by energy associated with QSE. Pb growth on top of In $\sqrt{31}$ shows a similar pattern to the In $\sqrt{3}$, with a rotation occurring due to higher temperatures instead of up to 12 ML of deposition. However, there is some evidence that the QSE of this system are different for growths along different orientations.

The Pb islands grown on In $\sqrt{31}$ below about 215 K grow in directions 0°, 8.4°, and 25.3° off of the Si[1$\bar{1}$0] because these directions match up well with the underlying In $\sqrt{31}$ lattice. This orientation is stable up to at least 11.5 ML of deposition, and for depositions of less than 4 ML there is a preferred height of 2 layers. Above 215 K the islands no longer appear in the diffraction pattern, leaving behind $\sqrt{3}$, whose composition is not known but is likely In. This is because the In gains enough energy to form very large islands that are larger than the transfer width of the instrument (the size of an object that the instrument can detect). On the other hand, Pb depositions on top of In $\sqrt{3}$ below 215 K results in a 1 x 1 pattern with very diffuse spots. Depositions or annealing above 215 K results in the Pb orientating along [11$\bar{2}$] and island heights of 4 layers. Pb growth on In 4 x 1 produced 4-layer islands, so the current results are in line with expectations.[37]

1.6 Techniques

All of the data used in this dissertation were taken with Spot Profile Analysis – Low Energy Electron Diffraction (SPA-LEED) or Scanning Tunneling Microscopy (STM). SPA-LEED uses an octopole electric field to sweep the diffracted electron beams across an electron counter, which provides two main benefits. The first is that the electron counter, in this case a channeltron, can measure the relative intensities much better than a phosphor screen which

is used in normal LEED. The second is that the channeltron opening has a finite width, which helps improve the resolution of the instrument, again, beyond the limit of a normal phosphor screen. The higher resolution is useful for determining lattice constants on the surface, and a quick glance at the diffraction pattern is enough to determine the lattice structure. SPA-LEED also excels at reporting statistics about the surface, ranging from surface roughness to step distribution and even island heights, island separation, and island size.[38] Lent and Cohen[39] published theory work that describes how the specular reflection of the beam will change based on the step distribution on the surface. It is composed of both a narrow and broad component, with the number of broad components depending upon the number of different layers exposed on the surface. The narrow component comes from the fact that no matter which step an electron diffracts off of, it is still reflecting off of a lattice position. The broad component represents the disorder on the surface, which holds information about the steps and islands on the surface and can be used to determine the heights and other properties mentioned above. Lent and Cohen[39] applied their results to high resolution LEED data from Gronwald and Henzler[40]. The Si on Si(111) data matched the theory perfectly, and they were able to determine that the Si steps on the surface were 1-layer thick, as well as put an upper bound on the area of a possible third layer of Si at 20% coverage. This will be covered in much greater detail in Chapters 2 and 3.

The STM, as its name implies, measures the tunneling current between a conductive tip and a sample to gauge the distance between the tip and the sample. One of the great strengths of the STM is that it can achieve atomic resolution, but it is unable to image insulators, as at least a little bit of current must flow through the sample.

The two instruments complement each other well because SPA-LEED produces a diffraction pattern that requires a fair bit of interpretation before it is useful, and the STM produces a topological map that is very easy to interpret. Conversely, the STM only provides data on a relatively small portion of the sample while SPA-LEED can provide statistics on millions of islands at once. Much more information about the two instruments can be found in Chapter 2.

1.7 Chapter Previews

Chapter 2 focuses on the instruments used to take the data in this dissertation and Chapter 3 takes an in depth look at a specific data analysis technique for LEED data called G(S) curves. G(S) curves can provide a great deal of structural information about the surface; including step heights, island size, and island separation. Chapters 4 (published in PRB 2008[20]), 5 (published in SS 2009[41]), and 6 revolve around the effects of QSE on the diffusion and critical island sizes of Pb and In on Pb films. Chapter 7 focuses on Pb depositions on the 2D In phases $\sqrt{3}$ and $\sqrt{31}$ to see how the phases affect the Pb growth and its strong QSE. Chapter 8 is the conclusion.

References

[1] M. Yakes, V. Yeh, M. Hupalo, and M. C. Tringides, Phys. Rev. B **69**, 224103 (2004). 1.1

[2] M. Hupalo, J. Schmalian, and M. C. Tringides, Phys. Rev. Lett. **90**, 216106 (2003). 1.1

[3] K. Budde, E. Abram, V. Yeh, and M. C. Tringides, Phys. Rev. B **61**, R10602 (2000). 1.1, 1.2, 1.2

[4] M. Hupalo, S. Kremmer, V. Yeh, L. Berbil-Bautista, E. Abram, and M. C. Tringides, Surf. Sci. **493**, 526 (2001), ISSN 0039-6028, URL http://www.sciencedirect.com/science/article/pii/S0039602801012626. 1.1, 1.2

[5] M. Hupalo and M. C. Tringides, Phys. Rev. B **65**, 115406 (2002). 1.1

[6] V. R. Stamenkovic, B. Fowler, B. S. Mun, G. Wang, P. N. Ross, C. A. Lucas, and N. M. Markovi, Science **315**, 493 (2007). 1.1

[7] J. Zhang, K. Sasaki, E. Sutter, and R. R. Adzic, Science **315**, 220 (2007), URL http://www.sciencemag.org/content/315/5809/220.abstract. 1.1

[8] V. Yeh, L. Berbil-Bautista, C. Z. Wang, K. M. Ho, and M. C. Tringides, Phys. Rev. Lett. **85**, 5158 (2000). 1.2

[9] Z. Zhang, Q. Niu, and C.-K. Shih, Phys. Rev. Lett. **80**, 5381 (1998). 1.2

[10] N. V. Smith, N. B. Brookes, Y. Chang, and P. D. Johnson, Phys. Rev. B **49**, 332 (1994), URL http://link.aps.org/doi/10.1103/PhysRevB.49.332. 1.2

[11] J. Chen, M. Hupalo, M. Ji, C. Z. Wang, K. M. Ho, and M. C. Tringides, Phys. Rev. B **77**, 233302 (2008). 1.2

[12] T. Nagao, J. T. Sadowski, M. Saito, S. Yaginuma, Y. Fujikawa, T. Kogure, T. Ohno, Y. Hasegawa, S. Hasegawa, and T. Sakurai, Phys. Rev. Lett. **93**, 105501 (2004), URL http://link.aps.org/doi/10.1103/PhysRevLett.93.105501. 1.2

[13] V. Fournée, H. R. Sharma, M. Shimoda, A. P. Tsai, B. Unal, A. R. Ross, T. A. Lograsso, and P. A. Thiel, Phys. Rev. Lett. **95**, 155504 (2005). 1.2

[14] M. Ja*l*ochowski, M. Hoffmann, and E. Bauer, Phys. Rev. B **51**, 7231 (1995). 1.2, 1.4

[15] Y. Guo, Y.-F. Zhang, X.-Y. Bao, T.-Z. Han, Z. Tang, L.-X. Zhang, W.-G. Zhu, E. G. Wang, Q. Niu, Z. Q. Qiu, et al., Science **306**, 1915 (2004). 1.2

[16] L. Aballe, A. Barinov, A. Locatelli, S. Heun, and M. Kiskinova, Phys. Rev. Lett. **93**, 196103 (2004). 1.2, 1.4

[17] N. Binggeli and M. Altarelli, Phys. Rev. B **78**, 035438 (2008). 1.2

[18] K. Takayanagi, Y. Tanishiro, M. Takahashi, and S. Takahashi, Journal of Vacuum Science Technology A: Vacuum, Surfaces, and Films **3**, 1502 (1985), ISSN 0734-2101. (document), 1.2

[19] Philip, page viewed October 19, 2006. This figure was adopted from the other reference but I grabbed it from this one., URL http://whome.phys.au.dk/~philip/q1_05/surflec/node23.html. (document), 1.2

[20] S. M. Binz, M. Hupalo, and M. C. Tringides, Phys. Rev. B **78**, 193407 (2008). 1.3, 1.7

[21] M. Hupalo, S. Binz, and M. C. Tringides, Journal of Physics: Condensed Matter **23**, 045005 (2011), URL http://stacks.iop.org/0953-8984/23/i=4/a=045005. 1.3

[22] K. Oura, *Surf. Sci.: an introduction*, Advanced texts in physics (Springer, 2003), ISBN 9783540005452, URL http://books.google.com/books?id=HBFtQgAACAAJ. 1.3, 1.3

[23] G. Ehrlich and F. G. Hudda, The Journal of Chemical Physics **44**, 1039 (1966), URL http://link.aip.org/link/?JCP/44/1039/1. 1.3

[24] J. W. Evans, D. E. Sanders, P. A. Thiel, and A. E. DePristo, Phys. Rev. B **41**, 5410 (1990). 1.3

[25] R. Caflisch, viewed on April 28, 2011, URL http://www.math.ucla.edu/~caflisch/thinfilmg.shtml. (document), 1.3

[26] H. Brune, Surf. Sci. Rep. **31**, 125 (1998), ISSN 0167-5729, URL http://www.sciencedirect.com/science/article/pii/S0167572999800016. 1.3, 1.3, 1.3

[27] J. A. Venables, G. D. T. Spiller, and M. Hanbucken, Rep. Prog. Phys. **47**, 399 (1984), URL http://stacks.iop.org/0034-4885/47/i=4/a=002. 1.3

[28] T. Chan, C. Z. Wang, M. Hupalo, M. C. Tringides, and K. M. Ho, Phys. Rev. Lett. **96**, 226102 (2006). 1.4

[29] N. Binggeli and M. Altarelli, Phys. Rev. Lett. **96**, 036805 (2006). 1.4

[30] M. Hupalo and M. C. Tringides, Phys. Rev. B **75**, 235443 (2007).

[31] Z. Kuntova, M. Hupalo, Z. Chvoj, and M. C. Tringides, Phys. Rev. B **75**, 205436 (2007). 1.4

[32] L.-Y. Ma, L. Tang, Z.-L. Guan, K. He, K. An, X.-C. Ma, J.-F. Jia, Q.-K. Xue, Y. Han, S. Huang, et al., Phys. Rev. Lett. **97**, 266102 (2006), URL http://dx.doi.org/10.1103/PhysRevLett.97.266102. 1.4

[33] X. Ma, P. Jiang, Y. Qi, J. Jia, Y. Yang, W. Duan, W.-X. Li, X. Bao, S. B. Zhang, and Q.-K. Xue, Proc. Natl. Acad. Sci. **104**, 9204 (2007), URL http://www.pnas.org/content/104/22/9204.abstract. 1.4

[34] Z. Hu, Y. Yang, B. Sun, X. Shao, W. Wang, and P. Zhang, The Journal of Chemical Physics **132**, 024703 (pages 5) (2010). 1.4

[35] A. D. Novaco and J. P. McTague, Phys. Rev. Lett. **38**, 1286 (1977). 1.5

[36] S.-J. Tang, C.-Y. Lee, C.-C. Huang, T.-R. Chang, C.-M. Cheng, K.-D. Tsuei, H.-T. Jeng, V. Yeh, and T.-C. Chiang, Phys. Rev. Lett. **107**, 066802 (2011). 1.5

[37] M. Yakes, J. Chen, M. Hupalo, and M. C. Tringides, Applied Physics Letters **90**, 163117 (pages 3) (2007), URL http://link.aip.org/link/?APL/90/163117/1. 1.5

[38] M. Henzler, Applications of Surf. Sci. **11-12**, 450 (1982), ISSN 0378-5963, URL http://www.sciencedirect.com/science/article/pii/0378596382900927. 1.6

[39] C. Lent and P. Cohen, Surf. Sci. **139**, 121 (1984), ISSN 0039-6028, URL http://www.sciencedirect.com/science/article/pii/003960288490013X. 1.6

[40] K. Gronwald and M. Henzler, Surface Science **117**, 180 (1982), ISSN 0039-6028. 1.6

[41] S. M. Binz, M. Hupalo, and M. C. Tringides, Journal of Applied Physics **105**, 094307 (pages 4) (2009), URL http://link.aip.org/link/?JAP/105/094307/1. 1.7

CHAPTER 2. Experimental Techniques: SPA-LEED and STM

2.1 Introduction

The two main techniques used to record the data in this dissertation were Spot Profile Analysis – Low Energy Electron Diffraction (SPA-LEED) and Scanning Tunneling Microscopy (STM). These two techniques are very different yet they still probe the physical structure of surfaces but that is why they work so well together. SPA-LEED is able to look at an area of around 0.1 mm^2 which means that it probes a relatively large area.[1] The STM usually only images 0.1 μm^2 at a time and covering a larger area takes on the order of hours. On the other hand, SPA-LEED data is in reciprocal space so even though the pattern and the spots themselves hold a lot of information it is not very easy to interpret. STM images are in real space allowing for relatively easy determination of the atomic locations and island shapes. While these quick facts are a good way to show that the two instruments complement each other it is short on details. Though, it should be mentioned up front that both instrument suffer from a common limitation, neither works very well with insulators since they both rely on the sample's ability to allow current to flow. The STM needs current to flow from the tip, to the sample, and then to the electronics to be measured. The SPA-LEED needs the sample to avoid charging because any charging can significantly alter the pattern.

2.2 Spot Profile Analysis – Low Energy Electron Diffraction

2.2.1 Diffraction and reciprocal space

Before addressing SPA-LEED it is beneficial to start with normal LEED because they work by the same basic process. Low energy refers to electrons from 30-200 eV and are used because they have wavelengths on the order of Angstroms which is the same order of magnitude of

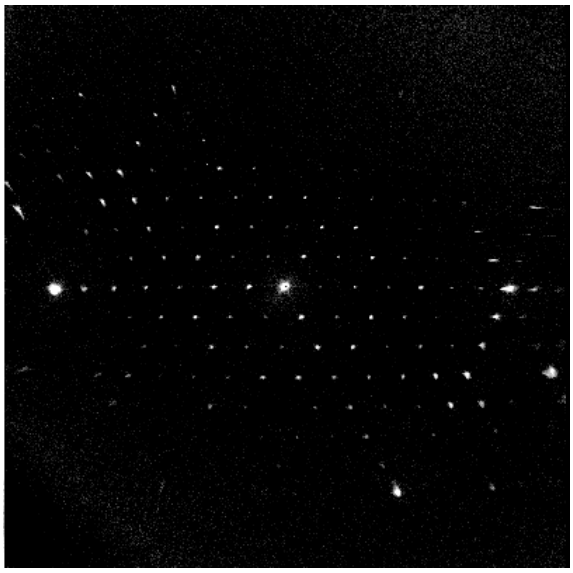

Figure 2.1 Example of a LEED pattern, more specifically a SPA-LEED pattern, of Si(111) 7 x 7.

the spacing between atoms, allowing the electrons to diffract off of the atoms. Specifically, the wavelength of an electron is:

$$\lambda_e = \frac{h}{\sqrt{2mE}} = \sqrt{\frac{150.4}{E}}\ \text{Å} \tag{2.1}$$

In the last portion of the equation, E is in eV and the result is in Å. Another reason low energy electrons are used is because they have a short mean free path in materials so the elastic signal that comes from the sample will be from the top few layers, ~5.[2] In other words, any information contained in what comes from the sample will pertain to the surface and not the bulk.[3]

The electron beam illuminates an area on the sample roughly 2 mm in diameter.[1] The beam does not have to be perpendicular to the sample but it generally is because that produces a symmetric pattern which is easier to work with. This is one of the advantages of using LEED instead of Reflective High Energy Electron Diffraction, which, because of its high energy electrons' ability to go deep into the sample must hit the sample at a glancing angle, producing a very distorted pattern.[3] Once at the surface, a percentage of the electrons will interact elastically with the atoms and move away from the sample. The percentage of the electrons that interact elastically with the sample depends upon the material and the electron energy. The

electrons interact destructively in most directions but interact constructively at very specific locations that satisfy Bragg's Law:

$$n\lambda_e = d\sin\theta \tag{2.2}$$

In this case, d is the distance between unit cells on the surface, i.e. the periodicity of the lattice. The equation is derived from the fact that for two electrons to interact completely constructively they must have the same phase. Since electrons that hit perpendicular to the flat surface with the same phase, the difference in path length from two adjacent atoms must be an integer multiple of the electron wavelength to keep them in phase. For a flat surface with a relatively simple crystal structure, Bragg's Law predicts the diffraction pattern very well and it is useful in interpreting more advanced results but it is not easy to work with for systems with multiple heights and it does not give the intensities of the spots. Another way to create the reciprocal lattice is by taking the Fourier Transform of the surface.[4] While a proof of that statement will not be provided it can be partially justified by the fact that diffraction notices correlations on the surface, or in less general terms, periodicity. That is exactly what the Fourier Transform does and it matches up with Bragg's Law, which also used the atomic periodicity to determine the diffraction spots locations. Therefore, the diffraction pattern is a measure of the periodicity of the surface. The derivation can be found in many places, including a well laid out derivation in Kittel[4] so it will not be repeated here. The important part is that the result of taking the Fourier Transform is:

$$n\left(\overrightarrow{r}\right) = \sum_{\overrightarrow{G}} n_{\overrightarrow{G}} e^{i\overrightarrow{G}\cdot\overrightarrow{r}} \tag{2.3}$$

$n(r)$ represents the real space lattice, n_G is the relative magnitude of the spot and $\vec{G}$ are the reciprocal lattice vectors. Since $n(r)$ represents the lattice it must be invariant under crystal translations. Solving equation 2.3 for $\vec{G}$ is not simple but there is an easy formulation that can be used.[4] The reciprocal lattice vectors are:

$$\vec{b_1} = 2\pi\frac{\vec{a_2}\times\vec{a_3}}{\vec{a_1}\cdot(\vec{a_2}\times\vec{a_3})} \tag{2.4}$$

$$\vec{b_2} = 2\pi\frac{\vec{a_3}\times\vec{a_1}}{\vec{a_1}\cdot(\vec{a_2}\times\vec{a_3})} \tag{2.5}$$

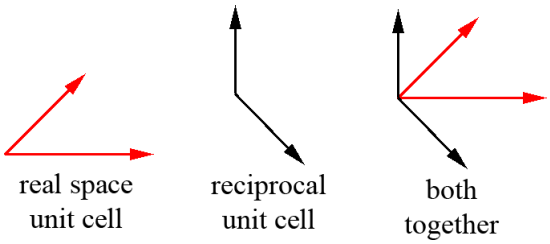

Figure 2.2 Hypothetical real space and reciprocal space unit cells shown separately and then together to emphasize their relationship to one another.

$$\vec{b_3} = 2\pi \frac{\vec{a_1} \times \vec{a_2}}{\vec{a_1} \cdot (\vec{a_2} \times \vec{a_3})} \tag{2.6}$$

$\vec{a_n}$ and $\vec{b_n}$ indicate the primitive vectors of the real space and reciprocal space unit cells respectively.[4] Since this dissertation is on surfaces, $\vec{b_3}$ appears to be irrelevant and $\vec{a_3}$ does not have a normal definition. However, since the lattice vectors represent the distances associated with the unit cell, it makes sense to set $\vec{a_3}$ to be perpendicular to the surface with a magnitude of infinity. This is because the next unit cell perpendicular to the surface is infinitely far away. This results in $\vec{b_3}$ being essentially zero which creates a reciprocal lattice rod perpendicular to the plane based at every point in the 2D reciprocal lattice. These lattice rods play an important role in the analysis techniques discussed below. Some rules of thumb that relate $\vec{a_n}$ to $\vec{b_n}$ are that $\vec{b_n}$ is always perpendicular to $\vec{a_n}$ and the longer $\vec{a_n}$ is, the smaller $\vec{b_n}$ is. To go from the reciprocal lattice back to real space switch all of the a's and b's in equations 2.4-2.6. The challenge to in going back to real space is being able to pick out the reciprocal unit vectors which is not always easy because surfaces have rotational symmetries and can also have different orientations on the surface (see the In $\sqrt{31}$ pattern in Chapter 7 for an example). One major downside to this method of calculating the spot locations is that it does not attempt to explain the spot intensities.

Kinematic Theory is very good at explaining a wide variety of spots and it also makes an attempt at estimating the spot intensities. Kinematic Theory asserts, incorrectly, that electrons are only scattered elastically once by the surface but does acknowledge the existence of the other layers via a structure factor, f, which will be discussed in more detail later. Kinematic Theory

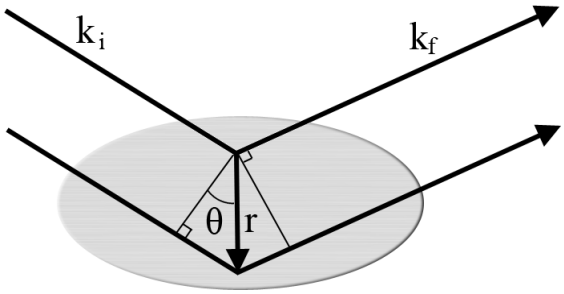

Figure 2.3 The difference in path length for the two waves is $rsin(\theta)+rsin(\phi)$ so the difference in phase is $(k_i - k_f) \cdot r$. See the text for more details. After Kittel [4]

says that the wave scatters equally in all directions so the wave from one atom is:

$$\Psi\left(\overrightarrow{k_i}, \overrightarrow{k_f}\right) = f\left(\overrightarrow{k_i}, \overrightarrow{k_f}\right) e^{-i\overrightarrow{k_f}\cdot\overrightarrow{r}} \tag{2.7}$$

k_i and k_f are the incoming and outgoing wave vector respectively and Ψ is the wave function describing the electrons. However, there are many different scattering locations so the method of interaction must be considered. Consider two electrons that are on parallel trajectories toward the surface and then scatter by the same angle, see Figure 2.3. They travel different distances but that can be easily calculated to see what their relative phase will be, and therefore the intensity of the electron wave at the angle they are now moving. The difference in distance traveled on the way toward the crystal is $rsin(\theta)$, the difference in phase angle is $2\pi rsin(\theta/\lambda)$ which is equal to $k_i \cdot r$. Likewise, the path away from the crystal is different in length by $-k_f \cdot r$. That means the total phase difference is $(k_i - k_f) \cdot r = K \cdot r$.[4] The total wave is then:

$$\Psi\left(\overrightarrow{k_i}, \overrightarrow{K}\right) = \int f\left(\overrightarrow{k_i}, \overrightarrow{K}\right) e^{-i\overrightarrow{K}\cdot\overrightarrow{r}} e^{i\overrightarrow{G}\cdot\overrightarrow{r}} dA \tag{2.8}$$

Since electrons are charged they scatter off of the potential distribution in the surface,[5] i.e., they do not scatter off of random locations like the situation used in Figure 2.3 and the above arguments. They only scatter off of the potential which mirrors the period of the atomic cores because they are the major feature in the potential distribution and it attenuates rather quickly because the electrons act to screen it. That is why the Fourier components of the lattice were added to equation 2.8 above. This leads to a new diffraction condition, the argument in the exponentials is very small unless $\vec{K} - \vec{G} = 0$, or in other words:[2,4]

$$\overrightarrow{K} = \overrightarrow{G} = \overrightarrow{k_i} - \overrightarrow{k_f} \tag{2.9}$$

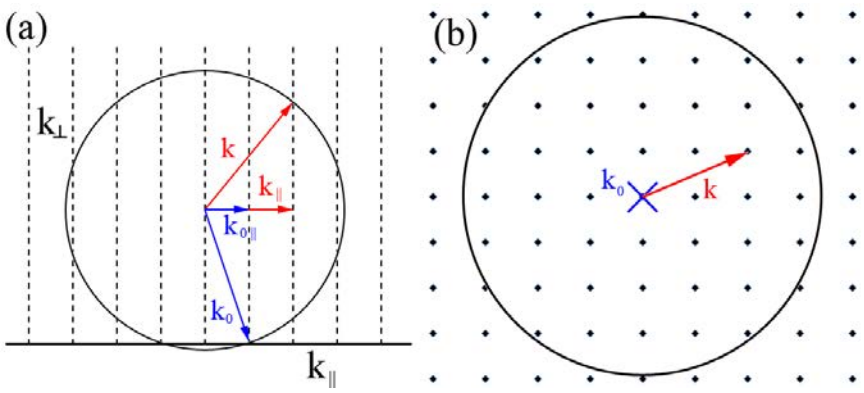

Figure 2.4 Ewald construction. (a) is a side view that shows the diffraction condition in equation 2.10 being satisfied. The vertical dotted lines are the reciprocal lattice rods. (b) is the top view of the Ewald Sphere with the circle indicating the extent of the sphere. This part of the figure assumes the incoming electron beam is perpendicular to the surface unlike (a) which introduced an angle to show the diffraction condition better.

Since the surface is flat there is no periodicity perpendicular to the surface so this can be simplified to:[3]

$$\overrightarrow{k_{\|i}} - \overrightarrow{k_{\|f}} = \overrightarrow{G_{hk}} \tag{2.10}$$

$$\left|\overrightarrow{k_i}\right| = \left|\overrightarrow{k_f}\right| \tag{2.11}$$

equation 2.11 comes from the fact that the electrons that diffract do so elastically. k_i and k_f are the wave vectors of the incoming and outgoing electron waves respectively and

$$\overrightarrow{G_{hk}} = h\overrightarrow{b_1} + k\overrightarrow{b_2} \tag{2.12}$$

Since k depends upon the energy of the electrons, the number of diffraction conditions that are met goes up as the energy goes up. $\vec{G}$ is the reciprocal lattice vector that points to the various reciprocal lattice points that make up the reciprocal lattice.

Another way to view this diffraction condition is called the Ewald Construction, it creates a geometric representation of equations 2.10 and 2.11. The first step is to draw the k_i vector to a reciprocal lattice point and then draw a sphere around the start of k_i (rotate the k_i vector until a sphere has been drawn). Then, for every intersection of the sphere and a reciprocal lattice point, or in the case of surface diffraction-reciprocal lattice rod, a spot will be created. An example of this is shown in Figure 2.4 with a side view showing the diffraction condition,

(a), and a top view showing all of the different reciprocal lattice rods that will produce a spot in the pattern, (b).

This construction, along with the fact that the surface creates reciprocal lattice rods, agrees with the simplified diffraction conditions laid out in equations 2.10 and 2.11. In normal LEED the angle that the k_f vector makes with k_i can be used to predict the physical location of the spots on the screen. In this way it is straight forward to see why LEED spots get closer together as the energy of the electrons increases, as k_i increases the curvature of the sphere near the main reflection, the specular, gets smaller and the spots are moved closer together because k_f now makes a smaller angle with k_i. This is also a good way to visualize the fact that to probe the reciprocal lattice rod all that must be done is to change the energy of the electron beam.[3]

The pattern created by diffraction is seen by accelerating the electrons into a phosphor screen but not want all of the electrons should be accelerated – just the ones that diffracted elastically from the surface. This is because only the electrons coming off of the surface at the same energy they went in were diffracted and contain coherent information about the surface structure, the electrons that lost energy do not. Therefore, before the electrons experience the accelerating potential to the screen they first go through a retarding potential to make ensure only electrons above a certain energy make it to the screen. The data is recorded via a camera, usually a CCD one connected to a computer.

All distances in reciprocal space are in units of inverse length but it is convenient to measure distances in terms of percent Brillouin Zone (% BZ). Brillouin Zone is the reciprocal space equivalent of the unit cell in real space and is composed of the reciprocal lattice vectors derived in equations 2.4-2.6. % BZ refers to the percent of the distance from the specular (one corner of the BZ) to the edges of the first BZ. Since different materials have different BZ using them as a measure of distance requires care. To solve this issue, the substrate's BZ is used for all measurements. One reason this method is so convenient is that it makes lattice lengths easy to identify. For example, if a spot is at 50% BZ then the unit vector that produced the spot is twice as long as the substrate's unit vector. Since spots move with electron energy in LEED care must be taken to ensure that the all spot location comparisons are done at the same energy.

From LEED it is possible to get an idea of how good the long range order of the sample is because the intensity of the spots are a function of how much of the surface is contributing to the pattern. Also, if there are spots that were not expected then the surface is not clean. The spot locations can give a rough idea of the crystal structure, for example, the arrangement of the spots indicates the surface periodicity. The distance those spots are from the specular indicates the length of the real space unit cell.

The spot intensities caused by different structures on the surface indicate the area of the surface that has that structure on it. Rewriting equation 2.8 to sum over all atoms instead of integrating over the entire surface is the first step to determining the mathematical relationship between the area of a phase and the spot intensity.

$$\Psi\left(\overrightarrow{k_i},\overrightarrow{K}\right)=\sum_n f\left(n,\overrightarrow{k_i},\overrightarrow{K}\right)e^{i\overrightarrow{K}\cdot\overrightarrow{r(n)}} \tag{2.13}$$

Remembering that Kinematic Theory replaces all f_n with their spatial averages the intensity is:[6]

$$I=\left|\Psi\left(\overrightarrow{k_i},\overrightarrow{K}\right)\right|^2=\left|f\left(\overrightarrow{k_i},\overrightarrow{K}\right)\right|^2\left|\sum_n e^{i\overrightarrow{K}\cdot\overrightarrow{r(n)}}\right|^2 \tag{2.14}$$

For any given successful diffraction condition the equation becomes:

$$I=\left|f\left(\overrightarrow{k_i},\overrightarrow{K}\right)\right|^2|n|^2=Fn^2 \tag{2.15}$$

There is more that can be said about the above equation but that will occur below. n is the number of atoms and scales with the area, therefore:

$$I\sim A^2 \tag{2.16}$$

This matches the result found in the literature.[2,6]

Unfortunately, the intensity of a single spot does not convey any information because the intensity depends upon many things, one of which is completely external to the surface, the intensity of the incoming electron beam. Another factor that is not directly related to the structure of the surface is temperature. The movement of the ion cores caused by lattice vibrations lowers the overall intensity, especially the peak intensity, of spots while increasing the background noise. This effect is called the Debye-Waller factor and was worked into LEED

theory by Laramore and Duke[7]. Those two factors limit the ability to compare intensities between days directly but they can be normalized against the specular which is also affected by the incoming electron beam intensity and thermal effects but is not as affected by differences in phases on the surface. This is because the specular is not very sensitive to the lateral positions of the atoms so different phases on the surface will not affect it nearly as much as it will the lattice vector spots of the various phases.[8] This information solves another problem. The experimentally acquired information is not just the reciprocal lattice vectors, G.

If, instead of attempting to evaluate the summation in equation 2.14, it is rewritten in terms of its major components:

$$I = \left| \sum_n f\left(n, \overrightarrow{k_i}, \overrightarrow{K}\right) e^{i\overrightarrow{K}\cdot\overrightarrow{r(n)}} \right|^2 = F\left(\overrightarrow{K}, \overrightarrow{k_i}\right) G(\overrightarrow{K}) \tag{2.17}$$

G is called the lattice factor and only depends upon the lattice vectors, the energy of the incoming electrons, and the long range order of the sample.[6] F, the dynamic form factor, is so named because it is supposed to represent processes covered in dynamic diffraction theory. Therefore it supposedly includes the structure factor of the unit cell even if the lattice has a basis, includes other atoms. It would also have to cover the fact that multiple scattering does occur which kinematic theory does not address directly. However, as mentioned above, the kinematic approximation replaces all F with their spatial averages; this is done to make the math doable but keeps kinematic theory from accurately predicting spot intensities. Similarly, G is normalized to 1 such that:

$$\int_{BZ} G\left(\overrightarrow{K_{\|f}}, \overrightarrow{K_{\perp f}}\right) dK_{\|f} = 1 \tag{2.18}$$

$$\langle F \rangle = \int_{BZ} FG \; dK_{\|f} \tag{2.19}$$

Since G has already been normalized to 1 over the BZ simply integrating the entire BZ's intensity produces the weighted average of the dynamic form factor.

The problem alluded to earlier is that the only data available experimentally is the intensity but, as a general rule, F is not the needed information. F has electron energy, angle, and surface dependence. This prevents comparing two spots caused by different phases or imaged at different energies. G is the needed value and the way to extract is to divide the intensity by

the integral of the intensity leaving the normalized function, G:[6,9]

$$\frac{I(\overrightarrow{K_{\parallel f}}, \overrightarrow{K_{\perp f}})}{\int_{BZ} I \; dK_{\parallel f}} = \frac{F\left(\overrightarrow{K}, \overrightarrow{K_i}\right) G(\overrightarrow{K})}{\int_{BZ} FG \; dK_{\parallel f}} = \frac{F}{\langle F \rangle} G \approx G \tag{2.20}$$

As long as F is relatively constant over the BZ then the resulting G is fairly accurate. More specifically, it was shown that as long as G has more drastic variations than F then the result has a high accuracy.[9] Dividing a spot by the intensity of the specular has a similar effect since it is relatively unaffected by lateral spot positions as already noted.

Another experimental method around F is to determine the structure factor experimentally, as opposed to merely getting rid of it. This requires a surface that is 100 percent the phase of interest and comparing its diffraction pattern to that of a phase with a known structure factor via this ratio:[8]

$$\rho = \frac{F_{adsorbate}}{F_{substrate}} = \sqrt{\frac{I_{\theta \gg 1 \; ML}}{I_{\theta = 0 \; ML}}} \tag{2.21}$$

2.2.2 SPA-LEED

Instead of using on a phosphor screen to detect the electrons, SPA-LEED utilizes an electron multiplier to count how many electrons are associated with each spot. This requires an octopole electric field to direct all of the different parts of the pattern into the electron multiplier one section at a time until the entire pattern has been scanned. The electric field also affects the electrons going from the gun to the sample so the fields have to be carefully controlled to make sure the electrons can both reach the sample and get back to the electron multiplier. The control of the electric fields as well as the recording of data requires the use of a computer. Counting the electrons with an electron multiplier has two benefits, the intensity of the spots are measured more accurately and the locations of the spots are known very precisely. Also, using the computer it is possible to scan along any direction in the pattern to produce 1D scans with each individual data point corresponding to less than 0.1% BZ. Though, that is not the claimed accuracy of the instrument. The full width at half maximum of the specular spot when imaging a clean surface is a measure of the accuracy of the instrument and it is usually at or below 0.3% BZ. Qualitatively speaking the idea behind using the FWHM as a guide to the resolution for the instrument is that for a perfectly periodic and infinite lattice the specular

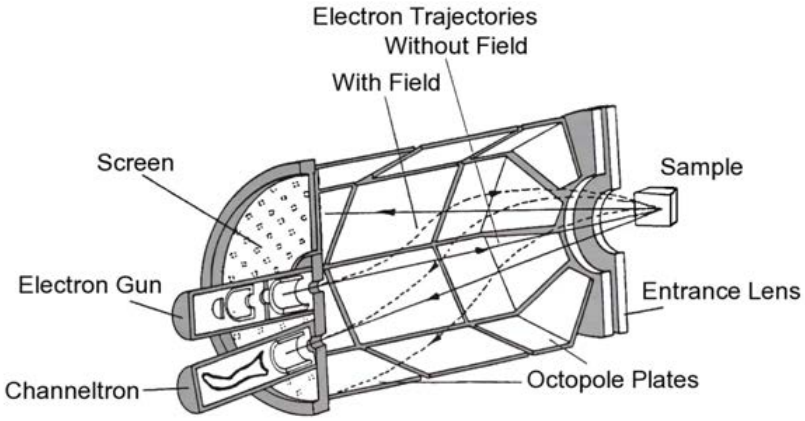

Figure 2.5 Inside view of a SPA-LEED unit. The electron paths are designated by dotted lines with arrows indicating the direction. The solid lines indicate the path of electrons without the otcopoles. From Omicron [1].

would have a width of 0. The fact that it is not 0 for a clean surface means that the instrument is limited by its specifications (like energy spread of the electrons, beam width, and detector width) or by the long range order of the sample. [10]

Another key advantage of SPA-LEED is that changing the energy will not change the spot locations, in terms of % BZ, because the computer will compensate for the change in voltage required to move the pattern across the channeltron. This is convenient if the deposited material does not show up strongly at the same energies as the substrate because it is easy to continue speaking in terms of % BZ of the substrate despite changing the energy of the electrons. [1]

Since the octopole continually adjusts the incoming and outgoing electron beams to make sure the outgoing beam of interest hits the channeltron, the angle the beam makes with the sample is continually changing. However, the angle between the incoming and outgoing beam does not change it always 4° because of the distances between the electron gun, the channeltron, and the sample. This has three effects on the pattern. The first is that the spots at different angles experience slightly different dynamic form factors since it depends upon the angle of incidence. The second is that as the energy changes, the size of the pattern on the screen does not change like it does for LEED. Though, the viewing area does go up with energy, it just does not change spot spacing. Lastly, as illustrated in Figure 2.6, the Ewald Sphere is effectively twice the size it is for normal LEED. The larger size nearly doubles the amount of reciprocal

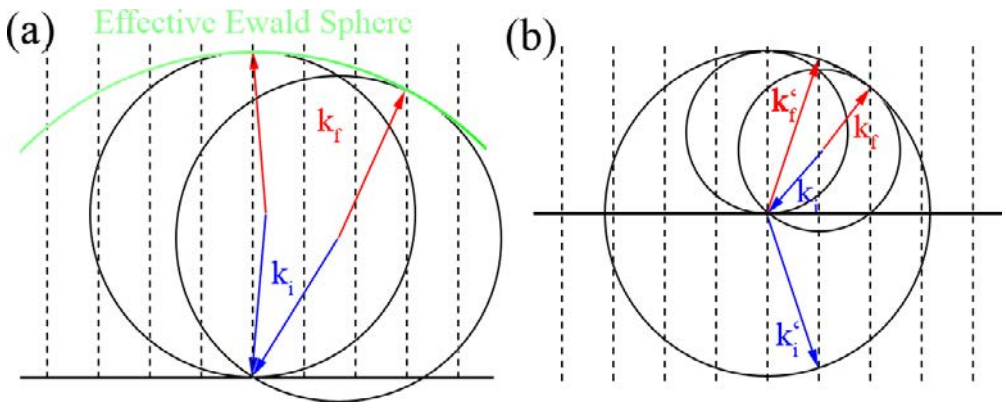

Figure 2.6 (a) The Ewald Sphere for SPA-LEED has nearly twice the radius of the normal construction since the K_i and K_f vectors are always 4° degrees apart and are rotated to see the entire pattern. The green arc across the top shows part of the effective sphere. Two sets of vectors are shown to illustrate the diffraction conditions. (b) A zoomed out view showing the entire effective sphere as well as two normal spheres and a set of vectors demonstrating the diffraction conditions. Modeled after an image in Zahl[11]'s 2008 SPA-LEED workshop talk.

space that can be viewed at any given energy.[1]

With the high resolution afforded by SPA-LEED it is easy to get the length as well as the direction of the reciprocal lattice vectors. Also, as the name suggests, the spot profiles can be used to determine extra details about the surface because any deviations from a perfect periodic surface will lead to less than perfect spots.[12] As mentioned above, the width of a spot is related to the size of the domains on the surface. If the sample is one continuous domain over the entire 0.1 μm^2 electron beam size then the sizes of the spots on the sample are limited by the instrument, more on this later. The smaller the domains that lead to a spot the broader the spot will be. This distance, like the locations of the normal diffraction spots is related to real space through the following ratio:[13]

$$\frac{\Delta k}{k_{10}} = \frac{a_0}{d} \tag{2.22}$$

Δk is the distance the spot of interest is from the specular, a_0 is the real space distance represented by k_{10} in reciprocal space, and d is the real space distance of the feature associated with Δk.

Another major source of imperfect spots is multiple layers exposed at the same time. For

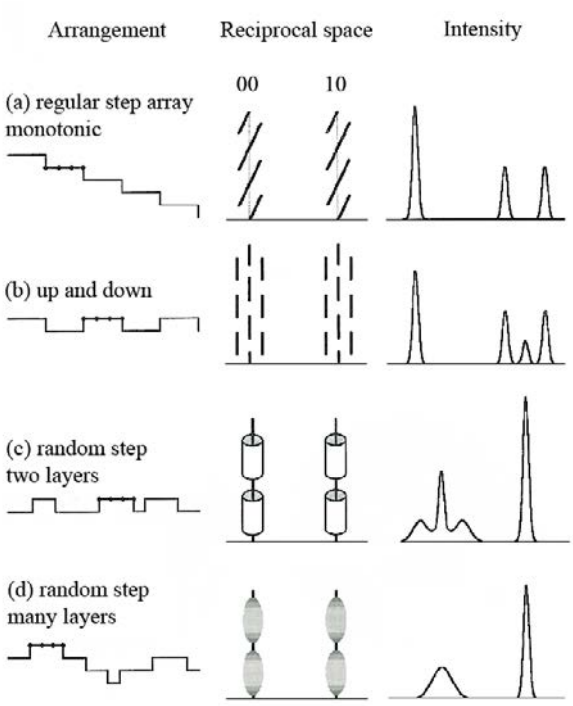

Figure 2.7 Example surface defects and how they affect the spots. (a) A regular step array produces spots that split and shift to the left as energy is increased. (b) Half of the surface being one height with the other half being another and having everything spaced uniformly produces a sharp spike at the in-phase conditions and three sharp spikes at the out-of-phase condition. (c) A more physically realistic two level system with the islands being somewhat random in size and location. (d) Many different layers exposed at the same time eliminates the shoulders in the out-of-phase conditions seen in (b) and (c) and replaces them with wings. This indicates that there is no longer any lateral length correlation between the heights. After Oura [3] and Henzler [12].

surfaces with a regular step array it produces spot splitting at certain energies and the spots shift a few % BZ as the energy changes, see Figure 2.7 (a). This is similar to the effect that is most directly relevant to this dissertation, islands of different heights and sizes on the surface. The differences in heights on the surface leads to the specular's intensity oscillating with energy between an in-phase condition and an out-of-phase condition, Figure 2.7 (b). If the electrons have just the right wavelength the electrons diffracting off of the substrate interfere destructively with the electrons diffracting off of the tops of the islands then the specular's peak intensity will be relatively low. If there is a dominant island height and the islands are spaced in some coherent fashion then in the out of phase condition the spots develop distinct shoulders, or

even extra peaks, instead of just becoming broader. The frequency (with respect to energy) with which the spots oscillate between in-phase and out-of-phase conditions depends upon the height difference between the layers present. The location of the shoulders indicates the most common distance between the islands while the width is related to the island sizes. The shape of the shoulders indicates the distribution of the island distances.[9,12,14] A deeper discussion of these points and a method for extracting the data can be found in Chapter 3.

2.2.3 Summary

LEED is a strong surface science instrument because it is very surface sensitive due to its small penetration depth of about 5 Å.[2] Because of its relatively large probe area it gets great statistics on the surface and the instrument does not need to be near the surface so it can take measurements at high temperature. LEED and a new version of Conical SPA-LEED are able to take in-situ measurements while depositing because they do not need to be aligned directly with the sample.[15] Recent work has been done by Klein et al.[16] has made taking SPA-LEED data at angles even more accessible.

However, not everything about SPA-LEED, and LEED in general, is good. SPA-LEED cannot take data in real time since the image must be scanned across the channeltron. Also, there is barrel distortion near the edges of the SPA-LEED's viewing.[2] The data taken is in reciprocal space and while it represents the real physical surface faithfully it is not a picture of it, which makes it harder to interpret. This is LEED's greatest weakness but is complimented well by the STM, which produces real space images of the surface. While the STM's data must also be interpreted with a discriminating eye it is much easier to understand.

2.3 Scanning Tunneling Microscopy

Scanning Tunneling Microscopy involves scanning a tip across a surface with an applied voltage which allows electrons to tunnel between the tip and the sample. Classically speaking, it is impossible for an electron to move from the tip to the sample at the low voltages used but as explained by quantum mechanics it is possible for objects to tunnel between two locations. If the object, distance, and barrier are all not too large it can happen readily. Exactly what is

going on is best left to a Modern Physics book but there is one more detail that is fundamentally important. The amount of the tunneling current is exponentially related to the distance the tip is from the sample, this result is from a 1D treatment which is accurate to first order in 3D:[17]

$$I \propto V d_s\left(E_F\right) e^{-2\frac{\sqrt{2m_e(\Phi-E)}z}{\hbar}} \tag{2.23}$$

This is what makes STM so sensitive to the height of a sample, any change in height is amplified by the exponential. A voltage must be applied to help overcome the potential barrier between the sample and the tip. In equation 2.23 $d_s(E_F)$ is the density of states at the Fermi Energy, V is the applied voltage, Φ is the work function of the donor material, E and m_e are the energy and mass of the electron, h is Planck's Constant, and z is the tip-sample distance in Å. I is the tunneling current.

The STM does not produce pictures, they are merely images constructed from the tunneling current. STM creates the image based on the current flowing to and from the tip but that only occurs if there are electrons available to flow. If the tip has a positive bias then electrons will tunnel to it from the sample. That means the tip will be probing the highest filled electron bands of the surface since that is where the electrons are most likely to come from. An added complication is that the tip must be able to accept electrons of that energy and momentum. If either the sample does not have available electrons or the tip cannot accept electrons of that energy and momentum then no current will tunnel. If the tip has a negative bias then the opposite occurs and the tip is probing the lowest unoccupied bands of the surface. This is reflected in the density of states term in equation 2.23.

Another way of saying that is that STM does not necessarily probe the locations of the atoms but rather the locations of the electrons. In some materials there is not a significant difference, for example, semi-conductors like Si, but in other materials it does. This is also why it is generally harder to get atomic resolution of metals, the free electron cloud has a large number of donors and acceptors of electrons. To get atomic resolution of a metallic surface the tip voltage must be set so that the tunneling current involves holes or electrons bound to the atoms. Some materials and arrangements of those materials can lead to electrons having a larger decay length, i.e., the stick out of the sample more, which would make the material

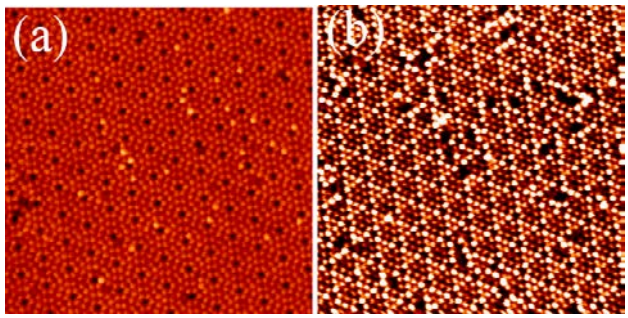

Figure 2.8 Both images are of clean Si(111) 7 x 7 reconstruction. Black spots that do not fit the periodic pattern are due to missing atoms in the surface and the irregular shaped bright spots are due to a foreign atom on the surface. (a) tip was +1.5 V with respect to the sample. (b), tip was at -1.5 V. The images look different because the tip was probing the highest occupied bands of the surface in (a) and the lowest unoccupied bands in (b).

appear higher than the atomic cores are.

Being sensitive to the electronic bands means that it is possible to do spectroscopies of the surface and get an idea of the electronic characteristics of the atoms. It is not perfect but it can easily tell the difference between semiconductors and metals and can even tell the difference between different thicknesses of Pb on Si.[18] Taking scans at different energies can also provide a lot of information about the electronic structure of the surface and can help the researcher determine what is merely an electronic affect and what is the actual atomic structure of the surface. That is the entire overview on how the STM works. As opposed to the SPA-LEED description, little effort was put into how to interpret the data because the images are of real space.

The Omicron STM used to acquire the data in this dissertation uses an XYZ stage with each direction being controlled by a separate piezo and a method of mechanical movement for larger displacements. The mechanical movement is directly controlled by the user and is great for approaching the tip from its resting location up close to the sample and for moving large distances across the surface of the sample. The electronics control the piezo movement for the final approach to the sample as well as during scanning. The STM is aware of its relative location in the x-y plane based on the voltages being applied to the piezoes.

There are two main modes to taking normal data in STM. The first is constant current

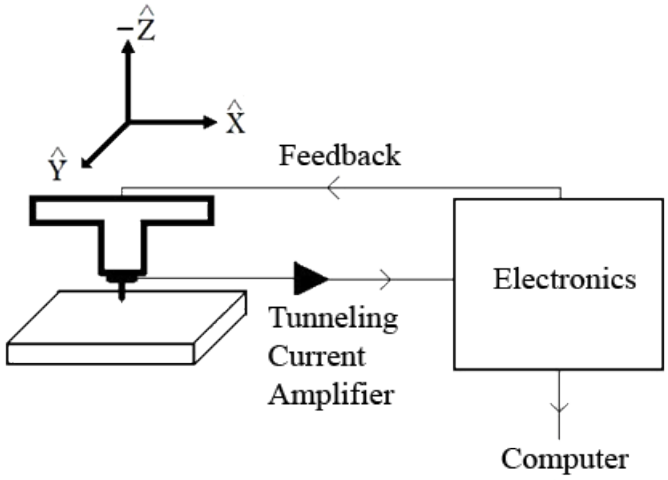

Figure 2.9 Schematic diagram of how STM works. Note that the computer is only an observer for most of the functions of STM.

mode where the voltage applied to the vertical piezo is constantly changed to keep the current the same. A typical scanning speed ranges from on the order of 100 nm/s up to 1000's of nm/s so the piezoes must react quickly to avoid allowing the tip collide with the surface . Not only is there no tunneling current when the tip is in contact with the sample, there is also almost certainly going to be damage to the tip and the sample in that area will be ruined. To allow for this quick movement the circuitry controlling the tip is just a feedback loop all done in the STM hardware. The computer collecting the data can, upon user request, change the strength of the feedback but it is not involved in the feedback in any other way. In constant current mode the STM images are created entirely based on the voltages being applied to the piezoes to move the tip.

The second STM mode is constant height. Just as the name suggests, in this mode the tip is kept at a constant height with respect to the chamber and its distance from the sample is calculated by the change in the current. Operating in this mode makes it possible for the tip to crash into or get out of range of the sample if its height varies by more than the distance between the tip and the sample, on the order of Å, unexpectedly. In this case the images are created based on the amount of current. All images shown in this dissertation were taken in constant current mode.

The general layout of the circuitry can be seen in Figure 2.9. There is a current amplifier

between the tip and the electronics. This is because even at the Ådistances that the tip operates at the tunneling current is in the pA to nA range so in order for the electronics to interpret it the current is first amplified.

2.4 Summary

The STM's ability to see individual atoms and their exact arrangement in real space makes it very user friendly. This compliments SPA-LEED in that it can directly measure island heights as well as island shapes and it is possible to get the relative height distribution without prior knowledge of the coverage. The tradeoff is that it takes on the order of hours to view the number of islands that the SPA-LEED can detect in just a few minutes.

References

[1] Omicron, *SPALEED Optics User's Guide*, Omicron NanoTechnology, version 2.1 ed. (2007). (document), 2.1, 2.2.1, 2.5, 2.2.2, 2.2.2

[2] M. H. von Hoegen, Zeitschrift fr Kristallographie **214**, 591 (1999). 2.2.1, 2.2.1, 2.2.1, 2.2.3

[3] K. Oura, *Surf. Sci.: an introduction*, Advanced texts in physics (Springer, 2003), ISBN 9783540005452, URL http://books.google.com/books?id=HBFtQgAACAAJ. (document), 2.2.1, 2.2.1, 2.2.1, 2.2.1, 2.7

[4] C. Kittel, *Introduction to solid state physics* (Wiley, 2005), ISBN 9780471415268, URL http://books.google.com/books?id=kym4QgAACAAJ. (document), 2.2.1, 2.2.1, 2.2.1, 2.3, 2.2.1, 2.2.1

[5] J. M. Cowley, *Diffraction Physics* (North-Holland Pub Co, 1981). 2.2.1

[6] R. Altsinger, H. Busch, M. Horn, and M. Henzler, Surf. Sci. **200**, 235 (1988), ISSN 0039-6028, URL http://www.sciencedirect.com/science/article/pii/0039602888905249. 2.2.1, 2.2.1, 2.2.1, 2.2.1

[7] G. E. Laramore and C. B. Duke, Phys. Rev. B **2**, 4783 (1970). 2.2.1

[8] J. Wollschlger and A. Meier, Applied Surf. Sci. **104-105**, 392 (1996), ISSN 0169-4332, proceedings of the Fifth International Conference on the Formation of Semiconductor Interfaces, URL http://www.sciencedirect.com/science/article/pii/S0169433296001778. 2.2.1, 2.2.1

[9] M. Horn and M. Henzler, Journal of Crystal Growth **81**, 428 (1987), ISSN 0022-0248, URL http://www.sciencedirect.com/science/article/pii/0022024887904283. 2.2.1, 2.2.1, 2.2.2

[10] T.-M. Lu and M. Lagally, Surf. Sci. **99**, 695 (1980), ISSN 0039-6028, URL http://www.sciencedirect.com/science/article/pii/0039602880905634. 2.2.2

[11] P. Zahl, *Third generation spa-leed* (2008), viewed on May 24, 2011, URL http://www.ifp.uni-bremen.de/index.php?page=spa_leed-workshop. (document), 2.6

[12] M. Henzler, Applications of Surf. Sci. **11-12**, 450 (1982), ISSN 0378-5963, URL http://www.sciencedirect.com/science/article/pii/0378596382900927. (document), 2.2.2, 2.7, 2.2.2

[13] M. Henzler, Applied Physics A: Materials Science & Processing **34**, 205 (1984), ISSN 0947-8396, 10.1007/BF00616574, URL http://dx.doi.org/10.1007/BF00616574. 2.2.2

[14] H. Busch and M. Henzler, Surf. Sci. **167**, 534 (1986), ISSN 0039-6028, URL http://www.sciencedirect.com/science/article/pii/0039602886907223. 2.2.2

[15] P. Zahl and M. H. von Hoegen, Review of Scientific Instruments **73**, 2958 (2002), URL http://link.aip.org/link/?RSI/73/2958/1. 2.2.3

[16] C. Klein, T. Nabbefeld, H. Hattab, D. Meyer, G. Jnawali, M. Kammler, F.-J. M. zu Heringdorf, A. Golla-Franz, B. H. Mller, T. Schmidt, et al., Review of Scientific Instruments **82**, 035111 (pages 7) (2011), URL http://link.aip.org/link/?RSI/82/035111/1. 2.2.3

[17] E. Meyer, H. Hug, and R. Bennewitz, *Scanning probe microscopy: the lab on a tip*, Advanced texts in physics (Springer, 2004), ISBN 9783540431800, URL http://books.google.com/books?id=v2oy14gjzwUC. 2.3

[18] M. Hupalo and M. C. Tringides, Phys. Rev. B **65**, 115406 (2002). 2.3

CHAPTER 3. High Resolution LEED Spot Profile Analysis

The LEED section of the last chapter focused on diffraction patterns from perfectly flat surfaces but the SPA-LEED section allowed a discussion on how different heights affect the diffraction pattern. The ability to analyze features in reciprocal space that are as small as 0.3% BZ opens up a lot of possibilities, including analyzing the profile of spots, particularly the specular. Analyzing the profiles over a range of energies allows us to discern things like step edge size and direction, as well as island sizes and distributions. In this dissertation, the focus will be on finding out as much about island dimensions on a surface as possible, which includes the island distribution, the size distribution, and the heights through the use of G(S) curves. This is the same lattice factor from earlier, but now instead of looking at various diffraction wavevectors at the same energy, it is looking at the same spot, in this case the specular, over different energies, or phase, S. That is, the x-axis of the curve has the value $S = K/(2\pi/d)$ and the y-axis is a measure of how in- or out-of-phase the specular is.[1] d is the height of one atomic layer. K is the momentum transfer of the electrons that are diffracting off of the surface. The graph itself is simple and only explicitly shows the height of the islands, but it is important to know the theory behind it to understand it and how to derive the other information.

3.1 $G(S)$ Introduction

When LEED patterns were introduced in the last chapter, the direction perpendicular to the surface was generally ignored because the surface was assumed to be flat. This leads to the creation of lattice rods originating at every reciprocal lattice point in the plane of the sample. Those rods are mostly uniform for a flat surface because the electrons only have a penetration depth of 5 Å, or 2 to 3 layers, not enough depth to create a strong periodicity in the lattice

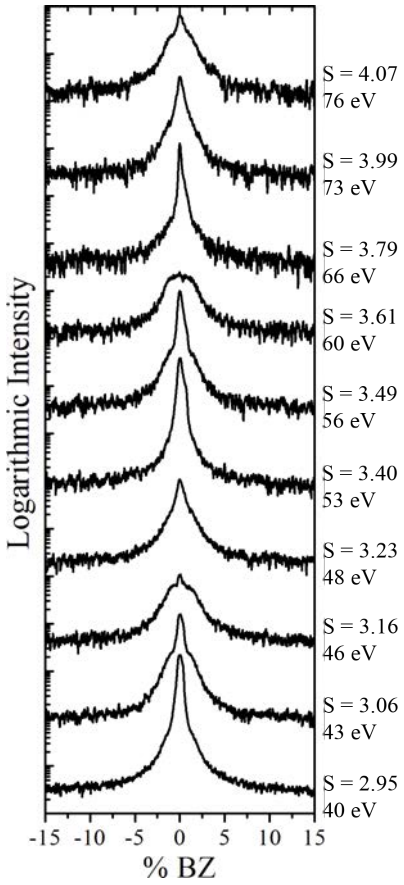

Figure 3.1 Progression of 1D scans of the specular of 3.0 ML of Pb on In v31 on Si(111) 7 x 7 at 170 K that differ by energy as marked. The flux rate was 0.1 ML/min. The peak intensity oscillates between high and low as the wavelength of the electron beam interacts with the heights on the surface. The scans are composed of 2001 points, but in this graph, each point's value has been averaged with its four nearest neighbors to reduce noise.

rods.[2] However, when the surface is not flat the lattice rods can start to show strong variation. Some examples of this were shown in Figure 2.5. The reason this occurs is that as soon as the crystal is not flat there is now a strong periodicity in the z direction, invalidating the assumption that the next unit cell in that direction is infinitely far away. The physical reason is that now electrons have two or more layers to diffract from, and like thin film reflection in introductory physics, this means that there are electron wavelengths, and therefore energies, that interfere constructively and some that interfere destructively. Therefore, at some energies the specular of the pattern will be very intense and sharp, while at other energies it will be

weak and broad, as seen in Figure 3.1. The period of the oscillation between the two extremes, with respect to energy, is an indication of the difference in height between the layers on the surface.

Therefore, to investigate this phenomenon it is necessary to take scans of the specular at many different electron energies (wavelengths). It is best to do this in a consistent fashion to make sure that all relevant features are recorded. The scans in this dissertation were taken at intervals of 1 eV with a width of 40 % BZ centered at the specular. These values were chosen because 1 eV provides a nice balance between energy resolution and time spent taking the data, and 40% BZ scans provide enough of the background to get a good estimate of its value no matter how wide the specular is. Taking a smaller scan, over 10% BZ instead of 40, for instance, will not provide better resolution because each data point is already over 10 times smaller than the instrument resolution, diminishing the usefulness of additional data points. As was mentioned in the introduction to SPA-LEED last chapter, the instrument resolution is around 0.3% BZ. The pixel resolution of a 40% BZ scan with 2001 points is about 0.02% BZ.

There are three main reasons that it is necessary to take a lot of scans, when a few quick scans at a few different energies are enough find a maximum and minimum of the specular's intensity. First, going through more than half of a period will provide better read on the value of the period. Second, a lot more information than just the height can be gained from doing proper fits, and more scans provide more accuracy when determining the fitting parameters. Lastly, fitting only a small number of curves can lead to complications from changing scattering factors or a surface with more than 2 layers. Scans should be taken in a range at least 30 eV in size to ensure any relevant heights are discovered, as will be explained later.

Some of the extra information that can be gained by fitting the scans is seen in Figure 2.7 (c), and again in Figure 3.2. The scan can be divided up into two main components: a narrow component, representing the long range order of the sample, and a broad component giving information about the islands (or steps) on the surface. At an in-phase condition, the electrons diffract off all heights of the surface in such a way that they are interfering constructively with each other, producing the normal strong, sharp specular. The other extreme is the out-of-phase condition, where the electrons diffracting off the different heights of the sample interact

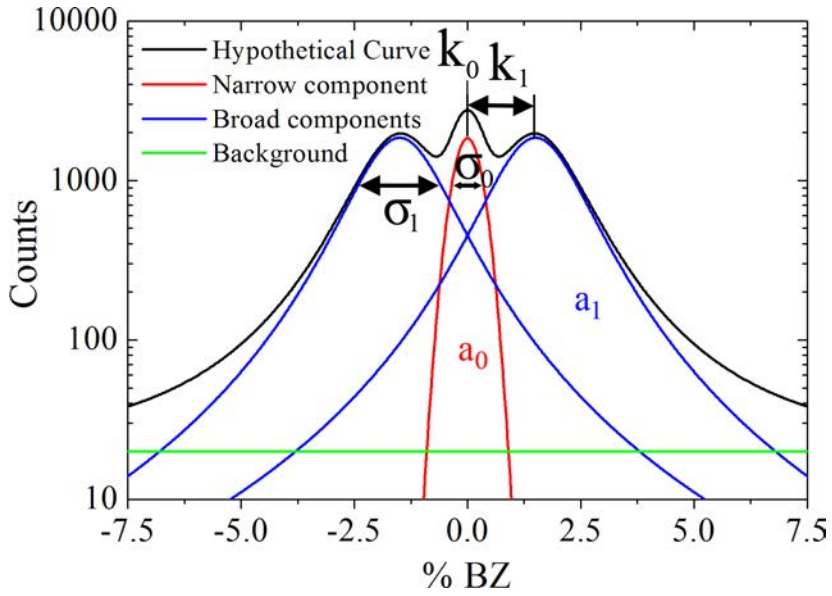

Figure 3.2 Idealized nearly out-of-phase condition showing the narrow and broad components, all are Lorentzian 3/2's, as well as the important variables: k_1 is the distance between the maxima of the narrow and broad components and represents the distance between the islands. σ_0 represents the FWHM of the narrow component, which is representative of the instrument's widening effect. σ_1 is the FWHM of one of the broad components and represents the average size and separation of the islands.

destructively, all but eliminating the sharp central peak of the specular, leaving the broad ring component. If the broad component is not a ring, but instead just an even number of spots, i.e. spot splitting, then that is an indication of steps on the surface. Steps only split the specular in certain directions because there tends to only be one or two sets of parallel steps on the surface, since they must follow the crystal structure, although this depends a great deal upon how the crystal is cut. Islands, on the other hand, can be separated by any angle, so they produce a ring around the specular instead of just splitting it. At any one location the height of the curve can be described by the summation of the two components (see Figure 3.2):[3]

$$I_T = I_N + I_B \tag{3.1}$$

The narrow component is generally considered to be a Gaussian, and is an indication of the long range order of the surface and the instrumental broadening.[4] The broad ring component represents the contribution from the islands. The mean value of the ring's peak represents the

average island separation, while the Full Width Half Maximum (FWHM) is related to the island size distribution. This could theoretically have any profile shape, but it is common for it to be a Lorentzian 3/2's shape which indicates a geometric distribution for the island separation.[2] The curve can be calculated for any specific island/terrace distribution via methods described in Pimbley and Lu[5] or in the other direction via Busch and Henzler[6].

The $G(S)$ curve is defined as the normalized central spike intensity.[2] Therefore, we not only need the intensity of the narrow component of the curve, but it must also be normalized. As discussed, this can be done by dividing by the intensity of another spot, in this case the entire intensity of the specular:[1]

$$G = \frac{I_N}{I_N + I_B} \tag{3.2}$$

I_N is the total intensity of the narrow component, and I_B is the total intensity of the broad component. Taking the ratio in this way eliminates instrumental broadening and changes of the total intensity due to the energy dependence of the scattering factor.[7] This also serves to normalize $G(S)$ to 1. A more mathematically intense definition of $G(S)$ will be given later once a few more terms have been defined. The value of $G(S)$ will oscillate between 1 and 0, but neither is generally reached in practice because the surface would have to be perfectly flat with exactly half of it one height and the other half another height. Despite the fact that the word "intensity" has already been used, it should be stressed that the total 2-D intensity of the spots must be used, not the areas or amplitudes of the 1D curves used to gather the data. To get the total intensity, the fitting function must be integrated around the center, which is most easily done in cylindrical coordinates.

$$I = \int_0^{2\pi} \int_0^{\infty} f\left(r, w, A, k\right)\ r\ dr\ d\theta = 2\pi \int_0^{\infty} f\left(r, w, A, k\right)\ r\ dr \tag{3.3}$$

f is the functional form used for the fitting, and w, A, and k are the fit parameters, in the case of a Lorentzian they would be area, width, and position of the center of the peak. Since it is assumed that the curve does not depend upon θ, integrating it from 0 to 2π is trivial, while integrating r from 0 to infinity requires the specific form of the function. For Lorentzian 3/2's

functions the total intensity is:

$$I = 2\pi \int_0^\infty \frac{A}{2w\left(1 + \left(\frac{r-k}{w}\right)^2\right)^{\frac{3}{2}}} \; r \; dr \tag{3.4}$$

For the narrow component, k can be ignored. For the broad component, a second curve must be integrated with $r + k$ instead of $r - k$.

3.2 Qualitative Description

There are two ways to visualize how this information is conveyed in the broad component, but neither is as clear cut as in the previous example. The first is to remember that the diffraction pattern is just a Fourier Transform of the surface, so distances from the specular indicate the frequency/period with which a structure repeats itself, which explains the spot location. As island size increases, more frequencies are needed to describe them properly, and they therefore produce a wider spot in reciprocal space, similar to the components of a square wave as opposed to a sinusoidal wave.

The second way to visualize scattering off of the islands is based on commentary from Henzler[8] about diffraction from an array of steps. In creating a model to describe the diffraction pattern of a surface with a regular array of steps, with each step having N+1 atoms on it, Henzler used an equation whose first term was exactly the intensity distribution from a grating with N+1 slits, with the second term being delta functions marking where the actual spots will be. The second function is based only on the step height and step width. From this, it can be concluded that if steps produce a pattern similar to grating spots, then it is a reasonable analogy to say that islands create a pattern similar to that of light passing through a large number of irregularly spaced holes in a piece of paper. The $G(S)$ curve holds other information as well. The width of the in-phase peaks is an indication of how rough the surface is, and sharper peaks indicate a larger number of exposed layers.[9] This follows intuitively from other diffraction results, such as in optical diffraction, where more gratings produce sharper spots.

3.3 Results from $G(S)$ Curves

As mentioned above, the three main pieces of information relevant to this dissertation that can be derived from $G(S)$ curves are the step height, island size, and island separation.[3] The step height is the most easily understood surface property because it harkens back to thin film reflection from introductory physics. If we take a step back from the $G(S)$ construction and look only at how the intensity of the specular changes with energy, the step height can still be calculated. The specular will be most intense, at an in-phase condition, therefore twice the distance between the upper and lower parts of the surface is equal to an integer multiple of the electron's wavelength (see Figure 3.3).[2]

$$\frac{2d}{\cos\theta} = n\lambda \tag{3.5}$$

For SPA-LEED the beam should be essentially perpendicular to the sample when scanning the specular, so let $\theta = 0$. The specular will be least intense if S equals a half integer multiple of the electron's wavelength. With two consecutive in-phase conditions mapped, the math to derive the step height is straightforward.

$$\mathrm{n}\ \lambda_1 = 2\mathrm{d} \tag{3.6}$$

$$(\mathrm{n}+1)\ \lambda_2 = \ 2\mathrm{d} \tag{3.7}$$

Where n is the number of wavelengths and λ_1 and λ_2 are the wavelengths associated with the first and second in phase conditions. Using $\lambda = h/(v(2m_eE))$ and solving for d results in:

$$d = \frac{h}{2\sqrt{2m_e}\ \ (\sqrt{E_2} - \sqrt{E_1})} \tag{3.8}$$

E_1 and E_2 are the energies of the electrons at the two consecutive in-phase conditions, h is the Planck Constant, and m_e is the mass of an electron.

That said, the step height can be determined more quickly from the $G(S)$ graph itself. The in-phase conditions are easy to spot on the $G(S)$ curve, since that is what the y-axis essentially already is. Looking back at equation 3.5, it makes sense to make the x-axis $2d/\lambda$, which is known as the phase, S. If the step height is just d, there will be an in phase condition at every integer value of

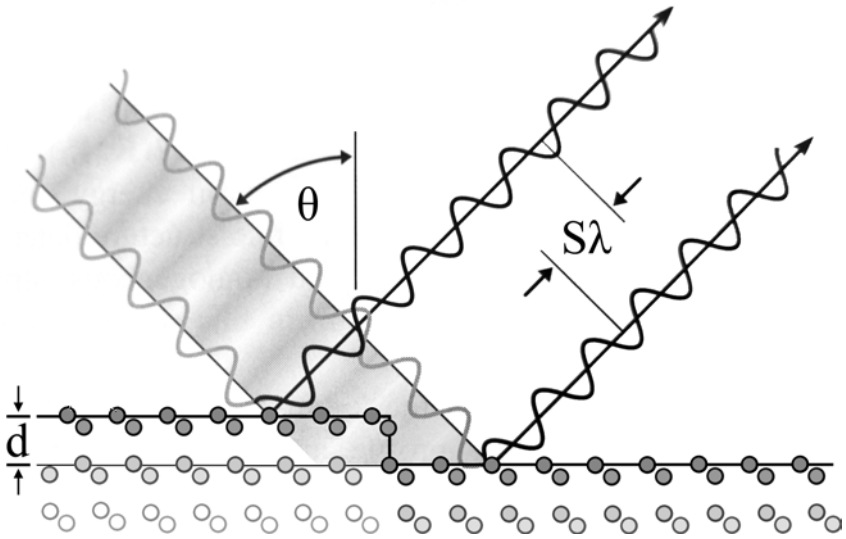

Figure 3.3 Diagram of a step on a surface illustrating how different heights effects the relative phase of electrons diffracted off of both heights. If $S\lambda$ is an integer then the two waves are in phase. Diagram after von Hoegen[2].

The above calculation and result is normally performed in terms of the momentum of the incoming and outgoing electron waves. The lattice factor, G, can be split up into parallel and perpendicular components, starting from equation 2.17:[2]

$$G\left(\overrightarrow{K}\right) = \left|\sum_n e^{ia\overrightarrow{K_\parallel}\cdot\overrightarrow{r(n)}}\ e^{id\overrightarrow{K_\perp}\cdot\overrightarrow{h(n)}}\right|^2 \tag{3.9}$$

a is the atom separation in plane, and d is once again the distance between layers. $h(n)$ is the height at atom n in terms of the step height d. The phase of the perpendicular component is:

$$S = \frac{K_\perp}{\frac{2\pi}{d}} = \frac{dK_\perp}{2\pi} \tag{3.10}$$

This is the value quoted on the first page of this chapter and will be used in the graphs, as it is a less specific case and more applicable to SPA-LEED than the previous derivation. Remember that $K = k_i - k_f$, momentum transfer, so a simple substitution for K is impossible and will not lead to the previous result.

Before addressing the other information that can be gained from the $G(S)$ curve, the more precise definition should be provided. Again, based on equation 2.17:

$$G\left(\overrightarrow{K}\right) = \left|\sum_n e^{ia\overrightarrow{K_\parallel}\cdot\overrightarrow{r(n)}}\ e^{id\overrightarrow{K_\perp}\cdot\overrightarrow{h(n)}}\right|^2 \tag{3.11}$$

Rewriting in terms of S and letting $K_{\parallel} = 0$, since we are interested in the specular only:

$$G(S) = \left| \sum_{n} e^{i2\pi S h(n)} \right|^2 \tag{3.12}$$

Change the sum from over all atoms to over the different heights as well as drop the phase information since it is not measured. p_h is the area of the surface that is of height h.

$$G(S) = \left| \sum_{h} p_h \cos 2\pi S h(n) \right|^2 \tag{3.13}$$

$$G(S) = \sum_{l} \sum_{h} p_{h+l} p_l \cos 2\pi S h(n) \tag{3.14}$$

$$G(S) = \sum_{h} C_h \cos 2\pi S h(n) \tag{3.15}$$

Therefore $G(S)$ is made up of cosine curves with frequencies of h. This strongly suggests Fourier Transform, so C_h, the amplitude of the cosines, can be rewritten as:

$$C_h = \sum_{l} p_l p_{h+l} = \frac{1}{2\pi} \int_{-\pi}^{\pi} G(S) \ cos(2\pi S h) \ dS \tag{3.16}$$

This can be used to find the different heights on the surface, even if the curve is too complicated to decipher by just looking at it. However, it does not quite provide the portion of the surface that the various heights occupy. C_h represents the normalized intensity amplitude of the various curves and not the areas causing the curves. Before moving on, it should be noted that having $G(S)$ be composed of a Fourier Transform of the surface heights is a very satisfying result. Each difference in height has its own frequency, and the surface can have multiple layers. The contribution from all of these simply adds together. To make this a true Fourier Transform that can be undone without changing anything, a factor of $1/(2\pi)$ must be added to the beginning of equation 3.15. For a two level system, h and $h+d$, there is a relatively simple way to determine the amount of the surface that is covered by the two layers. If the coverage is known, then the solution is simple:

$$p_{h+l} = \frac{\theta}{l} \tag{3.17}$$

θ is now once again its normal surface science definition of coverage in ML, h is the height of the reference layer, and l is the difference between the two layers in terms of the layer height d. However, if the coverage is not known, it will depend upon the strength of the oscillations

of the $G(S)$ curve, with the deepest oscillation occurring when half of the surface is covered. Remembering that the intensity of a spot scales with the area squared, all that has to be done is to compare the relative areas of the surface to the value of $G(S)$ at the out-of-phase condition:

$$G(S) = \frac{I_N}{I_N + I_B} \approx G = (p_h - p_{h+l})^2 = \left(\left(1 - \frac{\theta}{l}\right) - \frac{\theta}{l}\right)^2 = \left(1 - \frac{2\theta}{l}\right)^2 \tag{3.18}$$

This produces the same values for the minima of the $G(S)$ curve as the derivation of the entire curve done by Lent and Cohen [10].

$$G(S) = 1 - 2p_h(1 - p_h)(1 - cos(2\pi S)) \tag{3.19}$$

Unfortunately, since the phase information of the electron waves is lost, without at least an estimate of the coverage or surface structure it is impossible to tell which area is the lower height and which is the upper. However, that can be resolved by depositing more material, either through additional depositions or by restarting and depositing more to start with. The layer formed by the deposited material should expand, increasing or reducing the out-of-phase intensity depending upon whether or not it was the dominant scattered electron source to start with.

This logic can be expanded to three or even more, but the complexity increases rapidly. Simply picking out different layers can be difficult because in- and out-of-phase conditions can overlap. The only thing that can be done is to attempt to fit curves to the $G(S)$ function to try to determine what it contains. However, that will not reveal much without a known coverage, because there are generally many sets of p_h that describe the curve.

$$\theta = \sum_h h p_h \tag{3.20}$$

This reduces the number of possible sets of p_h but does not necessarily reduce it to one. The other two main surface properties, the island size and island separation, are derived from the location and size of the broad ring. Therefore, it is only seen at out-of-phase conditions, as in Figure 3.2. As mentioned earlier, the broad ring component of the curve can be transformed into a real space distribution of the islands and island sizes, but the calculations are not at all simple, so an approximation is commonly used. As is the case for all spots, the location of the

broad ring indicates the relevant distance for the feature. For your convenience, equation 2.22 with an addition to be discussed below:

$$\frac{\Delta k}{k_{10}} = \frac{a_0 \eta}{d} \tag{3.21}$$

Δk is the distance the spot of interest is from the specular, a_0 is the real space distance represented by k_{10} in reciprocal space, and d is the real space distance of the feature associated with Δk. The location of the out-of-phase ring indicates the average distance between the islands on the surface, and the width of it indicates the island sizes.[3,11] η in equation 3.20 is almost always assumed to be 1 but was inserted for completeness. It was reported by Bardotti et al.[12] that the actual average distance between islands is approximately 1.6-1.8 times smaller than what the location of the broad ring indicates. This conclusion was reached by comparing simulated diffraction patterns, high resolution LEED patterns, and STM data on the Ag on Ag(100) system. They consistently got values of around 1.6 for η when comparing the average island separation between the various methods. The value for η varies by model and is not known for all situations. η was referred to as λ in Bardotti et al.[12] but was switched for this dissertation to reduce confusion.

It should also be noted that the FWHM of the peak does not necessarily give the exact average size of the islands, because there are many different possible island size and separation distance combinations that lead to the same FWHM. This is because both factors can affect the width of the peak. For example, a larger variation in island separation will broaden the peak without the size of the islands changing. Therefore, there is an additional proportionality factor of 1-2 that must be included for an exact calculation of the average island size.[13,14] However, in conjunction with STM, simply being close is good enough to confirm results, so the approximation is perfectly acceptable.

3.4 Limitations

There are a number of limitations of $G(S)$ curve analysis, all of which are related to the fact that the phase information is lost from the electrons. The $G(S)$ curve represents the relative heights that appear on the surface, so if the only in-phase conditions are at integer values of S,

that does not necessarily mean that half the surface is not covered while the other half has one layer on it. It is also impossible to determine whether the more prevalent height on the surface represents the higher of lower layer unless the absolute coverage is also known, since the phase of the electrons is not known[2] unless other steps are taken (as discussed above). Additional complications arise if there is a third layer of noticeable size. If the two heights are 3 and 4 layers above the base layer, then the $G(S)$ curve would be expected to have three periods interacting in it, representing 4, 3, and 1 maximum per integer change of S. To make matters worse, it would be very hard to tell whether these layers were at heights 0, 3, and 4 or 0, 1, and 4. Even if the total coverage is known, there is no guarantee that there would be only a single surface arrangement that produces the $G(S)$ curve being analyzed.

Different scattering factors between the substrate and the islands on top of it could shift the location off the most out-of-phase condition with respect to coverage. For example, if the islands reflected twice as much as the substrate, then the perfect out-of-phase condition would occur at a lower island coverage than if the scattering factors were the same, which would produce an out-of-phase condition at exactly half of the surface covered.[15] In this scenario, since the intensity scales as the area squared the optimal coverage in the situation just mentioned is roughly 40% of the surface being covered by the islands. However, the distance between adjacent in-phase conditions stays the same. Scattering factors can also can also affect scans in the same $G(S)$ curve. The total intensity of the specular can change as the energy is changed and this can weaken transitions to and from the in-phase condition. While the ring does still shrink near in-phase conditions, if the amplitude of the in-phase condition is greatly reduced by the scattering factor, then it does not take much broad component to affect the resulting $G(S)$ curve. It is even possible that the scattering factor could make the peaks in the $G(S)$ curve lopsided, if a noticeable change in scattering factor occurs within a single period of oscillation.

3.5 Conclusion

The $G(S)$ curve is a very powerful surface science tool. It provides the height, island size, and island distribution on the surface. Because SPA-LEED probes such a large area the data from the $G(S)$ curve is very statistically significant. The downside, of course, is that unless the

surface is relatively well behaved or relatively predictable, the $G(S)$ could provide results that are just too hard to interpret in a meaningful and reliable way. In other words, for surfaces with multiple values of d or even just multiple exposed layers, it can be impossible to find an exact solution to the surface arrangement.

References

[1] M. Horn, U. Gotter, and M. Henzler, Journal of Vacuum Science & Technology B: Microelectronics and Nanometer Structures **6**, 727 (1988), URL http://link.aip.org/link/?JVB/6/727/1. 3, 3.1

[2] M. H. von Hoegen, Zeitschrift fr Kristallographie **214**, 591 (1999). (document), 3.1, 3.1, 3.3, 3.3, 3.3, 3.4

[3] M. Henzler, Applied Physics A: Materials Science & Processing **34**, 205 (1984), ISSN 0947-8396, 10.1007/BF00616574, URL http://dx.doi.org/10.1007/BF00616574. 3.1, 3.3, 3.3

[4] P. Klimesch, G. Meyer, and M. Henzler, Surface Science **137**, 79 (1984), ISSN 0039-6028. 3.1

[5] J. M. Pimbley and T.-M. Lu, Journal of Applied Physics **55**, 182 (1984), URL http://link.aip.org/link/?JAP/55/182/1. 3.1

[6] H. Busch and M. Henzler, Surf. Sci. **167**, 534 (1986), ISSN 0039-6028, URL http://www.sciencedirect.com/science/article/pii/0039602886907223. 3.1

[7] R. Altsinger, H. Busch, M. Horn, and M. Henzler, Surf. Sci. **200**, 235 (1988), ISSN 0039-6028, URL http://www.sciencedirect.com/science/article/pii/0039602888905249. 3.1

[8] M. Henzler, Surf. Sci. **19**, 159 (1970), ISSN 0039-6028, URL http://www.sciencedirect.com/science/article/pii/0039602870901159. 3.2

[9] J. Wollschlger, E. Z. Luo, and M. Henzler, Phys. Rev. B **44**, 13031 (1991). 3.2

[10] C. Lent and P. Cohen, Surf. Sci. **139**, 121 (1984), ISSN 0039-6028, URL http://www.sciencedirect.com/science/article/pii/003960288490013X. 3.3

[11] M. Horn and M. Henzler, Journal of Crystal Growth **81**, 428 (1987), ISSN 0022-0248, URL http://www.sciencedirect.com/science/article/pii/0022024887904283. 3.3

[12] L. Bardotti, C. R. Stoldt, C. J. Jenks, M. C. Bartelt, J. W. Evans, and P. A. Thiel, Phys. Rev. B **57**, 12544 (1998). 3.3

[13] M. Henzler, Surf. Sci. **132**, 82 (1983), ISSN 0039-6028, URL http://www.sciencedirect.com/science/article/pii/0039602883905332. 3.3

[14] T.-M. Lu and M. Lagally, Surf. Sci. **99**, 695 (1980), ISSN 0039-6028, URL http://www.sciencedirect.com/science/article/pii/0039602880905634. 3.3

[15] J. Wollschlger and A. Meier, Applied Surf. Sci. **104-105**, 392 (1996), ISSN 0169-4332, proceedings of the Fifth International Conference on the Formation of Semiconductor Interfaces, URL http://www.sciencedirect.com/science/article/pii/S0169433296001778. 3.4

CHAPTER 4. Height Dependent Nucleation and Ideal Layer by Layer Growth in Pb/Pb(111)

S. M. Binz, M. Hupalo, and M. C. Tringides

A paper published in *Physical Review B*, **78**, 193407 (2008)

4.1 Abstract

It has been puzzling why for Pb/Si(111), oscillations have been observed at temperatures as low as 18 K and were found to improve with decreasing temperature. With scanning tunneling microscope we have directly observed this ideal layer by layer growth. A dramatic dependence of the second layer island morphology on island height, expected from quantum size effects (QSE), is also found. Low density of fractal islands on stable vs high density on unstable Pb islands on a mixed height island confirms the role of QSE in kinetics. The low diffusion barrier and the fractal island morphology can explain the unusual layer by layer growth.

4.2 Introduction

Epitaxial growth has been of interest over the last three decades because novel types of nanostructures can be fabricated in controlled ways. Depending on the system, either layer by layer growth (i.e., a layer is completed before the next one nucleates on top) or three-dimensional growth is observed (when many layers are occupied simultaneously). Layer by layer growth is commonly observed at sufficiently high temperatures so diffusion of the deposited atoms is fast, and hopping from higher to lower layer occurs prior to the onset of nucleation.

A widely used experimental method to monitor in situ the quality of a grown film is diffraction intensity oscillations.[1–5] Strong sustained oscillations are evidence that the film is growing

smoothly, while monotonically decaying oscillations are evidence of three-dimensional growth. However, it was puzzling when sustained oscillations were observed well below room temperature because they imply a very low diffusion barrier, unless some nonthermal diffusion mechanism is operating; one possibility is transient mobility[6] related to the condensation energy that should be dissipated (i.e., to phonons or to electron-hole pairs, etc.) before an atom is eventually adsorbed on the surface. A different mechanism predominantly relevant for metal surfaces is downward "funneling."[7] If a cluster with the minimum number of atoms needed to form a stable binding site has not nucleated, the atom can "funnel" to the lower level.

Low-temperature oscillations have been seen during the growth of Pb/Si(111).[1,2] It became especially puzzling because the oscillation amplitude was larger as the temperature was reduced with the highest quality oscillations observed at the lowest temperature (18 K). Since neither of the two non-thermal mechanisms predicts this inverse dependence on temperature, these intriguing results have not been explained yet.

In addition, Pb growth has been of interest in quantum size effect (QSE)-driven growth observed with numerous techniques[8–13] and has resulted in an unusual degree of self-organization. Sharp uniform height island distributions have been observed [i.e., odd heights when measured from the wetting layer on the Si(111)-7x7]. Height selection can be explained from the variation of the confined electron energy with height, since for stable height islands the highest occupied band (HOB) is further away from the Fermi level than for unstable islands.[9] It is expected that this variation can also affect island reactivity by modifying the barriers of the atomistic processes controlling reactivity (adsorption, diffusion, nucleation, and bonding). It has been an active question to find how these barriers are modified with island height for stable and unstable heights.[14–18]

4.3 Experimental Details

In this Brief Report scanning tunneling microscope (STM) experiments were performed on the growth of Pb/Pb(111) at 40 K [with the initial substrate Pb islands grown on Si(111)-(7x7)] and almost perfect layer completion (within 95 %) is observed, before the next one starts to nucleate, which is in agreement with the strong low-temperature diffraction oscillations.

This is partially attributed to the very low diffusion barrier of Pb on Pb(111) (less than 80 meV). Furthermore, the second layer nucleation shows dramatically different morphology where growth on a stable height results in low-density fractal-like islands, but growth on an unstable height results in high density of smaller islands. These differences can be attributed to the variation of the electronic structure of the island with height. Remarkably, this difference in morphology is observed on a single mixed island grown over a substrate step; the stable five-layer part of the island has 60 times lower island density than the unstable four-layer part, indicating that the QSE stability condition normal to the surface is completely decoupled from the lateral degrees of freedom of the confined electrons. The low diffusion barrier and the fractal island morphology can account for the improved oscillations as the temperature is lowered.

If Pb islands are grown initially at 240 K, a wider range of heights can form (four, five, six, and seven layers) because at this higher temperature the islands reach large lateral sizes (they exceed 150 nm) which enhances island stability over longer times both for unstable and stable heights.[19,20] The unstable islands will eventually grow into stable islands but over the course of hours. An amount of 1.35 ML of Pb was deposited at 240 K on Si(111)7x7 followed by cooling the sample to 40 K. Small amounts of Pb were deposited at 40 K with flux rate of 0.4 ML/min. A five-layer island was selected to observe how the second layer grows with Pb deposition.

4.4 Results

Experiments were also carried out by depositing Pb directly on the Si(7x7) at 40 K (without first growing large islands at 240 K). Initially, an amorphous layer of Pb is observed which transforms to a crystalline layer at $\sim$4 ML.[1,2] Although it is easier to observe this crystallographic transition with diffraction, it is also seen with STM. A change in the grown morphology from a granular structure with well-separated random features is first observed, but after crystallization flat interconnected regions span the whole image. Only two layers are exposed at the growing front at all coverages, which confirms the layer by layer growth as in the diffraction experiments. However, results on isolated five-layer island grown at 240 K are shown because it is easier to monitor the coverage (from the uncovered regions on the island) and to assess

how ideal the layer by layer growth is.

Figure 4.1 shows the five-layer island evolution with increasing Pb coverage. In Figure 4.1 (a) a full view of the five-layer island is shown over an area of 403 x 162 nm^2. The other images [Figs. 1(b)–1(l)] show successive images after depositing small Pb amounts listed in the figure caption. The scale is 100x100 nm^2, which is outlined in Figure 4.1 (a) [except for Figure 4.1 (d) which has 73.45x73.45 nm^2]. Figure 4.1 (b) shows that on the flat clean surface, a periodic pattern of spatial period (8.3 nm) forms with an amplitude of less than 0.03 nm. Most likely this is an electronic effect that is a result of beating between the two different lattices at the Pb-Si interface. The period corresponds approximately to three times the 7x7 unit cell and is aligned with the $[1\bar{1}0]$ directions. This pattern is observed both on the five-and four-layer islands with the same contrast (the compact "blobs" are dark and the surrounding "sea" is bright), which shows that the island has perfect ABC stacking as dictated by the bulk structure underneath (of the Pb island). Islands grown with different stacking (ABC or ACB) result in reversal of the corrugation contrast after each monolayer increment.[21,22] Depending on the specific metal system the correct stacking is followed [Ag/Ag(111)],[23] but in other systems with stacking faults are also seen [Ir/Ir(111)].[24]

As will be discussed further below, the islands formed on the five-layer island have fractal shapes and lower density than the ones formed on the four-layer island. The island density at 40 K is higher by a factor of ∼60 than the island density on the five-layer island. With further Pb deposition, the fractal islands develop more branches (and the arm width is approximately constant 2.5 nm) until eventually they fill in the layer. It is instructive to focus on the completion of the sixth layer [in Figure 4.1 (g) by adding 0.4 ML to the previous image for a total of 1 ML] and the completion of the seventh layer [in Figure 4.1 (l) by adding 0.2 ML for a total of 2 ML]. In both cases, the growing layer is completed perfectly before islands nucleate in the next layer and all the "cracks" are healed. This is consistent with a large diffusion length. When the separation between cracks becomes comparable to the distance between the first nucleated islands [seen in Figure 4.1 (c)], coexistence between remaining "cracks" and newly nucleated islands is possible. However, the fractal morphology suppresses nucleation close to the "cracks" and induces their filling. The last part of the five-layer island to be completed is the outside

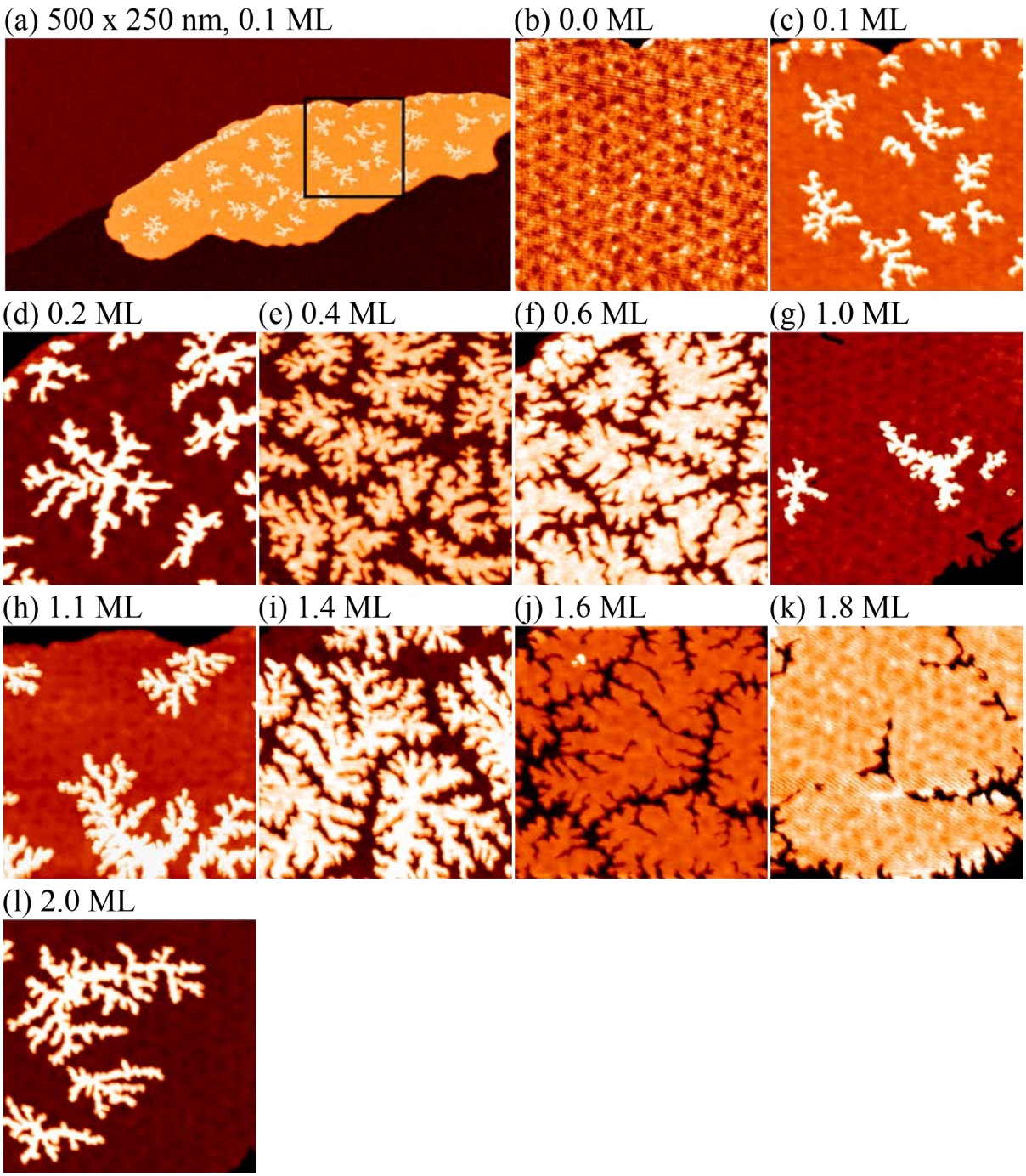

Figure 4.1 Stepwise deposition experiment at 40 K and a flux rate of 0.4 ML/min on top of a large 5-layer island which is pre-grown at 240 K. All images are 100 x 100 nm^2 and are outlined as the black squares in fig.(a) (except (a) which is 500 x 250 nm^2 and (d) which is 73.45 x 73.45 nm^2). Images (b-l) are all close up images of the various outlined parts in (a). The sequence of images shows the perfect layer-by-layer growth. The amount added above the initial growth at 240 K, $\Delta\theta$, is with the image label.

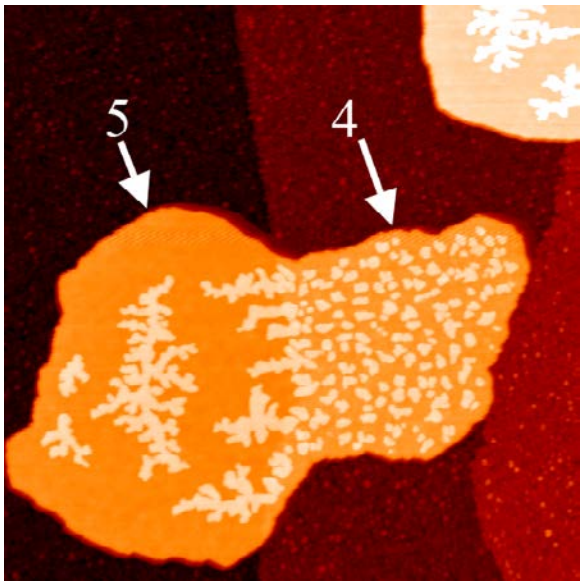

Figure 4.2 200 x 200 nm^2. An island that spans a single-step edge with 0.23 ML of Pb deposited at 0.1 ML/min. The left part of the island is five and the right part is four layers high. The island is flat with a 0.02 nm height difference between the two parts. The four-layer part has higher density of small compact islands while the five-layer part has lower density of bigger fractal islands because of QSE. The coverage is the same in the two parts so the island parts behave as if they are not connected.

edge of the five-layer island (not shown) for some still not understood reason. The layer by layer growth independently confirms that the Pb follows the ABC stacking; otherwise "cracks" would remain since regions of different stacking coming in contact would never heal.

The difference in the grown morphology depending on island stability is seen in a very intriguing way in Figure 4.2. The island shown was also prepared at 240 K, but because it extends over a substrate step the left part is five layers and the right part is four layers. After cooling down to 40 K and depositing 0.23 ML, the second layer nucleation morphology is very different on the two parts; they are acting independently as if they were not connected, i.e., the five-layer part has a few fractal islands while the four-layer part has a larger number of smaller compact islands. Integrating the coverage on the two parts (and correcting the expected larger contribution of tip convolution for the smaller islands) results in the same coverage for the two parts. The nucleation on the two parts suggests the presence of a large reflecting barrier on the island top running along the buried step underneath. Diffusion on top of each part is

restricted, forcing the deposited atoms to remain within each part (although the difference in height between the two parts is only 0.02 nm). Despite this initial difference of the second layer nucleation on the two parts, both layers are completed at the same time. Comparison of island densities and coverage on each part of the mixed island and separate islands of the same height support fully the conclusions that the coverage on each part is the amount fallen on each top and diffusion between the two parts is restricted.

4.5 Discussion

One can draw several conclusions from this experiment. First, there is likely a barrier on the island top related to QSE effects. This is a direct evidence that QSEs affect kinetic barriers and nucleation, and that reactivity changes can be dramatic (although the present system is a homoepitaxial system). The larger variation observed in the current experiment (the factor of ∼60 difference in island density) may also be related to the smaller island heights (four-layer vs five-layer) since QSE differences are larger at lower heights.

How can the dramatic difference in the observed morphology between the two island parts be explained? In Ma et al.[16] and Ma et al.[17] Fe deposition experiments on large Pb islands of heights 12–17 ML at 150 K have shown an island density variation with height of at most a factor of 1.3, which was attributed to the terrace diffusion barrier being lower by $E_4 - E_5 \approx -0.017$ eV on the unstable (E_4) vs stable (E_5) height island and the same critical size cluster $i = 1$ on both heights. (The critical size cluster is the minimum island size above which the island does not decay.) The current experiments suggest that at 40 K the origin of the different morphology is the difference in the critical size cluster and not of the terrace diffusion as in Ma et al.[16] and Ma et al.[17]. Assuming $i = 1$ as in Ma et al.[16] and Ma et al.[17] results in $E_4 - E_5 = 0.04$ eV with the positive difference inconsistent with previous work, i.e., how QSE affect terrace diffusion.[16,17,25] The island density difference in Figure 4.2 implies that the critical size cluster i is larger on the five than on the four-layer island. This should be expected since four-layer islands are unstable. The nucleation of even small monolayer islands on top of the four-layer island lowers their energy, since these new islands add Pb to create a stable height. On the other hand, nucleation on the top of five-layer islands, which are stable, increases their energy

because it adds atoms to create an unstable height, so it requires the aggregation of many more atoms in irregular fractal-like shapes. Edge diffusion must be extremely low at 40 K which can account for the fractal morphology; this is not surprising because it has been seen in other metal systems.[23,24,26]

To obtain a more quantitative estimate of possible values of the critical size cluster and terrace diffusion barriers on the two parts, the scaling theory of nucleation is employed as a first way to estimate the differences. Analyzing the four-layer island density under the simplest assumption that $i = 1$

$$n = \eta \left(\frac{D}{F}\right)^{-\frac{1}{3}} \tag{4.1}$$

and using $D = 1x10^{13} exp(-E_4/kT)$, where $\eta \approx 0.25$ is a numerical prefactor, $n = 0.03$ islands/nm^2 is the measured island density, the flux rate is $F = 1.66x10^{-3}$ ML/s, $T = 40$ K, the Pb(111) density is 9.41 unit cells/nm^2, we get $D = 828$ hops/s for the four-layer barrier $E_4 = 0.08$ eV.

For the 5-layer island we expect $i \gg 1$.[27] Based on the scaling theory of nucleation

$$D = F \left(\frac{\eta}{n}\right)^{\frac{i+2}{i}} e^{\left(\frac{E_i}{(i+2)k_bT}\right)^{\frac{i+2}{i}}} \tag{4.2}$$

with all the symbols defined earlier except the cohesive energy E_i. For fixed F, T, and sufficiently low E_i increasing i increases the diffusion activation energy. Since it is known[16,17,25] that the diffusion barrier for unstable islands E_5 must be lower than the barrier for stable islands E_4, for the measured island densities to have a difference in barriers $E_5 - E_4 > 0.01$ eV requires a minimum value of $i = 10$ and a maximum value of $E_i = 0.1$ eV. Increasing E_i makes the difference $E_5 - E_4$ smaller. This change in critical size cluster from 1 to 10 as a function of height is very dramatic, proving that QSE can be another controlling factor of the observed morphology. The terrace diffusion barriers (0.08 and 0.09 eV) are slightly higher than the barriers for stable height islands calculated by first principles in Chan et al.[25] to fit the nucleation data at higher temperature 180–210 K. At higher temperatures, other processes become important (i.e., transfer between the island top to the wetting layer, hopping from the top to the wetting layer, etc.). These barriers are "frozen" out at 40 K in the current exper-

iments which allows a more direct way to extract the controlling factor, which is the critical size cluster i.

4.6 Conclusions

In summary the ideal layer by layer growth, the low diffusion barriers, and the fractal-like island morphology can account for the enhancement of the diffraction oscillations at these low temperatures that have been puzzling so far. In addition the current experiments present strong evidence that geometry can control the electronic structure, adatom adsorption, nucleation, and possibly reactivity of the grown islands because of QSE. It is also remarkable that the presence of the step below completely separates the two parts of the mixed island so that they behave independently. This shows that the quantization along the normal direction of the confined electrons is separable and not coupled to the lateral degrees of freedom.

4.7 Acknowledgements

Work at Ames Laboratory was supported by the Basic Sciences, U.S. Department of Energy under Contract No. DE-AC02_07CH11358.

References

[1] M. Ja*l*ochowski, M. Hoffmann, and E. Bauer, Phys. Rev. B **51**, 7231 (1995). 4.2, 4.4

[2] A. Petkova, J. Wollschlger, H.-L. Gnter, and M. Henzler, Surf. Sci. **482-485**, 922 (2001), ISSN 0039-6028, URL http://www.sciencedirect.com/science/article/pii/S0039602801008664. 4.2, 4.4

[3] P. B. Howes, K. A. Edwards, D. J. Hughes, J. E. Macdonald, T. Hibma, T. Bootsma, and M. A. James, Surf. Sci. **331-333**, 646 (1995), ISSN 0039-6028, URL http://www.sciencedirect.com/science/article/pii/0039602895003827.

[4] K. A. Edwards, P. B. Howes, J. E. Macdonald, T. Hibma, T. Bootsma, and M. A. James,

Surf. Sci. **424**, 169 (1999), ISSN 0039-6028, URL http://www.sciencedirect.com/science/article/pii/S0039602898008802.

[5] M. C. Tringides, *Morphological Organizations in Epitaxial Growth and Removal* (World Scientific, Singapore, 1998). 4.2

[6] W. F. Egelhoff and I. Jacob, Phys. Rev. Lett. **62**, 921 (1989). 4.2

[7] J. W. Evans, D. E. Sanders, P. A. Thiel, and A. E. DePristo, Phys. Rev. B **41**, 5410 (1990). 4.2

[8] K. Budde, E. Abram, V. Yeh, and M. C. Tringides, Phys. Rev. B **61**, R10602 (2000). 4.2

[9] M. Hupalo and M. C. Tringides, Phys. Rev. B **65**, 115406 (2002). 4.2

[10] W. B. Su, S. H. Chang, W. B. Jian, C. S. Chang, L. J. Chen, and T. T. Tsong, Phys. Rev. Lett. **86**, 5116 (2001).

[11] A. Mans, J. H. Dil, A. R. H. F. Ettema, and H. H. Weitering, Phys. Rev. B **66**, 195410 (2002).

[12] M. H. Upton, C. M. Wei, M. Y. Chou, T. Miller, and T.-C. Chiang, Phys. Rev. Lett. **93**, 026802 (2004).

[13] C. M. Wei and M. Y. Chou, Phys. Rev. B **66**, 233408 (2002). 4.2

[14] L. Aballe, A. Barinov, A. Locatelli, S. Heun, and M. Kiskinova, Phys. Rev. Lett. **93**, 196103 (2004). 4.2

[15] A. G. Danese, F. G. Curti, and R. A. Bartynski, Phys. Rev. B **70**, 165420 (2004).

[16] L.-Y. Ma, L. Tang, Z.-L. Guan, K. He, K. An, X.-C. Ma, J.-F. Jia, Q.-K. Xue, Y. Han, S. Huang, et al., Phys. Rev. Lett. **97**, 266102 (2006), URL http://dx.doi.org/10.1103/PhysRevLett.97.266102. 4.5, 4.5

[17] X. Ma, P. Jiang, Y. Qi, J. Jia, Y. Yang, W. Duan, W.-X. Li, X. Bao, S. B. Zhang, and Q.-K. Xue, Proc. Natl. Acad. Sci. **104**, 9204 (2007), URL http://www.pnas.org/content/104/22/9204.abstract. 4.5, 4.5

[18] N. Binggeli and M. Altarelli, Phys. Rev. Lett. **96**, 036805 (2006). 4.2

[19] M. Hupalo and M. C. Tringides, Phys. Rev. B **75**, 235443 (2007). 4.3

[20] Z. Kuntova, M. Hupalo, Z. Chvoj, and M. C. Tringides, Phys. Rev. B **75**, 205436 (2007). 4.3

[21] W. B. Jian, W. B. Su, C. S. Chang, and T. T. Tsong, Phys. Rev. Lett. **90**, 196603 (2003). 4.4

[22] T. L. Chan, C. Z. Wang, M. Hupalo, M. C. Tringides, W. Lu, and K. Ho, Surf. Sci. **600**, 179 (2006), ISSN 0039-6028, URL http://www.sciencedirect.com/science/article/pii/S0039602806006108. 4.4

[23] E. Cox, M. Li, P.-W. Chung, C. Ghosh, T. S. Rahman, C. J. Jenks, J. W. Evans, and P. A. Thiel, Phys. Rev. B **71**, 115414 (2005). 4.4, 4.5

[24] C. Busse and T. Michely, Surf. Sci. **552**, 281 (2004), ISSN 0039-6028, URL http://dx.doi.org/10.1016/j.susc.2004.01.031. 4.4, 4.5

[25] T. Chan, C. Z. Wang, M. Hupalo, M. C. Tringides, and K. M. Ho, Phys. Rev. Lett. **96**, 226102 (2006). 4.5, 4.5

[26] H. Röder, K. Bromann, H. Brune, and K. Kern, Phys. Rev. Lett. **74**, 3217 (1995). 4.5

[27] J. G. Amar and F. Family, Phys. Rev. Lett. **74**, 2066 (1995). 4.5

CHAPTER 5. Quantum Size Effect Dependent Critical Size Cluster and Finite Size Effects

S. M. Binz, M. Hupalo, and M. C. Tringides

A paper published in *Journal of Applied Physics*, **105**, 094307 (2009)

5.1 Abstract

Pb nucleation on top of a unique Pb island grown on Si(7x7) (in the form of a "hub"-"moat"-ring) confirms that electron confinement causes large variations in critical size cluster i_c with island height. Because of smaller radial dimensions (less than 20 nm), the large variation of the nucleated island density on different layers cannot be a result of differences in terrace diffusion coefficients but i_c. These results have important implications on how adsorption can be dramatically modified by quantum size effects.

5.2 Introduction

Epitaxial growth has been one of the most widely used methods to build nanostructures and has been applied on numerous systems over the past three decades. One of the key goals is to find how the growth outcome (i.e., the growth mode, the geometry, dimensions of the grown nanostructures, etc.) becomes easily controllable. This in turn requires identifying the key energy barriers, which determine the growth and finding easy, reproducible ways to tune them.

This is especially promising at low temperatures because a hierarchy of energy barriers exists and only few barriers are sufficient to describe the growth outcome. For example, the initial stage of atom deposition on a substrate is measurable from the nucleated island density

$N(\theta, F, T)$, which can be easily measured in scanning tunneling microscope (STM) images as a function of the deposited amount θ, the flux rate F, and the temperature T.[1] This initial stage is commonly described by the scaling theory of nucleation with N determined from the ratio $(D/F)^{-\chi}$ where D is the terrace diffusion coefficient and $\chi = i_c/(i_c + 2)$ is the universal exponent that depends only on the critical size cluster i_c (the minimum number of atoms necessary for the cluster to be stable). This analysis has been used extensively to measure D or i_c because it is ideally suited to the STM. The critical size cluster depends on the element deposited and the substrate orientation. In most metal systems, $i_c = 1$ but in few cases $i_c > 1$ especially at higher temperatures with the transition temperature defined by the magnitude of the cohesive energy E_i (the bond strength of a dimer).[2] For metal systems in these cases, i_c was found to be not larger than 3.[3]

Recently it was found that for deposition of Pb on Pb(111) islands grown on Si, i_c depends on the island height in a very dramatic way.[4] A value of $i_c \sim 10$ was deduced from the large island density difference in two parts (four layer and five layer) of a single Pb island grown over a Si step. The four-layer island is an unstable height and the five-layer island is a stable height according to the energy of the confined electrons in the islands' quantum size effects (QSE).[5–8] This large difference (approximately a factor of 60 in N) is also seen on separate islands of the corresponding height. These results were obtained for growth temperature 40 K, where i_c should have a low value. The large difference in N is striking because the two parts of the island grown over a step are connected. The conclusion that $i_c \sim 10$ for the five-layer island was partially based on previous work at higher temperatures T=180 K[9] and $T = 150$ K[10] where it was found that the terrace diffusion barrier E_4 on four-layer islands is lower than E_5 (the diffusion barrier on five-layer islands). First principles calculations and general arguments that the density of states is higher for unstable than stable heights have also confirmed $E_4 < E_5$.[9] So terrace diffusion differences should result in higher island density on five-than on four-layer islands contrary to observations.

The conclusion that $i_c \sim 10$ on the same metal as a function of height at such low temperatures is very surprising. At the same time, it is promising in demonstrating that atomistic processes (nucleation) can be controlled by varying the island height (instead of the substrate).[11–13]

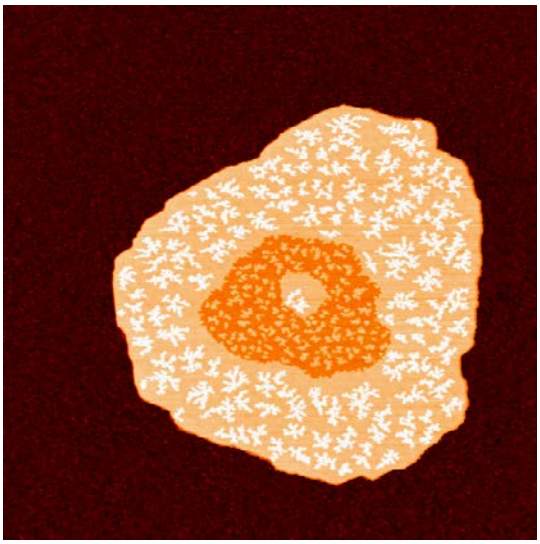

Figure 5.1 300 x 300 nm^2 0.2 ML of Pb was deposited at 40 K with a flux rate of 0.4 ML/min. The island density on the four-layer moat is six times higher than the density on the five-layer ring. This clearly illustrates the strong dependence of the island density on i_c since differences in diffusion should not be important for these systems with small radial dimensions.

5.3 Nucleation Experiments on Pb Ring Islands

To support this conclusion independently of Chan et al.[9] and Ma et al.[10], nucleation and submonolayer island density are studied on an island of smaller radial dimensions. It is known that when the diffusion length becomes several times the linear size of the system, the island density saturates to a level independent of T and F.[14,15] Any differences between different layers cannot be related to differences in diffusion barriers but differences in i_c as a function of layer.[16,17]

A special island shown in Figure 5.1 is five layers on the outside ring and on the inside smaller hub is surrounded by a four-layer moat. In the radial direction, the typical lengths range from 20 (on the hub) to 40 nm (the smaller width of the outside ring). A deposited atom can traverse the island several times radially on both layers:[9] the island density difference is expected to be less than on the bigger island[4] where the atom diffuses across the island fewer times. In addition, in the current experiments the flux rate was increased by a factor of 4 (over the flux in Figure 4.2 of Binz et al.[4]) to test the flux dependence for different layers.

The major result of the current experiments is that the reduced radial size supports the dramatically different i_c (without relying on the calculated diffusion barrier difference $E_4 < E_5$).[9] The flux dependence is also unusual and further confirms the large value of i_c for five-layer islands, but surprisingly N for the four-layer islands is flux independent.

The Pb island in Figure 5.1 was grown at 240 K on Si(111)-7x7 with three separate depositions of 1.0, 0.04, and 0.36 ML for a total of 1.4 ML. Most of the grown islands are either flat or only have rings; the ones in Figure 5.1 with the hub at the center are rare. The areas are 452 nm^2 (hub), 5679 nm^2 (moat), and 26,411 nm^2 (outside ring). The sample was then cooled down to 40 K where a further Pb deposition of 0.2 ML was carried out at a flux rate of 0.4 ML/min.

As shown before[14,15] when the diffusion length becomes comparable to the system size, the island density deviates from the scaling form $(D/F)^{-\chi}$ and eventually becomes independent of D and F. Using the larger of the two barriers for both layers $E_4 = E_5 \approx 0.05$ eV, we can estimate the lower bound to the diffusion length. It is given by $l = (4Dt)^{1/2}$ with $D = 10^{13} exp^{(-E/kT)}$, with k as the Boltzmann constant, $T = 40$ K, E is the diffusion barrier, F the flux rate, and t is the average time between two successive atom arrivals in area A, $t = 1/AF$. A normal prefactor of 10^{13} s^{-1} is assumed. For the hub with linear dimension 20 nm and $F = 0.4$ ML/min, $t \sim 0.035$ s. This implies that an atom moves $l = 840$ nm before the next Pb atom is deposited. The narrowest part of the moat is 20 nm so for $E_4 = 0.05$ eV, this leads to an atom traversing the moat 42 times radially; if the entire area of the moat is considered for a deposited atom to meet the next deposited atom, this leads to $l = 240$ nm; still 12 times the width of the moat. The narrowest part of the outside ring is 40 nm which leads to half the previous values of l. For $E = 0.05$ eV, the D/F ratio is $\sim 10^7/10^{-2} = 10^9$ in the regime where finite size effects and the breakdown of scaling should occur for these small sizes.[14,15] Even if a slightly larger barrier $E_4 = E_5 = 0.06$ eV is used,[9] D/F decreases by only an order of magnitude and the estimates for the diffusion length l are only reduced by a factor of $10^{1/2}$, still larger than the size of the hub and the narrow part of the ring. Under these conditions the island density should be independent of whether the nucleation is on the four or five layer. On the other hand for the flat mixed island grown over a substrate step[4] the island size is ~200

nm, so the island density is more sensitive to differences in the diffusion barriers of the two parts. In this case, to conclude $i_c = 10$ on the five layer requires the condition $E_4 < E_5$.[9]

However, for the ring island of Figure 5.1 the measured island densities were found to be strongly layer dependent. The island density on the outside five-layer ring is 0.006 islands/nm^2 and on the hub is 0.004 islands/nm^2. Both of these numbers are close to the island density 0.0041 islands/nm^2 on separate uniform five-layer islands at $T = 40$ K, $F = 0.4$ ML/min and with similar total area 15,000 nm^2.[18] The island density on the four-layer moat is six times higher (0.025 islands/nm^2), which is very close to the density measured on separate uniform four-layer islands (0.027 islands/nm^2), if only the freestanding islands on top of the surface of the moat are included (and not the islands at the inside edge of the ring because nucleation at the lower step has a much higher rate than the nucleation from monomer encounters). If the inside edge islands are counted then the island density on the four-layer part is increased to 0.032 islands/nm^2. The corresponding island densities for uniform islands and lower flux rate $F = 0.1$ ML/min are 0.023 islands/nm^2 for four-layer islands and 0.001 islands/nm^2 for five-layer islands; for the mixed island the density on the five-layer part was counted even lower at 4.6x10^{-4} islands/nm^2 because the islands which have nucleated at the boundary separating the two parts were not included in the island density of the five-layer part.

Figure 5.2 shows a different island grown under similar conditions but without a hub at its center. Most of the ring width is ∼15 nm so finite size effects should be more pronounced and very low island density should be expected (with more atoms falling off). The island density on the ring is 0.003 islands/nm^2 comparable to what is measured on separate islands.[18] The density on the center four-layer part is 0.026 islands/nm^2 if only the free-standing islands are counted (and 0.030 islands/nm^2 if the growth on the edge of the five-layer rings is counted). The island density on the two parts of the ring (the narrow and wide which differ by a factor of 4 in width) is the same, so this image by itself shows that the controlling factor must be i_c and not the diffusion barrier. If it was caused by diffusion we would expect the wider part to have a higher island density than the narrow part.

For nucleation theory,[1] the exact deposited coverage is not important as long as steady state is attained. Steady state condition applies before coalescence (for coverages less than

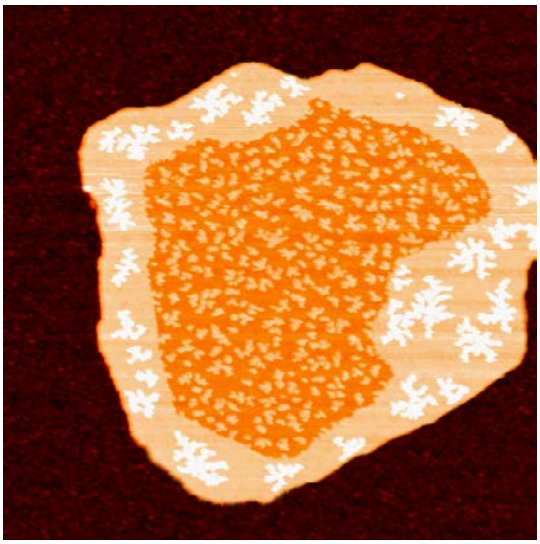

Figure 5.2 200 x 200 nm^2 A ring island with similar island densities on the two layers (as on separate larger islands of the same height) despite its small size. The width of the ring is ∼15 nm except at the widest part is 60 nm. The island density is the same ruling out differences in diffusion barriers (on four- vs five-layer islands) as being the cause of the island density variation.

∼0.3 ML). The coverage 0.2 ML used in the current experiment is below this value. In any case we measured the coverages on the three island parts to estimate how much Pb is falling off. To eliminate the effects of tip convolution only the flat top parts of the small nucleated islands were included in the calculations of the covered area. By using the histogram function only heights within 0.2 nm of the average height of the substrate were included in the coverage estimation.

The coverage on the ring, moat, and the hub of Figure 5.1 were 0.21, 0.22, and 0.11 ML respectively. For Figure 5.2 the coverage on the ring (which has area 10,057 nm^2) and center (which has area 11,314 nm^2) were 0.17 and 0.18 ML respectively. The expected coverage 0.2 ML based on the flux rate and the deposition time is very close (the flux rates were determined from the amount needed to fully complete a layer). The coverage on the center of Figure 5.1 and the narrower ring of Figure 5.2 is lower than 0.2 ML but this should not be important because steady state has been attained.

The current experiment was carried out at a higher flux rate (by factor of 4) than the flux in Binz et al.[4], it is interesting to discuss the flux dependence of the nucleated island density.

Since island densities are similar on separate[18] and ring islands, the flux dependence is the same for the two types of islands. They lead to the same conclusion that $i_c = 1$ for four-layer islands and $i_c > 1$ for five-layer islands (the larger value of $i_c = 10$ is deduced for nonzero cohesive energy $E_i = 0.1$ eV as in Binz et al.[4]). The flux dependence adds more evidence that the island density difference is because of i_c differences (and not the difference in the diffusion barrier). For the five-layer island the island density increases by a factor of 4 which suggests that $i_c \gg 1$. Otherwise if $i_c = 1$, we would expect the factor to be only $4^{1/3} = 1.6$ while for $i_c = 10$ the corresponding change in island density is $4^{5/6} = 3.2$ closer to the observed change of 4. Normally the critical size cluster is determined from the island size distribution.[19]

5.4 Discussion

For the four-layer island, the island density N is practically unchanged (within statistical fluctuations). It is still not clear what the reason for the flux independence is, but at least it implies that the nucleation rate is even higher than the case $i_c = 1$. One interpretation is that after Pb monomers reach a minimum density ~0.023 monomers/nm^2 (which corresponds to an average island separation of 7 nm), they attract all other monomers deposited. The origin of this minimum separation is unclear except it is close to 8.3 nm the observed corrugation on top of these islands.[4] However nucleation on two-layer Pb islands grown on top of Pb-α-$\sqrt{3}$x$\sqrt{3}$ corrugation was shown to affect island location[20] as a result of the different island stacking and not the island density with height as in the current experiments. (In addition, corrugation is seen on both heights and islands have the same stacking.)

These nucleation studies although performed for the growth of Pb on Pb islands (and also In on Pb islands,[18] which shows a factor of 2 difference in island density in similar experiments at 120 K) are very promising in terms of using QSE to affect reactivity. The connection between confinement, geometry, and energy barriers opens the possibility to control the rate of different atomic scale processes with island height. This possibility is intuitively justified in terms of the increased electron density of states whenever an energy level crosses E_F, so stronger bonding of adsorbates and higher chemical reactivity should be expected at unstable heights.

Previous work in the literature has shown rate variations with island height in other systems:

Fe diffusion on Pb islands (with a factor of 1.3-2 variation in island density).[10] Pb oxidation was found to oscillate with height (although the variation was not quantified in terms of oxide yield differences).[21] Oxide formation on Mg films was found to increase on unstable heights by a factor of 1.2.[11] A shift in desorption temperature by 6 % was also found for CO adsorption on epitaxially grown Cu films by inverse photoemission.[12] It is still not clear what the reason for the much larger variation of island density in the current work is; except that smaller height islands were used (four layers, five layers) where the difference in QSE energies and density of states is the highest.

The role of nanoclusters to enhance reactivity has been a very active area in nanocatalysis with other mechanism besides QSE. Well-ordered Au layers prepared on titania grown on Mo(112) substrates were used to show that the catalytic oxidation of CO was significantly higher on bilayer than on monolayer Au films.[22] Sintering processes of Pb 3D clusters of diameter less than 20 nm adsorbed on MgO were faster by orders of magnitude than clusters of mesoscopic diameters.[23]

5.5 Conclusions

In summary, Pb nucleation on top of uniquely shaped Pb islands with radial dimensions much smaller than the diffusion length shows that the differences in the nucleated island density is the same as for larger islands.[4] These results prove experimentally that the difference in terrace diffusion is not the factor causing the dramatic variation of the nucleated density with island height. The conclusion that the critical size cluster is larger on five-than on four-layer islands is directly confirmed from the experiment without the need of input from theoretical calculation of differences in the diffusion barriers. These results show that QSE can affect the nucleation and adsorption properties in a dramatic way on the same metal substrate not seen previously when the metal substrates used was varied.

5.6 Acknowledgements

Work at the Ames Laboratory was supported by the Department of Energy-Basic Sciences under Grant No. DEAC02_07CH11358.

References

[1] J. A. Venables, G. D. T. Spiller, and M. Hanbucken, Rep. Prog. Phys. **47**, 399 (1984), URL http://stacks.iop.org/0034-4885/47/i=4/a=002. 5.2, 5.3

[2] H. Brune, Surf. Sci. Rep. **31**, 125 (1998), ISSN 0167-5729, URL http://www.sciencedirect.com/science/article/pii/S0167572999800016. 5.2

[3] J. Evans, P. Thiel, and M. Bartelt, Surf. Sci. Rep. **61**, 1 (2006), ISSN 0167-5729, URL http://www.sciencedirect.com/science/article/pii/S0167572906000021. 5.2

[4] S. M. Binz, M. Hupalo, and M. C. Tringides, Phys. Rev. B **78**, 193407 (2008). 5.2, 5.3, 5.3, 5.4, 5.5

[5] F. Schulte, Surf. Sci. **55**, 427 (1976), ISSN 0039-6028, URL http://www.sciencedirect.com/science/article/pii/0039602876902508. 5.2

[6] P. J. Feibelman, Phys. Rev. B **27**, 1991 (1983).

[7] T. C. Chiang, Surf. Sci. Rep. **39**, 181 (2000), ISSN 0167-5729, URL http://www.sciencedirect.com/science/article/pii/S0167572900000066.

[8] B. J. Hinch, C. Koziol, J. P. Toennies, and G. Zhang, Europhys. Lett. **10**, 341 (1989), URL http://stacks.iop.org/0295-5075/10/i=4/a=010. 5.2

[9] T. Chan, C. Z. Wang, M. Hupalo, M. C. Tringides, and K. M. Ho, Phys. Rev. Lett. **96**, 226102 (2006). 5.2, 5.3, 5.3

[10] L.-Y. Ma, L. Tang, Z.-L. Guan, K. He, K. An, X.-C. Ma, J.-F. Jia, Q.-K. Xue, Y. Han, S. Huang, et al., Phys. Rev. Lett. **97**, 266102 (2006), URL http://dx.doi.org/10.1103/PhysRevLett.97.266102. 5.2, 5.3, 5.4

[11] L. Aballe, A. Barinov, A. Locatelli, S. Heun, and M. Kiskinova, Phys. Rev. Lett. **93**, 196103 (2004). 5.2, 5.4

[12] A. G. Danese, F. G. Curti, and R. A. Bartynski, Phys. Rev. B **70**, 165420 (2004). 5.4

[13] N. Binggeli and M. Altarelli, Phys. Rev. Lett. **96**, 036805 (2006). 5.2

[14] M. Schroeder and D. E. Wolf, Phys. Rev. Lett. **74**, 2062 (1995). 5.3, 5.3

[15] K. R. Roos and M. C. Tringides, Surf. Sci. **355**, L259 (1996), ISSN 0039-6028, URL http://www.sciencedirect.com/science/article/pii/0039602896006103. 5.3, 5.3

[16] M. Hupalo and M. C. Tringides, Phys. Rev. B **75**, 235443 (2007). 5.3

[17] Z. Kuntova, M. Hupalo, Z. Chvoj, and M. C. Tringides, Phys. Rev. B **75**, 205436 (2007). 5.3

[18] S. M. Binz, M. Hupalo, and M. C. Tringides (2009), the Complete Dataset. 5.3, 5.3, 5.4

[19] J. G. Amar and F. Family, Phys. Rev. Lett. **74**, 2066 (1995). 5.3

[20] H. Y. Lin, Y. P. Chiu, L. W. Huang, Y. W. Chen, T. Y. Fu, C. S. Chang, and T. T. Tsong, Phys. Rev. Lett. **94**, 136101 (2005). 5.4

[21] X. Ma, P. Jiang, Y. Qi, J. Jia, Y. Yang, W. Duan, W.-X. Li, X. Bao, S. B. Zhang, and Q.-K. Xue, Proc. Natl. Acad. Sci. **104**, 9204 (2007), URL http://www.pnas.org/content/104/22/9204.abstract. 5.4

[22] M. S. Chen and D. W. Goodman, Science **306**, 252 (2004), URL http://www.sciencemag.org/content/306/5694/252.abstract. 5.4

[23] C. T. Campbell, S. C. Parker, and D. E. Starr, Science **298**, 811 (2002), URL http://www.sciencemag.org/content/298/5594/811.abstract. 5.4

CHAPTER 6. Island Height Dependent Nucleation Driven by Quantum Size Effects and Unusual Island Growth in In/Pb(111)/Si(111)

6.1 Abstract

In was deposited onto epitaxially grown Pb(111) islands of 4 and 5 layers thickness to investigate possible quantum size effect driven differences between the two. A 2 times difference in island density was observed with the higher density being on the unstable height, as expected. A difference in diffusion and step edge barriers caused by Quantum Size Effects (QSE) can explain the differences. Second layer nucleation is slow to occur because In diffuses very quickly and the step edge barrier off of the Pb/In island is small. Because of this, nucleation is slow until the Pb starts to be surrounded by approximately 4 nm of In with the same height as the Pb/In island. In has a much higher propensity to nucleate on these new, all In, sections for a number of possible reasons.

6.2 Introduction

Quantum Size Effects (QSE), effects that manifest themselves only when dealing with dimensions on the order of atoms or tens of atoms, have been shown to cause a wide range of effects on materials, including determining the shape and dimensions of structures on surfaces.[1,2] QSE are caused by the confinement of otherwise free electrons by crystal dimensions that are on the order of the Fermi wavelength of the electrons. The system has a lower energy when the confined electron energies are far from the Fermi energy, as discussed in the introduction of this dissertation. The lower their energy, the less the electron wave functions extend beyond the surface, the less energy associated with the QSE. QSE only effect crystals with at least one dimension on the order of the atomic scale because if the crystal is much larger than the electron's

wavelength then any energy associated with part of the electrons' path is very small, especially compared to the energy of the crystal. This is how QSE can control island shapes, generally manifested on surfaces as the thicknesses of films. The confining dimensions also changes the overall electronic structure of the material by limiting the energies available to some electrons which effects electronic based properties, like the electrical resistivity.[3] This will be discussed more thoroughly later in the chapter. Since QSE can control electrical resistivity it stands to reason that they have an effect on other electron related properties, like bonding. Bonding and chemical reactivities are an important property of materials and this has therefore become an area of intense research in recent years.

Controlling the bonding properties of a material by changing its height allows for the possibility of creating catalysts that work better and last longer than currently used catalysts. Speaking strictly of solid catalysts there are three main steps to the process: the initial reaction of one or all reactants with the catalytic surface, diffusion of the reactants and the eventual creation of the final product, and the product(s) breaking away from the surface. Each of those steps is critical to the success of the catalyst and if they can all be controlled with QSE then there are a lot of possibilities for new catalysts. However, each individual property cannot be adjusted on its own because any one part of a film is limited to one thickness and therefore one set of properties (diffusion, adsorption, desorption). For example, it has been shown by Danese et al.[4] that in the CO on Cu(100) system, the adsorption energy of the CO oscillates in tune with the density of states at the Fermi energy. Danese et al.[4] showed via inverse photoemission that when the density of states at the Fermi energy was at its highest the temperature of thermal desorption of CO was higher. The density of states near the Fermi Energy is partially controlled by QSE. Regardless of the film thickness there are always some electrons at the Fermi energy because the film only constrains the perpendicular component of the electrons' momentum. When the Highest Occupied Band (HOB) in the z-direction is far from the Fermi energy, see Figure 1.1, the density of states is suppressed at the Fermi energy. The opposite is true when the HOB is near the Fermi level. The exact mechanism behind the relation between higher reactivity is still in doubt but Danese et al.[4]'s basic argument was that having more electrons at the Fermi energy increased the reactivity of the surface because there are more

electrons available to interact with atoms or molecules approaching the surface.

Aballe et al.[5] proved that specific thicknesses of Mg adsorbed O_2 much more readily than other thicknesses. Low Energy Electron Microscopy was used to image the surfaces with many different layers of exposed Mg while exposing it to O_2. With x-ray photoelectron spectroscopy the intensity of the oxidized Mg 2p peak was tracked and the rate of O_2 adsorption was approximately linear with the density of states at the Fermi Level. Combined with another study by Aballe et al.[6] they showed that QSE not only changes the density of states at the surface but also the electron density decay length – 1 over the distance from the surface that it takes for the electron density probability to decay by a factor of e. They went further and showed that the electron decay length has a larger effect on the reactivity of a surface, at least for the O_2 on Al on W(110) system and probably others, than the density of states. This is, in part, because Hellman et al.[7] stated that electron tunneling between the surface and the O_2 molecules controls the initial sticking of O_2 to the surface. For the O_2 on Al(111) system the van der Waals force is not strong enough to keep the O_2 on the surface, therefore the O_2 molecule must be dissociated before the O will stay on the surface. That is where the decay length of the electrons in the substrate comes in, the longer the decay length the more likely an electron from the surface will tunnel to the O_2 molecule. The model used by Hellman et al.[7] assumed that as soon as an electron tunneled to the O_2 molecules, they dissociated and stuck to the surface, chemisorbing the O to the Al. So, QSE can have a strong effect on the first step of catalysis by changing the adsorption energy and reaction distance.

That leaves the ability of the reactants to find each other on the catalytic surface which depends upon, among other things, diffusion barriers. These too have been shown to be greatly affected by QSE. Ma et al.[8] and Chan et al.[9] have shown that stable and unstable thicknesses of Pb islands on Si(111) have different barriers with the unstable thicknesses having the lower diffusion barrier in both cases. Ma et al.[8] deposited Pb onto Si(111) creating large islands that spanned many single step high Si terraces and therefore had multiple thicknesses. They then deposited Fe which resulted in an oscillating Fe island density depending upon the Pb layer thickness. With that it was argued that the diffusion barrier on even (unstable) and odd (stable) Pb thicknesses were different. Chan et al.[9] reported vertical island growth of Pb on

Si(111) that differed between stable and unstable Pb island heights. Layers on stable islands grew from the center while they started on the edges of unstable heights. In conjunction with theoretical calculations they argued that this unusual growth pattern was caused by faster diffusion on the unstable heights along with a higher Ehrlich Schwoebel Barrier (also known as the step edge barrier, the barrier keeping atoms from falling off a terrace or island) on the unstable heights.

Our recent work in this area was Pb on Pb(111) on Si(111) at 40 K and it produced a particularly strong effect with the island density on the 4-layer thick Pb(111) being up to 60 times that on the 5-layer thickness. See Chapters 4 and 5 for details.[10,11] We concluded that it must be from a change in critical island size, which, while not as directly related to catalysis as the diffusion barriers, still indicates a change due to QSE that could be useful. To investigate if the effect would be seen in a more realistic system, a heteroepitaxial one at higher temperatures, we followed up by depositing In onto Pb(111) on Si(111) 7 x 7 at 110 K.

6.3 Experimental setup

An Omicron VT STM was used to image a Si(111) substrate with Pb islands of height 4 and 5 layers, created by depositing about 1.1 ML of Pb at 240 K. Immediately after deposition the system was cooled down to 110 K, this helped ensure that the 4- and 5-layer islands did not coarsen away, allowing further deposition onto them.[12,13] In was then deposited in various increments at a flux rate of 0.07 ML/min for all data except those shown in Figure 6.1 which had a slightly lower flux rate of approximately 0.05 ML/min. The flux rate was determined by calculating the change in volume of the In islands growing on the Pb wetting layer using the Scala Pro histogram function. The areas used were at least 9500 nm^2 and were chosen to be at least 10 nm from the Pb island edges to minimize any effects they may have on the distribution of In on the surface. 10 nm is sufficient because diffusion of In on this surface is low after initial depositions at this temperature. This behavior was not necessarily expected given the normally high mobility of In on many other surfaces, including on Pb $\sqrt{3}$ x $\sqrt{3}$ and will be discussed later in this chapter.[14]

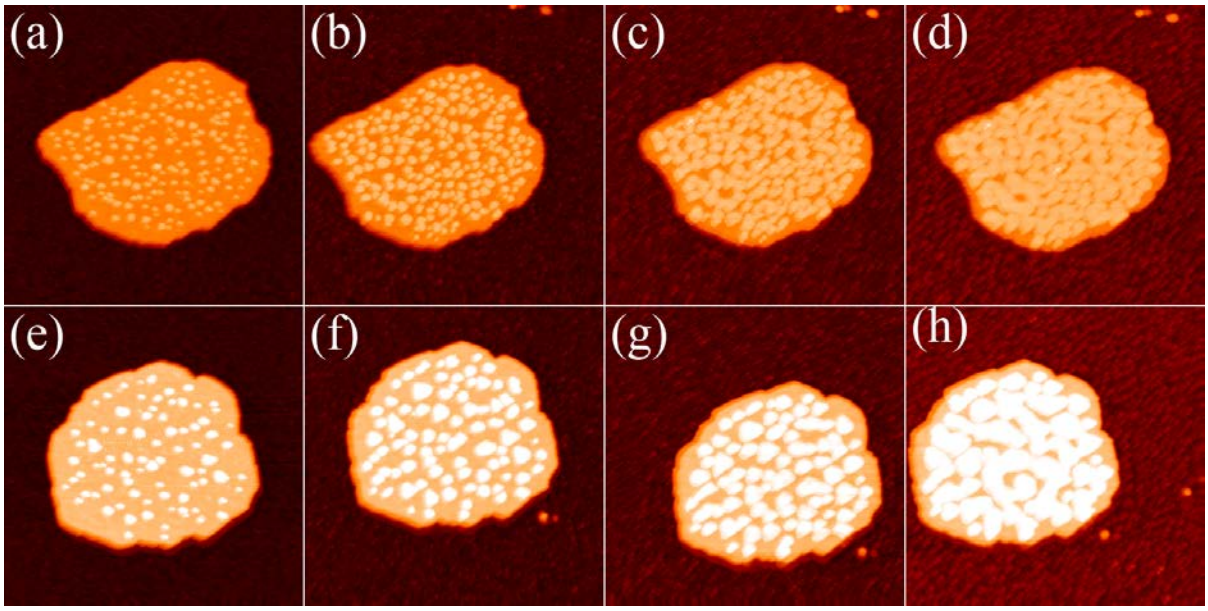

Figure 6.1 The island density on the 4 layer island is roughly twice that of the 5 layer island because the diffusion rate on the 4 layer island is lower. As more In is deposited the In islands grow and then merge, finishing the In layer perfectly. All images are 200 x 200 nm and the columns have experienced the same conditions (same experiment). The top row shows the 4-layer island and its area is 12,600 nm^2 and has a peak of 173 islands in (b). The other row shows the 5-layer island, it is 12,200 nm^2 and has 83 islands in (f).

6.4 Results

Upon depositing In onto the Pb islands two trends appeared almost immediately. The first is that the 4-layer Pb islands have approximately twice the In island density as the 5-layer Pb islands. This is seen in Figure 6.1 (b vs. f) where the maximum island density on the 4-layer Pb island is 0.016 islands/nm^2 and on the 5-layer Pb island it is 0.007 islands per nm^2 on a surface with 0.3 ML deposited. Figure 6.2 (a vs. f and k) shows similar results with 0.42 ML deposited onto smaller islands, the three island densities are 0.012, 0.005 and 0.005 islands/nm^2 for the 4- and then the 5-layer islands respectively. These numbers are a bit lower but that is because the islands have already started to merge. The overall averages for the 4- and 5-layer islands are 0.0014 and 0.006 islands/nm^2, respectively. This is very similar to the effect seen in Binz et al.[10] but is quite a bit weaker. In that system the island density on the 4-layer Pb

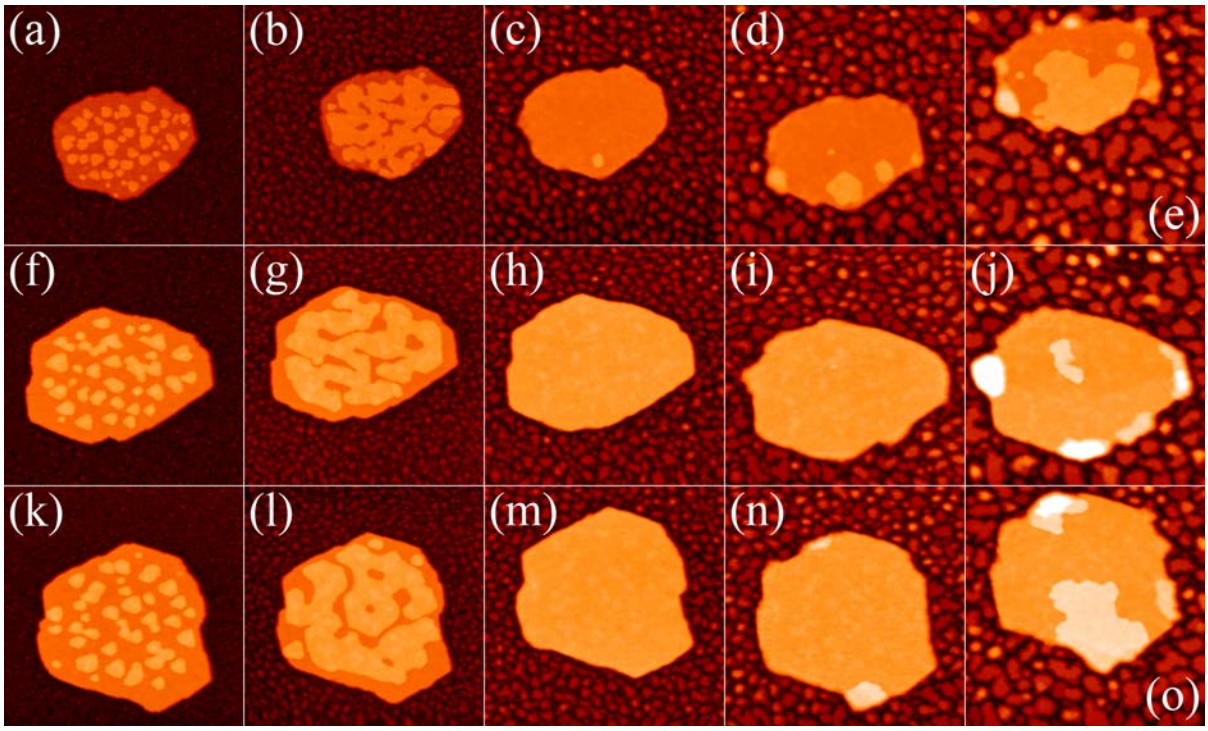

Figure 6.2 All images are 135 x 135 nm. Once again, the 5-layer islands (f-j, 5740 nm^2 and k-o, 6780 nm^2) have half the island density that the 4-layer island (3600 nm^2) does (a-e). As more In is deposited the first layer completes perfectly at which point most of the In starts to fall off the islands, especially on the 5-layer island. Some of the In that falls off attaches to the side of the islands and grows them laterally where most of the 2^{nd} layer nucleations occur. 3D growth dominates in these regions. Deposited amount for columns (a): 0.42, (b): 0.84, (c): 1.26, (d): 1.68, (e): 2.24 ML Actual Coverage on top of islands: (a): 0.26, (b): 0.65, (c): 1.0, (d): 1.11, (e): 1.52, (f): 0.27, (g): 0.61, (h): 1.0, (i): 1.0, (j): 1.29, (k): 0.26, (l): 0.62, (m): 1.00, (n): 1.03, (o): 1.31 ML.

islands was 0.03 islands/nm^2, even higher than in this system, while the island density on the 5-layer Pb islands was 0.0005 islands/nm^2, even lower than what is seen here. One important difference, however, is the flux rate. In the Pb on Pb experiments of Binz et al.[10] the flux rate was 0.1 ML/min while the flux rate of In deposition in the current experiment was 0.07 ML/min. Low flux rates act to lower island densities for otherwise identical systems so the lower flux rate may be contributing to the lower island density in the In on Pb case.

It is interesting to note that after the initial deposition onto the islands in Figure 6.1, during which 0.17 ML grew on the 4 layer island, there was still significant island nucleation in the

second deposition. 15 sets of islands merged during the second deposition yet the number of islands went up by 14, 29 new islands nucleated. Not all of the experiments had the same deposition times but they did all exhibit a surprising amount of nucleation after the initial depositions.

The second major trend is that a significant amount of the deposited In falls off of the Pb islands. The analysis later on will focus on other data but it can be seen even in the data shown in Figure 6.1 where after the first deposition there is 0.17 ML on the 4 layer island and 0.12 ML of In on the 5 layer island. As the number and size of the In islands increase the amount of the deposited In that stays on the Pb islands increases as would be expected because there are now more locations for the In to attach to.

As more In is deposited the first In layer completes perfectly before the 2^{nd} layer begins. This is even stronger layer-by-layer growth than seen in the Pb on Pb case.[10] However, the first layer is where the similarity ends because it is immediately clear that the second layer of In is going to grow very differently, Figure 6.2 (c, h, and m). On the originally 4-layer islands the In nucleates a second layer relatively easily but the island density is much lower than what grew directly on the Pb. Only 4 islands nucleated in the center of the 4-layer island in Figure 6.2 and they do it over the course of three separate depositions for a total of roughly 1 ML deposited. Nucleation of islands is even harder on the now 6-layer islands. Only one island nucleates in the center of the island in Figure 6.2 (row f) and it takes approximately 0.70 ML of deposition to do it. Over the same period no islands nucleate in the center of the island in Figure 6.2 (row k). However, it is not uncommon to have 2 or even sometimes 3 islands nucleate in the center of the 6-layer islands.

A lot of In is being deposited that does not stick to the top of the islands, some of it falls off of the island completely while quite a bit goes into expanding the islands laterally. This creates an incomplete ring of solid In around the Pb islands, encasing them in In. The parts of the islands that are all In are about 0.1 nm taller than the Pb plus 1 layer of In sections.

Most of the nucleation of the second layer of In occurs along the edges of the islands. More specifically, on the all In sections. Generally, In areas wider than 4 nm nucleate new In islands. Once nucleated they quickly grow, horizontally onto the rest of the island and vertically with

the peak in Figure 6.2 (j) already 1.5 nm, 4 layers, above the first layer of In on the island.

Throughout this whole process the wetting layer is slowly forming islands of its own. After 0.14ML or less of deposition the Pb wetting layer is covered in small In "blobs". By 0.42 ML, Figure 6.2 (a column) the density of small islands has reached its peak of 0.055 islands/nm^2, and select islands start to grow larger. The islands that grow remain flat topped and slowly adsorb other islands and grow taller. In Figure 6.2 (c column) some of these islands have started to grow 3 dimensionally, some of which are the same height as the 4+1-layer islands. The wetting layer islands closest to the Pb islands slowly merge with the larger islands helping to determine their shape. This generally happens all at once in such a way that they go from being just like all the rest of the wetting layer islands to being the same height as the larger island they joined after just one deposition.

6.5 Discussion

6.5.1 Expectations and model of the system

The effects seen in In on Pb film growth are similar to effects seen in Binz et al. [10] for Pb on Pb film growth at 40 K, though it is quite a bit weaker. There are a number of possible reasons that the effect is smaller in this experiment, the two obvious ones are that this experiment used In instead of Pb as the final deposition element and this experiment was done at 110 K, not 40 K. In is a smaller element and therefore naturally has a higher diffusion rate and, perhaps in this case a lower critical island size, i_c. i_c is the largest collection of atoms which have a higher probability of decaying to nothing than growing into permanent islands. In diffusion barriers on Ag(001) and Cu(001) have been shown to be significantly higher than the barrier estimated for Pb on Pb in Binz et al. [10], ∼0.09 eV, with 0.31 [15] and 0.28 eV. [16], respectively. Van Siclen [17], using the embedded-atom method, calculated the diffusion of In on Cu(001) to be 0.32 eV, within 15% of the experimental value. Van Siclen [17] also calculated the barrier for In on Cu(111) and got 0.02 eV which is significantly lower. [17] Since the surface structure appears to be have a larger role in determining the barrier than the element it stands to reason that In will diffuse quickly on Pb(111). Also, somewhere between 40 K and 195K even the

Pb on Pb system loses the large critical island size that caused the bulk of the island density difference associated with Pb growth on 5 layers of Pb so observing a smaller island density difference at 110 K is not surprising. Two times is quite a bit less than 60 times but it is still a strong and robust effect.[18] For example, it is still larger than the effects seen for Fe on Pb.[8]

Nucleation theory can be used to get rough estimates for the diffusion barriers, E_d, and critical island size, i_c. Qualitatively speaking, based on the number of islands and the fact that they continue to nucleate during further depositions despite a large number of islands already existing the critical island size is probably 0 or 1 on both the 4 and 5 layer Pb islands but the fact that In is falling off rules out 0. Furthermore, critical island sizes for metals deposited onto metals are commonly 1 at low temperatures where atoms have less energy to break free from bonds.[19,20] In the homoepiaxial systems of Fe(100), Cu(100), Ni(100), and Pb(100) the critical island size below around 300K, and in some cases higher, is 1 while above around 300K it is 3.[21] An example of heterogeneous deposition, Cu on Ni(100) has a critical island size of 1 until 320 K when it changes to $i_c = 3$.[22] i_c jumped to 3 from 1 because of the square lattice and is not expected for the In on Pb(111) system. On a square lattice both $i_c = 1$ and 2 have at most one bond between the various atoms so $i_c = 2$ is not any more stable than $i_c = 1$. However, on a hexagonal lattice, like that of Pb(111), three atoms can arrange themselves in such a way that each atom is bound to the other two atoms for a total of two bonds each.[23] Similarly, it is possible to estimate the relative diffusion barriers on top of the 4 and 5 layer thick Pb films. Since i_c is 1 on both film thicknesses and there is a higher island density on the 4 layer film, it has a higher diffusion barrier. This is because, all else being equal, the slower diffusion rate will lead to a higher density of islands. When an atom lands on the surface it is more likely to nucleate a new island if it takes it a long time to diffuse to an existing island.

This can be addressed in deeper detail by addressing the fact that the nucleation of new islands is occurring on islands, not infinite films. Nucleation of islands on large terraces is usually treated by a mean field theory, such as the one introduced in the introduction (equation 1.7).[24] Mean field theories are so prevalent because the associated assumptions, like assuming the monomer density is constant on a surface, make the math associated with nucleation models a lot easier and they are easy to follow and relatively accurate. However, when nucleating on

islands those assumptions are not necessarily true and things can be even further complicated by the fact that atoms can fall off islands as is the case with In on Pb. This is not a small problem, even though the average atom diffusion length was at least an order of magnitude lower than the size of the island, more than half of the atoms still fell off. To get around this problem Krug et al.[25] approached the problem directly instead of using models designed for other films. The final result has limitations as well but the underlying framework can go a long way in helping to make sense of what is going on.

When an atom is deposited onto a flat surface it will move around, if its energy is not significantly smaller than the diffusion barrier, it will succeed. On a large flat area this atom will almost certainly meet other adatoms and nucleate a new island long before reaching the step edge. However, on a relatively small island the atom could visit all sites on the top of the atom long before another atom arrives on top of the island. Krug et al.[25] refers to this situation at the Lonely Atom Model. The specific assumptions required will be mentioned in more detail below but keep in mind that any atom that lands on the island will be there a long time. That means that an atom will have enough time to visit each lattice point on the island. The time it would take to do that is called the traversal time, τ_{tr}:

$$\tau_{tr} \sim \frac{A}{\nu} \tag{6.1}$$

A is the area of the top of the island in terms of the lattice unit cell and ν is the hopping rate as defined by:

$$\nu = \nu_0 e^{\frac{-E_d}{k_b T}} \tag{6.2}$$

These terms have the same definition as they did in the above discussion but for the sake of convenience: ν_0 is the attempt frequency and is generally set to be 10^{13}, E_d is the diffusion barrier, k_b is Boltzmann's constant, and T is the temperature in Kelvin.

The approximation sign is used in equation 6.1 instead of an equal sign because the atom on the surface is doing a random walk. Every time it moves from one place to the next the direction is completely random so the described traversal time to actually visit each lattice site is an underestimation.

A more interesting, though less intuitive, time is the average time that an atom stays on the island, τ. It is an easy enough concept to think about but quantifying it in measured variables is a bit more difficult. For now, let it be defined as the total amount of time atoms have spent on the surface, T_T, divided by the number of atoms that have been deposited, n.

$$\tau = \frac{T_T}{n} \tag{6.3}$$

The total number of atoms deposited is just the flux rate, F, times the time of deposition, T, and the area, A.

$$n = FTA \tag{6.4}$$

From this it is possible to get that the average time between depositions is just the inverse of FA.

$$\Delta t = \frac{1}{FA} \tag{6.5}$$

This is another important time because it defines, roughly, the amount of time between atoms arriving on the island. If an atom falls off in less than this time then there will not be an atom for a newlu arriving atom to nucleate an island with. For example, if τ is the same order of magnitude or larger than Δt, then a new island will nucleate on the original island rather quickly. If τ is much smaller than Δt, then nucleation is relatively unlikely, but not impossible. In this regime the chance of nucleation depends upon fluctuations and is the regime of the LAM.[26]

Before moving on, τ still needs to be recast into something that can be calculated. n and T_T are not known natively so they will need to be removed. Another way of expressing T_T is that it equals the average number of atoms at any one lattice point at any time multiplied by T and A.

$$T_T = \overline{n}TA \tag{6.6}$$

Putting this into equation 6.3 leads to:

$$\tau = \frac{\overline{n}A}{\Delta t} \tag{6.7}$$

Where T divided by n was replaced with Δt. The simplest way to proceed is to assume that the adatom density is uniform across the entire surface, this occurs when the chances of an

atom falling off is much smaller than staying on the island. This is true because that gives the atom a long time to diffuse across the surface and randomly visit each section and it does not automatically fall off when it gets close to the edge, meaning the adatom density at the edge is the same as everywhere else.[27]

The number of atoms on the island depends upon two things, the rate of atoms being deposited onto the surface and the rate of atoms falling off. In the case that the adatom density is evenly distributed the rate of atoms falling off is simply the number of edge lattice sites, times the probability of an atom being there, times the chances of it falling off the island, or $L < n > \nu$'. ν' is fundamentally the same as equation 6.2 with two key differences because it represents the rate with atoms fall off of the island. The diffusion barrier is replaced by the Ehrlich Schoewbel barrier, E_s, which is generally larger than the diffusion barrier, and ν'_0 is 10^{10}.

$$\nu' = \nu'_0 e^{\frac{-E_s}{k_b T}} \tag{6.8}$$

L is the length of the perimeter of the island in terms of the unit cell length and is therefore trivially related to A as long as the shape of the island is known. Formalizing this relationship:

$$A = \alpha L^2 \tag{6.9}$$

where α depends upon the shape of the island, it is $1/4\ \pi$ for circular islands.

The number of atoms on the island is a competition between the deposition rate, FA, and the rate of atoms falling off the island, $L < n > \nu$':

$$FA = L\overline{n}\nu' \tag{6.10}$$

If that statement does not look reasonable at first remember that $< n >$ will continue to increase until the equation is true. Rewriting equation 6.7 with the above equation results in:

$$\tau = \frac{\alpha L}{\nu'} \tag{6.11}$$

ν' is not something that is always known but there is a common value that can be used which will allow a rough estimate for τ. Now all three important times, equations 6.1, 6.5, and 6.11, associated with nucleation on an island of limited size have been defined.

In does fall off of the Pb films in this experiment and according to the above discussion it could be due to a low flux rate or a small step edge barrier. However, In continues to fall off of the Pb islands even after islands have been nucleated. This indicates that the step edge barrier must not be large. An estimate for the barrier can be obtained by assuming that the In atoms arriving after islands nucleate must fall off of the Pb island before coming into contact with the existing islands. Therefore, they must fall off more quickly than the island traversal time, equation 6.1. For this calculation the island will be assumed to be a perfect circle with an area similar to that of the islands in Figure 6.2, 6000 nm^2, 10.15 nucleation sites per nm^2 as per the Pb(111) lattice, $\alpha = 1/4\pi$, and then $L = 875$ unit cell lengths. The diffusion barrier will be assumed to be on par with that of Pb on Pb diffusion, $\tilde{0}.09$ eV. With those parameters the time to visit each site on the island is $8.1{*}10^{-5}$ seconds. Therefore, the average time on the island must be less than that, applying equation 6.11 results in the step edge barrier having to be below 0.067 eV. Therefore, the barrier is likely of the same order of magnitude as the diffusion barrier.

6.5.2 Critical island size

In an attempt to put the above conclusions on firmer ground the island size density was analyzed as was done by Amar and Family [23] and used successfully by Pomeroy and Brock [28], among others. Amar and Family's theory does not directly assume any specific lattice so it should work on anything. Though, since they tested it on a triangular lattice (as well as a square lattice) it is clear that it will work with the hexagonal lattice of Pb(111) since it is essentially an equilateral triangle lattice. Also, since it is based solely on island size distribution it is independent of temperature and therefore diffusion rate. The only catch is that at higher temperatures the islands will be larger (generally speaking) the area that needs to be scanned to get good statistics would be much larger.

Amar and Family [23] asserted that the island size density can be written in terms of coverage, θ, average island size, S, and a scaling function that depends upon the critical island size, i_c,

and the normalized island size distribution, s/S.

$$N_s(\theta) = \frac{\theta}{S^2} f_i\left(\frac{s}{S}\right) \tag{6.12}$$

The above relationships were from simulations to which scaling theories were applied. To keep the function $f(u)$ from changing the scaling introduced by theta and S^{-2} two restrictions were placed on $f(u)$. The integral of $f(u)$ and $f(u) * u$ over all lengths must both be equal to 1. Futhermore, based on simulations of fractal islands with $i_c = 1$[29] they knew there that for small values of u, $f(u)$ was approximately linear and that it should approach 0. The islands will be larger for larger i_c, reducing the number of small islands so the u term in the scaling function is assumed to actually be u^{i_c}. Lastly, it is assumed that the average island size will also be the most likely island size so the peak of f(u) should occur at 1 with an exponential drop afterwards. This all leads to the following function and conditions:

$$f_i(u) = C_{i_c} u^{i_c} e^{-i_c a_{i_c} u^{\frac{1}{a_{i_c}}}} \tag{6.13}$$

$$\frac{\Gamma\left[\left(i_c+2\right)a_{i_c}\right]}{\Gamma\left[\left(i_c+1\right)a_{i_c}\right]} = \left(i_c a_{i_c}\right)^{a_{i_c}} \tag{6.14}$$

$$C_{i_c} = \frac{\left(i_c a_{i_c}\right)^{(i_c+1)a_{i_c}}}{a_{i_c}\Gamma\left[\left(i_c+1\right)a_{i_c}\right]} \tag{6.15}$$

$$\int_0^\infty f(u)\,du = \int_0^\infty f(u)\,u du = 1 \tag{6.16}$$

C_i and a_i are constants to ensure the two integral constraints are maintained and were determined numerically to be $C_i = 1.11, 1.97, 3.24$ and $a_i = 0.27,\ 0.30,\ 0.31$ for $i_c = 1, 2, 3$ respectively. The values for $i_c = 1$ and 3 were compared with Pomeroy's results.[28] For some reason C_3 does not match, Pomeroy reported 3.33, but the other numbers do agree and the exact location of the $i_c = 3$ line will not prove to be decisive. It is, however, reassuring that the other three numbers matched.

Figure 3 (a) shows a sample of the data for In on 4-layer Pb islands. It includes data from several different coverages and experiments that were normalized and then combined into one data set. The bulk of this process was straight forward but it should be mentioned that to get the final y-axis positions, the weighted average of all of the individual contributions was taken via the island size. For example, if there were two Pb islands and when their data was

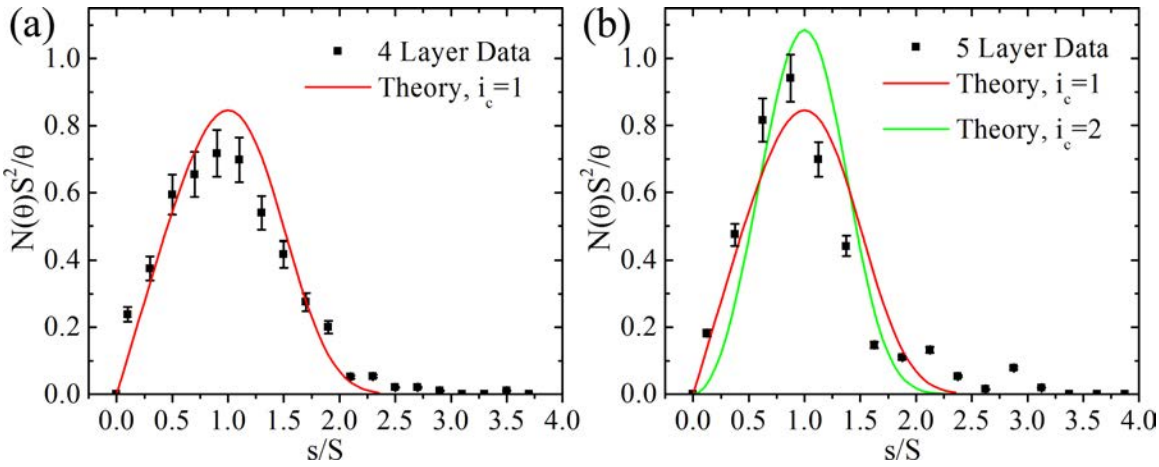

Figure 6.3 Rescaled island size distribution for In islands grown on top of 4 (a) and 5 (b) layers of Pb. Both match the scaling function associated with $i_c = 1$ though for the 5-layer the connection is less obvious. See the text for details.

normalized separately one was 5000 nm^2 and the 0.3 bin had a value of 0.5 and the other was 7500 nm^2 and the 0.3 bin had a value of 0.7. The final y-axis value was calculated like this: (5000*0.5+7500+0.7) / 12500 = 0.62. When a contributing data set had 0 islands for a bin it was weighted as 1 island at a height of 0 to ensure that one or two unusual islands did not get overrepresented in the final data. The experimental data for the 4-layers of Pb follows the theoretical $i_c = 1$ curve fairly well, providing solid evidence that i_c does in fact equal 1 in this situation. The peak is below the theoretical curve but not alarmingly so and the $i_c = 0$ curve is drastically different with the peak intensity occurring very near 0 and then decreasing linearly for a while before an exponential tail. This is because for $i_c = 0$ there is no diffusion so atoms stay where they land so most islands only have one or two atoms in them.[19,24] The average island size of the In islands that contributed to this graph varied between the individual images and coverages but they were all above 70 atoms so i_c was definitely not 0.

Figure 3 (b) is the same thing but for 5-layer islands. This curve's result is not quite as straight forward because the peak of the data is offset to the left of 1 and the peak height is somewhere between the theoretical curves of $i_c = 1$ and $i_c = 2$. The shift to the left is due to the fact that some of the coverages included in the data had some islands that were starting to merge (0.26 ML). Merging is to be expected at coverages as low as 0.2 ML so this is not

surprising.[24] The data was included anyway to provide better statistics for those experiments. The coalescence raises the average island size, moving it to a value larger than the peak of the normal island size distribution that is created at lower coverages. This resulted in the peak shifting to the left and up. Therefore the critical island size of the In growing on the 5 layers of Pb is also 1.

There are a number of sources of error for these graphs, the most prominent two are the coverage estimate and the areas of the islands. The coverage was estimated by locating the peak of the In layer and taking all of the histogram from 0.07 nm below that peak and above as being part of that layer. STM images are a convolution of the STM tip and the surface of the sample so not every feature in the image is caused by the surface. The large length of the sides of the islands is caused by the STM tip so the sides in the area should not be included. 0.07 nm was chosen because it minimizes the amount of the sides of the islands included while still including all of the layer itself, i.e., the normal distribution of heights. In most data it places the cutoff just below base of the In layer's peak so relatively little of the background in the histogram is included. However, since the absolute flux cannot be used to guide the cutoff decision, it is merely an estimate. Moving the cutoff 0.01 nm higher or lower changes the estimated coverages by 5-12%. This is the source of the error bars in the Figure 6.3. Since the coverage enters into the y-axis of the graph as a divisor the error bars are essentially a direct representation of the 5-12% error in the coverage estimate.

As for the areas of the individual islands, whenever that comes into play the data is first binned or averaged. It is assumed that those two actions along with taking into account the error in the coverage estimate removes any significant error associated with the areas of the individual islands. The same cutoff was used to determine which pixels were in an island and which ones were not that were used to calculate the coverage. Therefore the two errors are linked and in the equation actually act to cancel each other out since one is in the numerator and the other is in the divisor.

To make sure that the bin size was statistically significant the number of relevant bins was not allowed to be above the square root of the number of islands in the graph. This turned out to not be a problem since the bin size was made large enough so that the up to 12 percent

errors in the island areas, similar to the coverage estimate, could not change the distribution significantly. This is why the bin sizes were 0.2 and 0.25 times the size of the average island size.

6.5.3 Diffusion barriers

Confident that $i_c = 1$ it is possible to estimate the diffusion barrier for the In using the following equation based on nucleation theory:[24]

$$n_x = \eta\left(\Theta, i_c\right)\left(\frac{1}{F}\frac{v_0 e^{\frac{-E_m}{k_b T}}}{2d}\right)^{\frac{-i_c}{i_c+2}} e^{\frac{E_{i_c}}{(i_c+2)k_b T}} \tag{6.17}$$

v_0 is the frequency with which the atoms on the surface attempt to move and it is commonly 10^{13} second^{-1}. d is the dimension of the motion and is generally set to 0.5. The η function has a rather complicated background but for coverages around 0.1 ML and $i_c = 1\eta$ is about 0.25,[30] E_i is the binding energy, a measure of the strength of the bond between an atom and an island. It is set at 0.2 eV. T = 110 K, k_b is Boltzmann's Constant and the flux rate, F, was 0.00083 ML/sec for Figure 6.1 and 0.0012 ML/sec for Figure 6.2.

The maximum In island density achieved on the 4-layer Pb island in Figure 6.1 was 0.0138 islands/nm^2 leading to a diffusion barrier value of 0.069 eV. Doing the same calculation for the 4-layer Pb island in Figure 6.2, using its island density (0.0125 islands/nm^2) and that experiment's flux rate the diffusion barrier is 0.063 eV. The numbers agree with each other quite well suggesting that the almost 4 times difference in area of the two islands had little to no effect - as would be expected based on their similar island densities and the fact that the average diffusion length (8 nm vs. 80 or more nm for the width of the islands) is an order of magnitude lower than the size of the islands. That means that even on the smaller island the In islands nucleated and grew as if they were on a large terrace, partially validating the use of a mean field theory to calculate the diffusion barrier despite the fact that the growth is occurring on an island. Though, as will be discussed in more detail later, In is falling off which means the flux rate used in the calculation is not quite right. The diffusion barrier associated with the average island density is 0.064 eV.

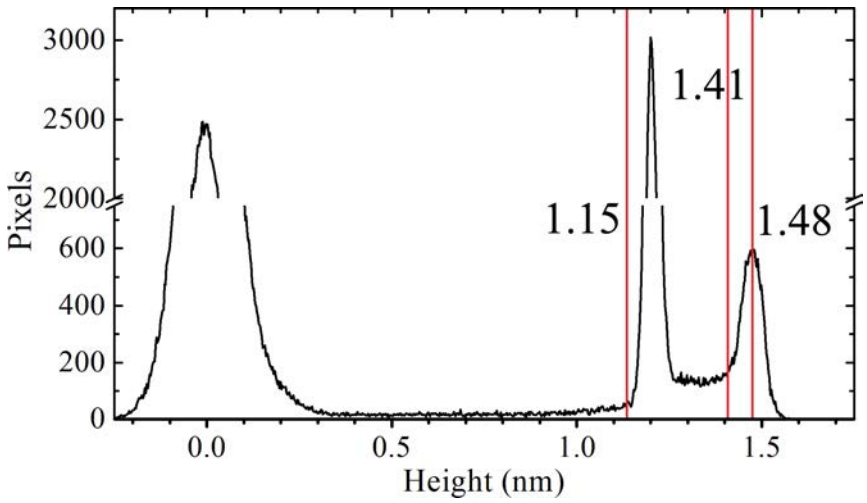

Figure 6.4 Example histogram used to calculate the In coverages on top of the Pb islands. Areas above 0.07 nm below a peak and above are considered to be part of the same level. Everything below that are the sides of the islands and should not contribute to the area calculation. This is a histogram of Figure 6.2 (f). The In layer is 0.28 nm above the Pb (111) film, very close to the 0.274 nm height for FCC In.

The In island density on 5 layers of Pb in Figure 6.1 was 0.0068 islands/nm^2 which lead to a diffusion barrier of 0.05 eV. 0.0054 islands/nm^2 is the In island density associated with the two 5 layer island in Figure 6.2 and that corresponds to a lower a diffusion barrier of 0.04 eV which is 20 percent lower than the result from Figure 6.1 but they agree that the 5-layer barrier is quite a bit lower than the 4-layer diffusion barrier. This larger difference could be due to the fact that the island in Figure 6.1 is twice as large and had a smaller percentage of In falling off of it. This may not have affected the 4 layer growths as much because the higher diffusion barrier mitigated its affects. The average distance between the outside ring of In islands to the nearest side of the Pb island average about 6 nm while on the 4-layer islands it was 4 nm. The diffusion barrier associated with the average island density is 0.04 eV.

The diffusion barriers that resulted from equation 6.17 are what was expected based on the island density but it is bit different than expectations based on previous results. Chan et al. [9] found that the Pb diffusion on Pb islands was faster on 4 layers of Pb than on 5 while the opposite is true here. The other major difference is that the diffusion barriers for Pb on Pb were 0.08 and 0.09 eV [10] for the 4- and 5-layer islands, respectively, while in the In on Pb case

they are estimated to be 0.05 and 0.04 eV. Different diffusion barriers for different types of adatoms is not surprising, though in the Fe on Pb case the diffusion barrier was higher on the stable height as well, 0.204 vs. 0.187 eV.[8] Also, reversing the trend for diffusion barrier from the 4 layer being 0.01 eV lower in Pb on Pb case to being 0.1 eV larger in the In on Pb case than the diffusion barrier on the 5 layer is quite the change.

One factor complicating the simple analysis above is that In is falling off of the Pb islands, which is in line with expectations because the step edge barrier tends to be smaller for heterogeneous systems.[31] Agreement is always good to see but it poses a problem for the calculations that were done because they depend upon a known and constant flux rate. With atoms falling off the effective flux rate is lower than what was used and variable so the barriers could be higher than what was calculated. This is because with In falling off the monomer density on the Pb film will be lower than the flux rate suggests. With all else being equal, having a lower monomer density reduces the island density because with fewer monomers on the surface new atoms are less likely to nucleate new islands. However, this logic says nothing about how much the monomer density will be affected and therefore might not have a large effect on the final island density. The fact that islands as large as 12,000 nm^2 have very similar densities to that of islands around 5,000 nm^2 and the fact that the average diffusion length of the atoms was quite a bit smaller than the size of the islands suggests the In falling off has little effect on the final island density.

The coverage on the shown 4-layer island, Figure 6.2 (a-e), after depositing 0.14 ML is just 0.024 ML and after 0.42 ML of deposition the coverage in Figure 6.2 (a) and 2 (f) is 0.26 and 0.27 ML, respectively. That means that approximately 80 and 15 percent of the In falls off in the first and second depositions, respectively, and that the two heights are affected roughly the same. This, in conjunction with the diffusion rate being low, indicates that the step edge barrier, ES (Ehrlich Schwoebel barrier), is on the order of the diffusion barrier, if not smaller.

Since both island heights have roughly the same amount of Pb falling off, it is not the reason that equation 6.17 resulted in the 5-layer island having a higher diffusion rate. Having In fall off is effectively lowering the flux rate but it is doing so equally for both heights.

Another possible reason for the weakened difference in island density is that charge between

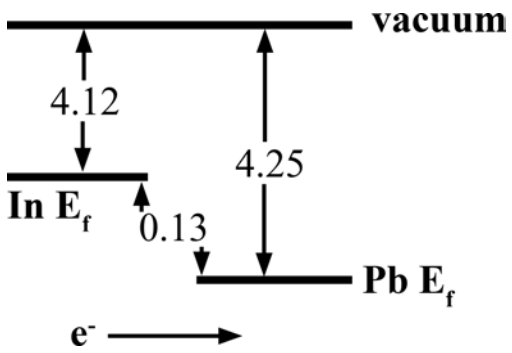

Figure 6.5 Pb(111)s polycrystalline work function is 4.25 eV, Ins is 4.12 eV. This means that charge will transfer to the Pb causing its Fermi Energy to increase.

the In and the Pb has shifted the Fermi Energy enough to make 4 layers of Pb slightly less unstable and 5 slightly more unstable. Yeh et al.[32] showed the charge transfer between Pb islands and the underlying substrate could change the preferred island heights. In this system all Pb islands were grown on Si(111) meaning that the stable heights are 5 and 7. However, In deposited on top of the Pb means that there will be some charge transfer between the In and the Pb. While this charge transfer is relatively small it could change the dynamics enough to make the island density on the 4 lower and higher on the 5.

6.5.4 Charge transfer

A main goal is to understand the factors that control the role QSE and height play in the degree they affect reactivity: why for Pb on Pb the effect is more than a factor of 60 while for In on Pb only factor of 2. This short section proposes a possible mechanism and some parameter that can possibly account for it and can be the subject of other future studies The stability of a film depends upon how close to the top level confined electrons energy(HOB) are to the Fermi Energy (see figure 1.1) so shift in the Fermi Energy can make a film less stable and more reactive. For the purposes of this quick comparison the Fermi Energy will be reported with respect to the vacuum potential, i.e., the work function of the metal. The work function of polycrystalline Pb and In are 4.25 and 4.12 eV respectively.[36]. The values of the work function depend upon the exposed crystal plane so using the polycrystalline value is not ideal but is sufficient to show the possible affect.

Pb has the larger work function, therefore, electrons will transfer to the Pb from the In, see Figure 6.5. This charge transfer will raise the Fermi Energy of the Pb film making the HOB of the 4-layer island slightly more stable and slow down surface diffusion. The Fermi Energy of the 4-layer film will shift slightly more than the 5-layer film and at the new position the 4-layer film will have most likely a lower density of states per unit area. Therefore, the 4-layer films diffusion will be affected more strongly.

6.5.5 Step edge barriers

One more number of interest can be estimated, the step edge barrier. After initial depositions there is a ring of area along the outside edge of the Pb islands where there are no In islands, a denuded zone. It is seen most prominently in Figure 6.2 (a, f, and k). It was assumed that all of the In that falls in the circle the ring surrounds will stick to one of the existing islands and therefore have no chance of falling off the Pb island and that all of the In that falls on the ring itself has an equal chance of reaching either the In islands or the edge of the Pb island. Determining how much of the In that lands on the ring stays on the island can be an indication about how large E_s is. Figure 6.6 has a line to indicate what was considered to be part of the ring. The line is not straight between islands because the goal was to outline where an atom could land and still reasonably reach the edge. An atom that fell in one of those deep gaps is likely to hit an island on its way out of the gap than it is to make it to the edge of the Pb island.

When depositing 0.28 ML of In to get to Figure 6.2 (a), from an initial coverage of 0.05 ML, only 35.7% of the In deposited onto the ring stayed on the Pb island while 64.2% of the In that landed on the ring from a 0.42 ML deposition stayed on going to Figure 6.2 (b). Doing the same calculation for the 5-layer island's step from Figure 6.2 (f) to (g) shows that 37.8% of the In that hits the ring stays on the island. The numbers are rather disparate but nothing should be read into it, as deposition occurs the islands grow changing the dynamics of atomic movement. Also, the width of the ring changes a great deal from minimum to maximum value and it is not unreasonable to think that a change in behavior could accompany the change in average width. What can be taken from it is that there is an even chance for the In to attach

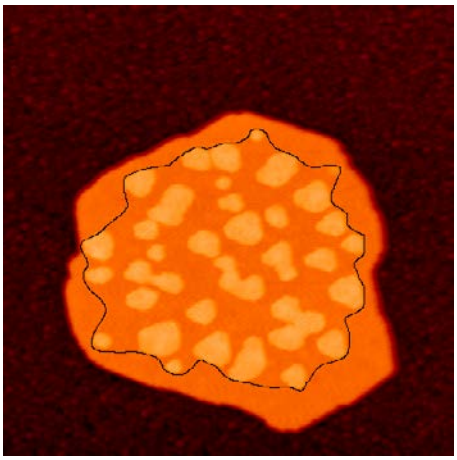

Figure 6.6 5-layer Pb island with the area in which arriving atoms are estimated to join an island 100% of the time circled. The area outside of this circle is a ring in which atoms can either fall off the Pb island or join one of the In islands. The coverage is 0.26 ML.

to an existing island or to fall off indicating that the step edge barrier is on the same order as the diffusion barrier.

6.5.6 High coverage In depositions

Figure 6.2 (c, h, and m) shows that continuing to deposit In results in a perfectly completed layer of In on top of both Pb island heights. Nucleation of a 2^{nd} In layer is usually quick on the formerly 4-layer thick Pb islands with it occurring shortly after the first layer is completed or even sometimes before. While the 2^{nd} layer on the 5+1-layer Pb islands could take depositions of 0.42 ML or more to nucleate. The 5+1-layer island in Figure 6.2 (row f) took almost exactly 0.42 ML (6 min) to nucleate an island on the second layer while the average is higher than that because some 5 layer islands never have a 2^{nd} layer nucleate in the center like that (more on this later), Figure 6.2 (row k).

The dramatically reduced nucleation rate indicates one or both of the following: E_d is small or $i_c > 1$. It has been reported in Chen et al.[14] that diffusion of In on In wetting layer (on Pb α-phase) is very fast at 150 K so a small E_d is in line with expectations. Having $i_c > 1$ is not expected and does not fit with the fact that 2^{nd} layer islands continue to nucleate on the formerly 4-layer islands. Also, Heinrichs et al.[26] and the papers they reference state that for

$i_c < 3$ the ability to nucleate on an island depends upon fluctuations. It basically comes down to pure chance if two atoms are on the surface at the same time and collide. Loosely speaking, that is what is seen on the 5-layer islands, they have anywhere from 0 to 3 islands nucleated. Not exactly hard proof but it fits with expectations and makes sense. E_s could also be small but that alone could not guarantee just a few nucleation events or guarantee a lot of In will fall off.

Could In have moved up from the wetting layer? In tends to have good mobility on In and once 3D growth commences on the Pb island the In has no problem climbing up the sides of the In from the Pb/In island (as in Figure 6.2 (j)) but since none of the islands grew substantially more than they should based on how much In landed on them it is impossible to prove that In climbed up the sides of the Pb/In islands from the wetting layer.

It was mentioned earlier that not all 5 layer islands have a 2^{nd} layer of In nucleate on them, that is because some of the In that "falls" off of the Pb island goes to growing the island laterally. This is most easily seen in its pure form (no further 3D growth) between Figure 6.2 (h) and (i). The all In sections of the island are approximately 0.1 nm taller than the mostly Pb parts but it is not a sharp change and neither surface is particularly flat, both vary by at least 0.1 nm across the surface.

It is not too surprising that the In behaves quite differently on top of the all In sections of the islands, in Figure 6.2 (j) all but one nucleation on the 5-layer island in the image that occurred, did so on the all In sections whose width was 4 nm wide or wider.

There are a number possible things that make the In sections of the islands much more susceptible to nucleation but they all have one thing in common, raising the monomer density. Some possibilities: diffusion is low, the barrier to fall off those sections is higher, a small barrier prevents In from going back to the Pb sections, and some In is coming up the sides of the island. Given the results of Chen et al.[14] and the current observations of In climbing up at least 6 layers it is unlikely that the diffusion rate on the all In sections is lower than it is on the mostly Pb sections. Given that the 3D growth does not readily spread to the mostly Pb sections there is almost certainly an energy difference between the two parts which is evidence for there being a barrier there. There is direct evidence that In climbs up the sides of the In islands during the

3D growth but none to suggest where that In comes from or how much it happens for lower portions of the island since in no deposition did the island as a whole grow significantly more than was deposited directly onto it.

If In was going up the sides of the island it was not very much because In mobility on the substrate was greatly reduced once In islands started to form. The island density on the wetting layer is 0.055 islands/nm^2 in Figure 6.2 (b and g) which means that, on average, an In atom could not go more than 2.4 nm before running into an existing island, and this is an upper limit since the islands are not actually point islands like the quick calculation assumed. It is pretty clear, even as early as just 0.84 ML deposited that there would be no large movement of In across the surface.

6.5.7 Wetting layer

In's reaction to the Pb wetting layer is relatively odd. It is not its usual very mobile self that it is on Pb α-phase or Si(111) 7 x 7.[39] Instead it forms little blobs no higher than 0.3 nm, they are similar to but slightly larger than blobs seen in In on Pb-α phase[39] as well as Pb on In $\sqrt{31}$. The big difference comes into play when more In is deposited. Instead of the In quickly flowing to islands the blobs collect the In and start to grow. After they reach a height of around 5 layers they start to grow 3 dimensionally, growing very tall and no longer having a flat top. Because of all of these small islands growing, In mobility on the surface is greatly reduced. Even at higher coverages like those in Figure 6.2 (column d) it is uncommon for the distance between two adjacent islands to be more than 8 nm. Since there is less In on the Pb islands than falls on them it is safe to say that more In falls of the islands than joins them, at least at the lower coverages already discussed. This means that the small In islands on the wetting layer are efficient at grabbing new In so the average diffusion distance for them is likely less than the distance between islands, or less than 8 nm. Therefore, any In that falls off of the Pb islands does not travel more than about 8 nm so calculating the flux rate based on areas at least 10 nm away from a Pb island should give a consistent and unbiased result.

6.6 Conclusions

In depositions onto 4- and 5-layer Pb islands produce a similar result as that reported by Binz et al.[10] and Ma et al.[8] with an effect halfway between the two in strength – a 2 times difference in island density. This difference is caused by the current experiments being done at 110 K and using the lighter and more mobile element, In. The Ehrlich-Schwoebel barrier has roughly the same value as the diffusion barrier, the barriers are all at or above 0.04 eV. Nucleation of the 2^{nd} layer of In is much harder than the first with nucleations on the all In sections being preferred, and 3D growth is favored as it is in Chen et al.[14]

The fact that such a large difference in island density can be seen at a higher temperature and in a heterogeneous system is further evidence that QSE have an active future in shaping future catalysts.

References

[1] M. Hupalo, S. Kremmer, V. Yeh, L. Berbil-Bautista, E. Abram, and M. C. Tringides, Surf. Sci. **493**, 526 (2001), ISSN 0039-6028, URL http://www.sciencedirect.com/science/article/pii/S0039602801012626. 6.2

[2] F. Krok, F. Buatier de Mongeot, M. Goryl, J. J. Kolodziej, and M. Szymonski, Phys. Rev. B **81**, 235414 (2010). 6.2

[3] M. Ja*l*ochowski, M. Hoffmann, and E. Bauer, Phys. Rev. B **51**, 7231 (1995). 6.2

[4] A. G. Danese, F. G. Curti, and R. A. Bartynski, Phys. Rev. B **70**, 165420 (2004). 6.2

[5] L. Aballe, A. Barinov, A. Locatelli, S. Heun, and M. Kiskinova, Phys. Rev. Lett. **93**, 196103 (2004). 6.2

[6] L. Aballe, A. Barinov, N. Stoji?, N. Binggeli, T. O. Mentes, A. Locatelli, and M. Kiskinova, Journal of Physics: Condensed Matter **22**, 015001 (2010), URL http://stacks.iop.org/0953-8984/22/i=1/a=015001. 6.2

[7] A. Hellman, B. Razaznejad, Y. Yourdshahyan, H. Ternow, I. Zori, and B. Lundqvist, Surface Science **532535**, 126 (2003), ISSN 0039-6028, ¡ce:title¿Proceedings of the 7th International Conference on Nanometer-Scale Science and Technology and the 21st European Conference on Surface Science¡/ce:title¿, URL http://www.sciencedirect.com/science/article/pii/S0039602803001110. 6.2

[8] L.-Y. Ma, L. Tang, Z.-L. Guan, K. He, K. An, X.-C. Ma, J.-F. Jia, Q.-K. Xue, Y. Han, S. Huang, et al., Phys. Rev. Lett. **97**, 266102 (2006), URL http://dx.doi.org/10.1103/PhysRevLett.97.266102. 6.2, 6.5.1, 6.5.3, 6.6

[9] T. Chan, C. Z. Wang, M. Hupalo, M. C. Tringides, and K. M. Ho, Phys. Rev. Lett. **96**, 226102 (2006). 6.2, 6.5.3

[10] S. M. Binz, M. Hupalo, and M. C. Tringides, Phys. Rev. B **78**, 193407 (2008). 6.2, 6.4, 6.5.1, 6.5.3, 6.6

[11] S. M. Binz, M. Hupalo, and M. C. Tringides, Journal of Applied Physics **105**, 094307 (pages 4) (2009), URL http://link.aip.org/link/?JAP/105/094307/1. 6.2

[12] M. Hupalo and M. C. Tringides, Phys. Rev. B **75**, 235443 (2007). 6.3

[13] Z. Kuntova, M. Hupalo, Z. Chvoj, and M. C. Tringides, Phys. Rev. B **75**, 205436 (2007). 6.3

[14] J. Chen, M. Hupalo, M. Ji, C. Z. Wang, K. M. Ho, and M. C. Tringides, Phys. Rev. B **77**, 233302 (2008). 6.3, 6.5.6, 6.6

[15] R. Fink, R. Wesche, T. Klas, G. Krausch, R. Platzer, J. Voigt, U. Whrmann, and G. Schatz, Surface Science **225**, 331 (1990), ISSN 0039-6028, URL http://www.sciencedirect.com/science/article/pii/003960289090454G. 6.5.1

[16] G. Schatz, R. Fink, K. Jacobs, U. Kohl, G. Krausch, J. Lohmller, B. Luckscheiter, B.-U. Runge, and U. Whrmann, Physica Scripta **1993**, 554 (1993), URL http://stacks.iop.org/1402-4896/1993/i=T49B/a=030. 6.5.1

[17] C. D. Van Siclen, Phys. Rev. B **51**, 7796 (1995), URL http://link.aps.org/doi/10.1103/PhysRevB.51.7796. 6.5.1

[18] M. Hupalo and M. C. Tringides, Phys. Rev. B **65**, 115406 (2002). 6.5.1

[19] B. Fischer, Ph.D. thesis, Ecole Polytechniqie Federale De Lausanne (1998). 6.5.1, 6.5.2

[20] J. Evans, P. Thiel, and M. Bartelt, Surf. Sci. Rep. **61**, 1 (2006), ISSN 0167-5729, URL http://www.sciencedirect.com/science/article/pii/S0167572906000021. 6.5.1

[21] M. Bartelt, L. Perkins, and J. Evans, Surface Science **344**, L1193 (1995), ISSN 0039-6028. 6.5.1

[22] B. Müller, L. Nedelmann, B. Fischer, H. Brune, and K. Kern, Phys. Rev. B **54**, 17858 (1996), URL http://link.aps.org/doi/10.1103/PhysRevB.54.17858. 6.5.1

[23] J. G. Amar and F. Family, Phys. Rev. Lett. **74**, 2066 (1995). 6.5.1, 6.5.2

[24] H. Brune, Surf. Sci. Rep. **31**, 125 (1998), ISSN 0167-5729, URL http://www.sciencedirect.com/science/article/pii/S0167572999800016. 6.5.1, 6.5.2, 6.5.3

[25] J. Krug, P. Politi, and T. Michely, Phys. Rev. B **61**, 14037 (2000). 6.5.1

[26] S. Heinrichs, J. Rottler, and P. Maass, Phys. Rev. B **62**, 8338 (2000). 6.5.1, 6.5.6

[27] J. Tersoff, A. W. Denier van der Gon, and R. M. Tromp, Phys. Rev. Lett. **72**, 266 (1994), URL http://link.aps.org/doi/10.1103/PhysRevLett.72.266. 6.5.1

[28] J. M. Pomeroy and J. D. Brock, Phys. Rev. B **73**, 245405 (2006). 6.5.2, 6.5.2

[29] J. G. Amar, F. Family, and P.-M. Lam, Phys. Rev. B **50**, 8781 (1994), URL http://link.aps.org/doi/10.1103/PhysRevB.50.8781. 6.5.2

[30] J. A. Venables, G. D. T. Spiller, and M. Hanbucken, Rep. Prog. Phys. **47**, 399 (1984), URL http://stacks.iop.org/0034-4885/47/i=4/a=002. 6.5.3

[31] K. Bromann, H. Brune, H. Rder, and K. Kern, Phys. Rev. Lett. **75**, 677 (1995). 6.5.3

[32] V. Yeh, L. Berbil-Bautista, C. Z. Wang, K. M. Ho, and M. C. Tringides, Phys. Rev. Lett. **85**, 5158 (2000). 6.5.3

[33] A. Mans, J. H. Dil, A. R. H. F. Ettema, and H. H. Weitering, Phys. Rev. B **66**, 195410 (2002).

[34] C. Kittel, *Introduction to solid state physics* (Wiley, 2005), ISBN 9780471415268, URL http://books.google.com/books?id=kym4QgAACAAJ.

[35] S. Ciraci and I. P. Batra, Phys. Rev. B **33**, 4294 (1986).

[36] Science, *Handbook of Chemistry and Physics* (CRC Press, 1987). 6.5.4

[37] N. W. Ashcroft and N. D. Mermin, *Solid State Physics* (Sanders College Publishing, 1976).

[38] Z. Zhang, Q. Niu, and C.-K. Shih, Phys. Rev. Lett. **80**, 5381 (1998).

[39] J. Chen, Ph.D. thesis, Iowa State University (2009). 6.5.7

CHAPTER 7. Pb on In $\sqrt{3}$, In $\sqrt{31}$, and In "1x1"

7.1 Abstract

SPA-LEED was used to investigate Pb deposited on top of three In phases, $\sqrt{3}$, $\sqrt{31}$, and "1 x 1" which were grown on Si(111). Pb grown on In $\sqrt{31}$ exhibited quantum size effects and has a preferred height of 2 and then 4 ML between 170 and 215 K. This was confirmed with STM. Pb crystals on In $\sqrt{31}$ aligned along 4 different directions, Si[$1\bar{1}0$] and 7.2°, 8.9°, and 25° clockwise and counterclockwise to Si[$1\bar{1}0$]. This was interpreted through a lattice matching model between the adsorbate and the substrate. Pb on top of In $\sqrt{3}$ aligned along Si[$11\bar{2}$] and Si[$1\bar{1}0$]. Pb on In "1 x 1" aligned along Si[$1\bar{1}0$]. All alignments depended upon temperature.

7.2 Introduction

The Pb and In on Si(111) system has produced a wide range of interesting phases and results. Including, strongly preferred 7 layer Pb islands on Si(111),[1,2] the devil's staircase phases of Pb on Si(111),[3] and Pb on In 4 x 1 which produced Pb islands with preferred widths and heights while growing very long.[4] One of the remaining phases of particular interest is In $\sqrt{31}$ on Si(111) because it is aligned off of a Si symmetry axis, similar to In $\sqrt{3}$ x $\sqrt{3}$ R30°[5] but even that is aligned along Si[$11\bar{2}$]. In $\sqrt{31}$ It has two different domains with each rotated 8.9° from the Si[$1\bar{1}0$] direction.[6] In general rotations of single layers is not special, they were first theorized in 1977 by Novaco and McTague[7] and have since been observed in many systems.[8–10] However, it does provide an opportunity to approach the Pb, In, and Si system in a slightly different way, allowing comparisons between rotation angles and lattice mismatch.

In on Si(111), like Pb, has a number of two dimensional phases that develop in the sub-monolayer regime. Figure 7.1 (a) shows a phase diagram by Kraft et al.[5] and the rest of the

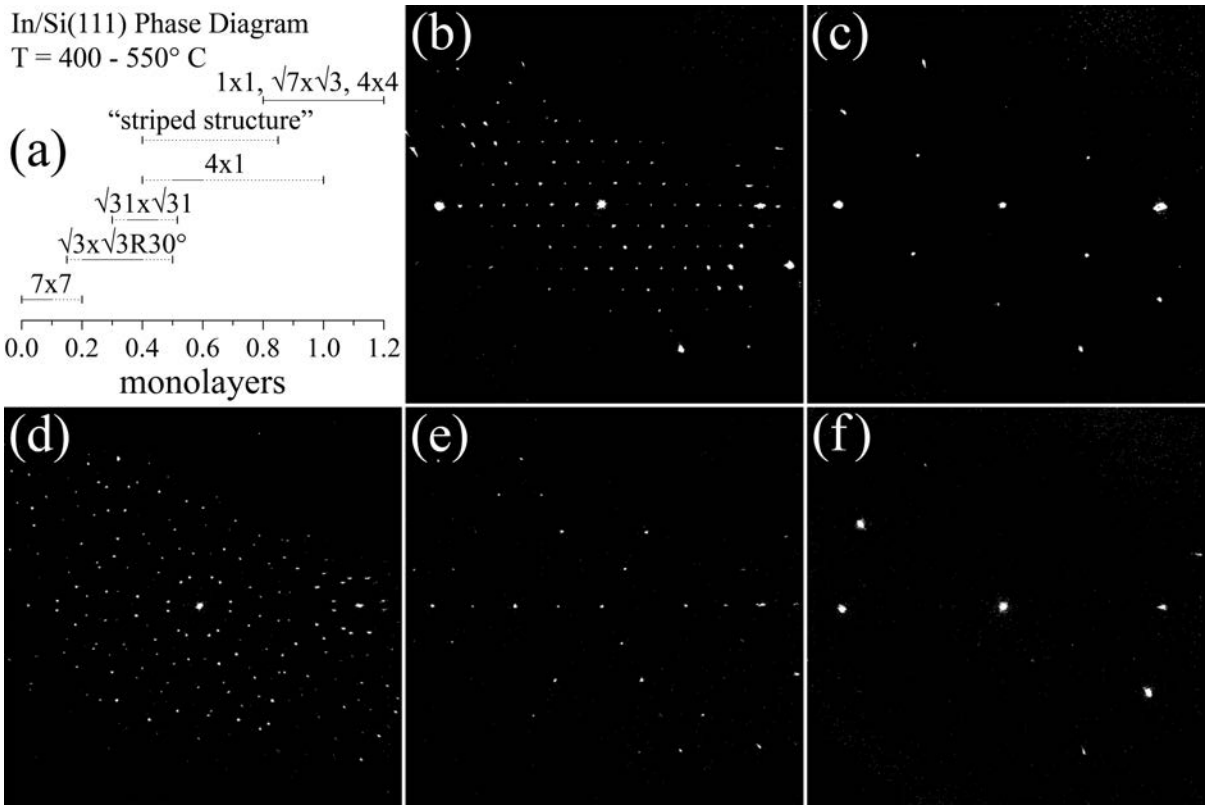

Figure 7.1 (a) Phase diagram of submonolayer In phases on Si (111), modified fromKraft et al.[5]. (b-f) are 2D SPA-LEED patterns of some of the phases seen in the phase diagram. (b) Si (111) 7 x 7 reconstruction, (c) In $\sqrt{3}$, (d) In $\sqrt{31}$, (e) In 4 x 1, (f) In "1 x 1". (c) and (e) were taken by Michael Yakes in 2002. All data was taken at 38 eV, the specular is in the center of each pattern.

figure is composed of SPA-LEED images of the phases discussed in this chapter. Kraft et al.[5] was not claiming that each phase has a large range of coverages but that they show up on the surface at a large range of coverages. This is expected since there is no single surface structure associated with 0.7 ML so the phases above and below it are required to use all of the In atoms using the least amount of energy possible. It is still possible to create large single phase domains but it requires careful control of the coverage and temperature of the sample.[11,12] In terms of coverage, In $\sqrt{31}$ x $\sqrt{31}$ R8.9° (In $\sqrt{31}$) is wedged between In 4 x 1 (In 4 x 1) and In $\sqrt{3}$ x $\sqrt{3}$ R30° (In $\sqrt{3}$). Saranin et al.[6] and reference 34[13] from his paper have more specific estimates of the coverage of the phases with In $\sqrt{31}$ at 0.55 ML and $\sqrt{3}$ at 1/3 ML. 4 x 1 has a coverage of 1 ML but was hotly debated for a while. Saranin et al.[6], in the same study where

they found the $\sqrt{31}$ coverage, said that the coverage of In 4 x 1 was 0.75 ML. Other models suggested the coverage was as low as 0.5 ML[5,14] or as high as 1.0 ML.[15] In 1999 Bunk et al.[16] used surface x-ray diffraction and found that a model with 4 In atoms per 4 x 1 unit cell fit the data best. Mizuno et al.[17] followed up in 2003 with LEED based I-V analysis comparing 45 different models derived from the above experiments and one not yet mentioned[18] using transmission electron microscopy. Mizuno et al.[17]'s conclusion is that the 1.0 ML model from Bunk et al.[16] is the most accurate. The last phase to be addressed in this paper is In "1 x 1" R30°, its form and coverage are still under debate but it is either a phase in and of itself or composed of two different $\sqrt{7}$ x $\sqrt{3}$ structures with a coverage of between 1 and 1.2 ML.[19] Evidence gathered in the present experiments suggests it is a unique phase as was Pavlovska et al.[20]'s conclusion because "1 x 1" spots are seen without any $\sqrt{7}$ x $\sqrt{3}$ spots but this is not a central topic of the dissertation so it will not be dwelled on. Pavlovska et al.[20]'s conclusion was that the "1 x 1" R30° phase had a coverage of 1.08 ML based on the size of the unit cell. However, "1 x 1" exhibits a number of odd traits, for example, Ofner et al.[21] showed that the "1 x 1" spots stick around even after very large In depositions suggesting it is not just a single layer.

Figure 1 (b-f) shows the Si(111) 7 x 7 reconstruction and each of the aforementioned In on Si(111) phases as seen by Spot Profile Analysis - Low Energy Electron Diffraction (SPA-LEED), in order of increasing coverage . They will be discussed in more detail later.

7.3 Experiment

SPA-LEED was used to study Pb islands grown on top of In $\sqrt{31}$ and In $\sqrt{3}$ and to a lesser extent In "1 x 1" R30° at temperatures ranging from 170 K to RT. SPA-LEED was used because of its strength at reporting long range order of films as well as the atomic structure of those films – including the relative orientation between the various atomic structures on the surface. Lastly, its ability to produce good statistics about surface structures was used to determine the heights, widths, and spacing of islands on the surface. See Chapters 2 and 3 for details.

The experiments were done on the aforementioned In films which were grown on the Si(111)

7 x 7 reconstruction. The 7 x 7 was prepared by flashing the sample to 1520 K through electron bombardment, allowing the crystal to cool to 1070 K, keeping it there for 30 seconds, and then allowing the crystal to cool to approximately RT. The In films were prepared by depositing 0.6 ML of In onto a RT Si (111) 7 x 7 surface and then annealing the sample with electron bombardment from a filament with 4.9 W of power for 4 minutes to create In $\sqrt{3}$ (about 820 K) and 2.3 W for about 15 minutes to create In $\sqrt{31}$ (about 810 K).[20] If the surface was not entirely In $\sqrt{3}$ or In $\sqrt{31}$ further annealing or depositions were required. For example, if the sample had In $\sqrt{31}$ and In 4 x 1 on the surface but the goal was In $\sqrt{31}$ the sample would be annealed for a bit longer to desorb more of the In. This results in a surface with more In $\sqrt{31}$. The long anneals at low power were designed to make the sample's temperature be as uniform as possible to minimize the amount of "extra" phases. To create In "1 x 1" R30° 1.2 ML of In was deposited and then the sample was annealed to around 570 K.[20,22] The sample was then cooled with liquid nitrogen to the appropriate temperature and Pb was deposited at a rate of 0.1 ML/min. The annealing experiments were done in one of two ways, either heating via a filament or by simply letting the sample warm up to room temperature naturally. All scans were done at 38 eV unless otherwise noted.

To correct for the persistent distortion in the 1-D scans related to barrel distortion[23] the Si(111) 7 x 7 spots were used to correct the locations of the Pb spots in conjunction with the still visible Si (10) spots. The 7 x 7 spot locations are a known quantity and can be used to calculate the magnitude of the distortion at any point along the scan. The exact algorithm was to pick the two 7 x 7 spots closest to the relevant Pb spot and then calculate the correction that moves those two spots into their theoretical position. This function is a straight line which was then shifted to the right or left to make sure that the Si (10) spot is at 100% BZ.

This method will be referred to as the 'normal correction' for 1D scans later in the chapter. It should be noted that this method is only accurate for local spots since the distortion itself is not linear. It is also important to note that the correction can only be applied to scans that were produced with the same electron energy and focusing settings. This is one of the reasons that 38 eV was used for every scan. To produce the 1D scans in the figures a 3^{rd} order polynomial was used to approximate the local correction and allow for a continuous function. The spot

locations reported in the paper and on the figures are from the local correction described above.

The normal 1-D correction method does not work well when dealing with In $\sqrt{31}$ because those scans are 8.4° counter-clockwise of the Si[1$\bar{1}$0]. This is unavoidable since there are not many Si 7 x 7 spots along that direction so it was used anyway with the understanding that the correction becomes less and less applicable the further away from the specular the spot is. Therefore, 80% BZ 2D scans of the Si 7 x 7 and In $\sqrt{31}$ patterns were taken of the area that the Pb spots would appear. The scans were 401 x 401 pixels so each pixel represented about 0.2% BZ. The 2D correction was applied in three ways where possible and the results were averaged to limit the error caused by having a maximum resolution of 0.2% BZ. In most cases there was an In $\sqrt{31}$ spot almost exactly where the Pb spot is so the distortion of the $\sqrt{31}$ spot was directly subtracted from the Pb spot. This same method was applied with 7 x 7 spots but did not work in all cases because the 7 x 7 spot locations were not always close to the Pb spots. The third method was to choose two 7 x 7 spots such that they were close to the Pb spots and so that all were on a straight line. The change in correction between the two Si spots was assumed to be linear and the correction with the appropriate value being applied to the Pb spot.

7.4 Pb on In $\sqrt{31}$

7.4.1 Introduction

In $\sqrt{31}$ does not appear to be particularly stable because it is difficult to create a surface with just In $\sqrt{31}$ on it.[5] Temperatures as low as 640 K have been shown to allow In to desorb but the temperature must be high enough to allow the underlying Si to reconstruct to allow the In $\sqrt{31}$, more on this in a bit. However,Wei et al.[12] were able to create perfect films by controlling the temperature very accurately with direct heating and by controlling the deposition accurately. This method still required further annealing or depositions to get the coverage just right. Through practice the percentage of non-In $\sqrt{31}$ phases on the surface were minimized and experiments were not continued unless there was no visible sign of In 4 x 1 of In $\sqrt{3}$ on the surface.

Figure 2 (a) shows the real space diagram of In $\sqrt{31}$ as reported by Saranin et al.[6] To determine the real space diagram Saranin et al.[6] took a series of STM images at different coverages. The different coverages resulted in different percentages of the possible phases. They knew that $\sqrt{3}$ has a coverage of 1/3 ML and were able to determine the coverages of the other two phases involved, $\sqrt{31}$ and 4 x 1. These calculations lead to a coverage of 0.53 $\pm$0.02 ML, in terms of the unreconstructed Si 1 x 1 surface. To determine the coverage of the top Si layer Saranin et al.[6] looked at data in the center of a very large Si terraces, no number was given but images related to this topic had terraces on the order of 500 nm. The idea was that as Si was pulled out of the 7 x 7 reconstruction (with a coverage of 2.08 ML) it had to go somewhere, as long as it could be found and counted that would provide the coverage of the interface layer. Si islands did form with a height of 2 layers so the interface layer plus the area covered by the islands should be 2.08 ML. Doing the math resulted in a coverage of 0.88 +/-0.03 ML for the interface layer.

According to the atomic resolution images of the In $\sqrt{31}$ there are 17 locations with empty electron levels. Assuming all of those are atoms results in a coverage of 0.55 ML (17 In atoms / 31 Si atoms), just above but within the range of the experimental results. The atoms are arranged in two triangles, one of 6 atoms and the other containing 10 with the 17^{th} atom residing at the corners of the unit cell. Saranin et al.[6] was also able to determine that the corner atoms occupy Si T4 sites and that the central atom, or protrusion as Saranin et al.[6] is careful to call it in the 10 atom triangle, is located in an H3 site. He came to this conclusion by comparing atom locations to the nearby In $\sqrt{3}$ atom locations. The rest of the atoms are not in any normal positions of a Si(111) lattice. Saranin et al.[6] came up with the model shown in Figure 7.2 by satisfying the coverage and atom locations described above. It also manages to have no dangling bonds with most of the In atoms only bonding with the top layer of Si except the three corner atoms of the 6 atom subunit which also bonds to a Si atom in the second layer.

Starting with Saranin et al.[6]'s real space model it should be possible to calculate the reciprocal lattice vectors to duplicate the experimental diffraction pattern. This math will be done in terms of the Si(111) unit cell to make the math simpler and the $[1\bar{1}0]$ direction will be

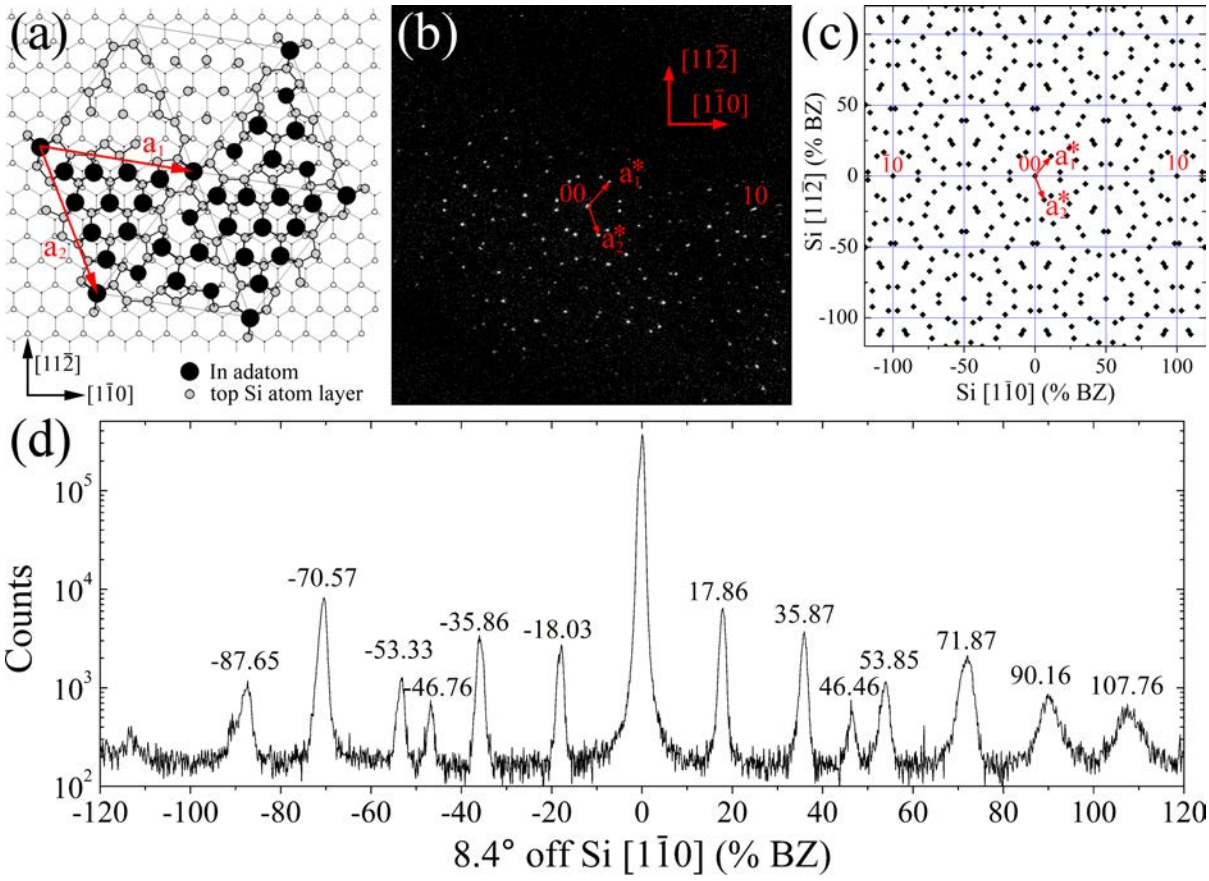

Figure 7.2 (a) Real space model of In $\sqrt{31}$, slightly modified fromSaranin et al.[6]. The unit cell vectors a_1 and a_2 are shown. (b) SPA-LEED pattern of In $\sqrt{31}$ with the reciprocal lattice vectors marked. (c) Calculated In $\sqrt{31}$ pattern based onSaranin et al.[6] model as seen in (a). It matches (b) very well. (d) 1D scan along a direction 8.4° off of Si [1$\bar{1}$0], along the In $\sqrt{31}$ unit cell. The peaks are every $100/\sqrt{31}$% exactly as expected. The spots at around 46.5% BZ are from a different orientation of the $\sqrt{31}$ lattice that just happens to be near the 8.4° line so they are not spaced the same as the rest of the spots. The two sides are not symmetric due to the targeted correction used that was only applied to the right side. The Si 00 and 10 spots are labeled. See text for details.

the positive x direction. The real space unit cell vectors are:

$$\overrightarrow{a_1} = 5.5\hat{x} - \frac{\sqrt{3}}{2}\hat{y} \tag{7.1}$$

$$\overrightarrow{a_2} = 2\hat{x} - 3\sqrt{3}\hat{y} \tag{7.2}$$

Using equations 2.4-2.6, remember that a_3 is in the $\hat{z}$ direction:

$$\overrightarrow{b_1} = 2\pi\frac{a_2 \times a_3}{a_1 \cdot (a_2 \times a_3)} \tag{7.3}$$

$$\overrightarrow{b_1} = 2\pi\frac{\left(2\hat{x} - 3\sqrt{3}\hat{y}\right) \times \hat{z}}{\left(5.5\hat{x} - \frac{\sqrt{3}}{2}\hat{y}\right) \cdot \left(\left(2\hat{x} - 3\sqrt{3}\hat{y}\right) \times \hat{z}\right)} \tag{7.4}$$

$$\overrightarrow{b_1} = 2\pi\frac{-2\hat{y} - 3\sqrt{3}\hat{x}}{\left(5.5\hat{x} - \frac{\sqrt{3}}{2}\hat{y}\right) \cdot \left(-2\hat{y} - 3\sqrt{3}\hat{x}\right)} \tag{7.5}$$

$$\overrightarrow{b_1} = 2\pi\frac{-2\hat{y} - 3\sqrt{3}\hat{x}}{-\frac{31}{2}\sqrt{3}} \tag{7.6}$$

$$\overrightarrow{b_1} = \frac{12\pi}{31}\hat{x} + \frac{8\pi}{93}\sqrt{3}\hat{y} \tag{7.7}$$

$$\overrightarrow{b_2} = 2\pi\frac{a_3 \times a_1}{a_1 \cdot (a_2 \times a_3)} \tag{7.8}$$

$$\overrightarrow{b_2} = 2\pi\frac{\hat{z} \times \left(5.5\hat{x} - \frac{\sqrt{3}}{2}\hat{y}\right)}{\left(2\hat{x} - 3\sqrt{3}\hat{y}\right) \cdot \left(\hat{z} \times \left(5.5\hat{x} - \frac{\sqrt{3}}{2}\hat{y}\right)\right)} \tag{7.9}$$

$$\overrightarrow{b_2} = -\frac{2\pi}{31}\hat{x} - \frac{22\pi}{93}\sqrt{3}\hat{y} \tag{7.10}$$

The SPA-LEED data is in terms of the Si(111) recirpocal unit cell whose length is 1.89 Å^{-1} so b_1 and b_2 must be divided by that to scale the vectors properly. Half of the spots shown in Figure 7.2 (c) are associated with the scaled lattice vectors. The other half are from the other orientation of the $\sqrt{31}$ lattice, rotated (8.94°*2) 17.88° counter-clockwise from the first lattice. The result is a pattern that matches the experimental data found in Figure 7.2 (b). The first ring of spots in Figure 7.2 (b) is at about 18% BZ from the specular right in line with the $1/\sqrt{31} = 17.96\%$ BZ expected value. However, 2D scans of this scale are not ideal for determining lattice vectors because each pixel represents about 0.6% BZ. For that reason, 1-D scans are used.

Figure 2 (d) shows a 1-D scan along a line 8.4° below the Si[1$\bar{1}$0] direction. After applying the normal correction described above one more corrective step was taken to make up for the

fact that this line is not along Si[1$\bar{1}$0] like the 7 x 7 scan used to correct it. The 107.76% spot and the specular were set to the values they would be if this surface is indeed In $\sqrt{31}$ and a linear correction was applied based on those two spots. After that, there is a spot every $1/\sqrt{31}$, or 17.96% BZ. All spots from -35.86% BZ up through 107.76% BZ are very close to the calculated values proving that it was In $\sqrt{31}$, all spots are within 0.1% BZ except the 90.16% spot which is 0.36% BZ off. Below -53% BZ the secondary correction started to be less and less accurate resulting in some spots being quite a bit off. The spots around 46.46% BZ are not a multiple of $1/\sqrt{31}$, it is a spot from a different orientation of $\sqrt{31}$ that just happens to fall close to the 8.4° line. Based on the spot location calculations the spot should be at 47.52% BZ and 10.2° off from the Si[1$\bar{1}$0] line. This spot corresponds to 2 $\vec{b_1}$ and 1 $\vec{b_2}$ of the other lattice.

7.4.2 Pb depositions

As Pb is deposited at 170 K most of the In $\sqrt{31}$ spots disappear by 0.5 ML coverage with only the spots at 17.96% BZ staying until at least 1.5 ML of Pb has been deposited. Around 1.5 ML the first Pb spot appears along Si[1$\bar{1}$0] and approximately 8.5° clockwise and counterclockwise to it. This suggests that the wetting layer is roughly 1.3 ML because Pb crystals have had a chance to form and grow large enough to be seen in the diffraction pattern by 1.5 ML. Further depositions leads to spots showing up at 25° and 35° off the [1$\bar{1}$0] direction, an unusual though not unprecedented occurrence in the Pb and In on Si(111) system. Pb on Si and Pb on α- and β-phase all have slight rotations of up to 6° off of the Si[1$\bar{1}$0] direction but none are off by 25°. Note that the spots at 35° are actually 25° spots by symmetry (the next [1$\bar{1}$0] equivalent vector is 60° off of [1$\bar{1}$0]). Figure 7.3 (d) is a 1D scan along the Si[1$\bar{1}$0] direction of 3.5 ML of Pb deposited at 170 K and it shows the new spots at about 110.7% BZ. The correction of the spots in the 2D pattern followed the method described earlier in the chapter. Figure 7.4 includes information that was used to do the corrections based on the In $\sqrt{31}$ spots. Table 7.1 shows the average of the results for all three corrections. The average distance from the specular is 110.5% BZ, 0.8% larger than normal Pb crystal which is 0.384 nm / 0.35 nm*100 = 109.7% BZ according to equation 2.22. Therefore, the experimental value is just beyond the standard deviation of 0.6% BZ. However, since the resolution of the image

Average Spot Locations (% BZ)		Distance	Angle
x	y	(% BZ)	(degrees)
-110.2	0	110.2	0
-109.6	16.1	110.7	8.36
-99.2	46.8	109.7	25.26
-90.4	63.7	110.5	35.17
109.9	16.6	111.2	8.58
110.4	0.9	110.4	0.48
108.9	-16.8	110.1	-8.75
101.0	-47.7	111.7	-25.27
90.2	-63.1	110.0	-34.99

Table 7.1 Pb spot locations based on 2D SPA-LEED patterns. The distance from the specular is 110.5 ±0.6% BZ which indicates that the spots are indeed Pb. The plus/minus is from the standard deviation. The angles are 0.3°, 8.6°, 25.3°, and 35.0° away from Si[1$\bar{1}$0]. The data was collected from images with 3.5 ML of Pb deposited at 170K.

is 0.2% BZ per pixel and the center of the peaks were picked by hand an additional 0.4% BZ error was present. Therefore this is indeed Pb(111) on the surface.

The large diffuse spots at ±8.5° and 0° indicate that the islands have a relatively wide distribution of alignments near those angles. The spots at 25° are much more compact and therefore the island alignment is much more uniform. An image of this is seen in Figure 7.3 (a) where the width of the 25° spots at their base are 3.6% BZ and the ±8.5° and 0° spots are an average of 6.4% BZ wide at the base. The 25° spots continue to gain intensity until at least 6 ML, Figure 7.3 (b). Above 6 ML the intensity stays roughly the same until at least 11.5 ML. The rotations of the spots are seen at least through 11.5 ML at 195 K. Upon annealing all spots get more intense until about 265 K when the 25° spots decrease in intensity and the 8.4° spots level off in intensity. This means that the 25° spots are not stable at room temperature while the 8.5° spots seem to be reasonably stable and aligning along [1$\bar{1}$0] is more likely at higher temperatures, this has also been seen in the experiments where Pb was deposited at higher temperatures and will be revisited later. Figure 7.3 (c) is an image of the surface with 4.0 ML of Pb deposited at 170K and then annealed overnight to RT. Depositing Pb at higher temperatures follows a similar trend but the 25° spots stop appearing around 215 K. The large difference in temperature between when the 25° spots do not form while depositing and when

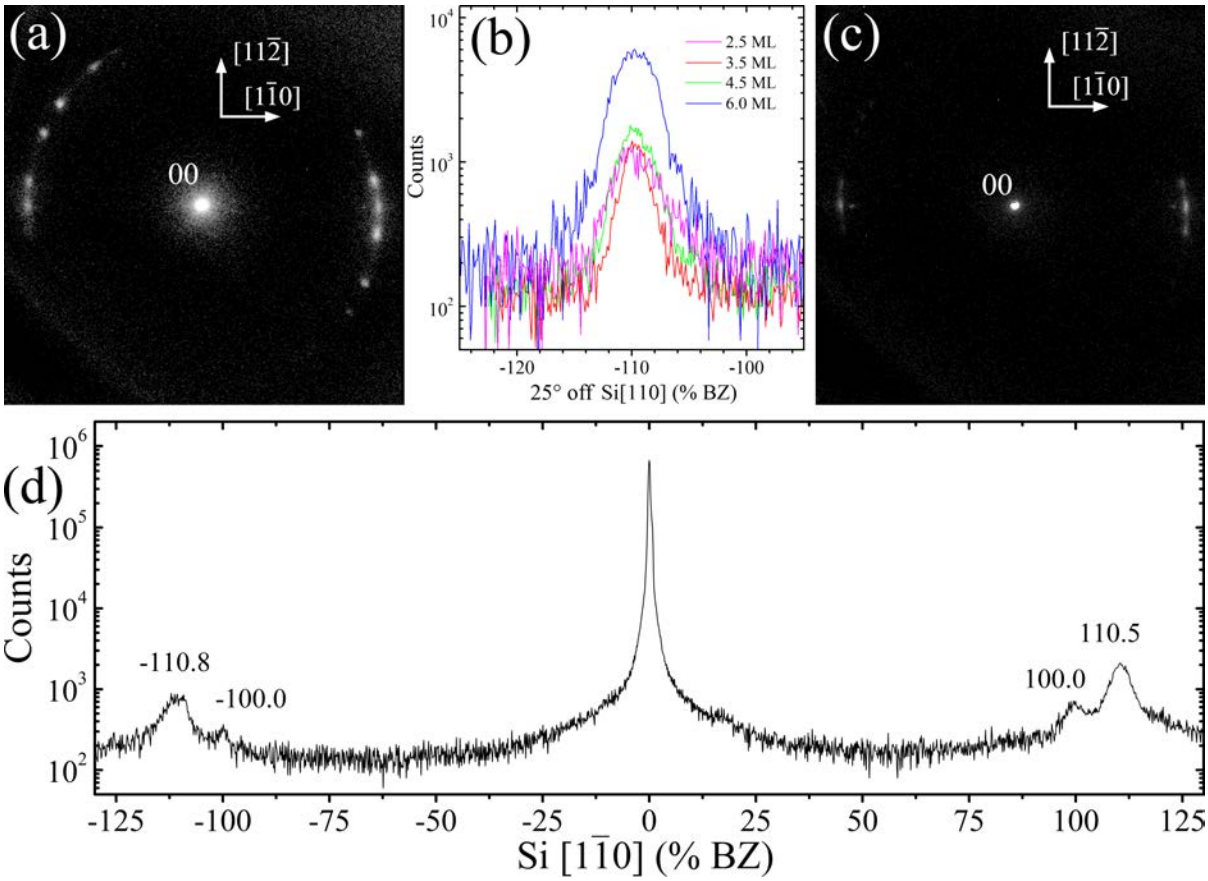

Figure 7.3 (a) (a) 2D SPA-LEED pattern of 6.0 ML of Pb deposited on In $\sqrt{31}$ at 170 K. There are Pb spots along Si[1$\bar{1}$0], and 8.5° and 25° degrees off of Si[1$\bar{1}$0]. (b) The 25° spot at different coverages continues to increase in intensity until at least 6 ML of coverage. The lines are scaled by the relative specular intensities. This shows that the Pb rotation is metastable at least up until this coverage. (c)The Pb aligned along 25° is not stable at RT and disappears very nearly completely after an overnight anneal. The other two orientations are stable to RT. This data was taken on a surface with 4 ML of Pb depositd at 170 K on top of In $\sqrt{31}$ and then anneal overnight. The intensity of all of the spots is down suggesting a rough surface. (d) 1D scan along Si[1$\bar{1}$0] shows that the new spots are indeed Pb. This was taken with 3.5 ML of Pb deposited at 170 K the surface.

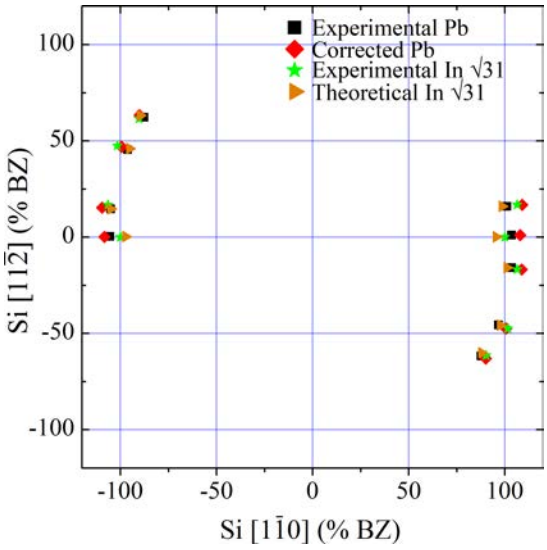

Figure 7.4 The locations of the experimental Pb and $\sqrt{31}$ spots as well as the corrected Pb locations and the theoretical $\sqrt{31}$ locations. This shows how the correction was done and that the $\sqrt{31}$ spots were generally very close to the Pb spots allowing for direct and accurate corrections.

they decay due to annealing is probably due to two things. The first is that in the deposition experiments the atoms have enough energy to arrange themselves in their preferred arrangement right away and do not have to overcome the extra barrier associated with breaking away from an already established island or configuration. Second, the time it takes for the 25° islands to decay at those temperatures could be on the order of the timescale of the anneal time which was about 3 hours. This means that the Pb islands aligned along 25° are no longer metastable at temperatures around 215 K.

7.4.3 Pb alignment discussion

Pb islands align along three different directions, there are only three other systems involving Pb and Si that has Pb growing along non-Si[1$\bar{1}$0] directions, Pb deposited onto Si(111) 7 x 7, Pb α-phase, and Pb β-phase and they are not stable to RT.[24,25] Another major difference is that in the case of Si(111) 7 x 7, Pb α-phase, and Pb β-phase the angles are only 6°, 5.6°, and 3° respectively.[8,24,25] What is so special about this particular system and why these angles? Novaco and McTague[7] postulated that rotations could explain some of the data that had recently been published about rare gases on homogeneous substrates. They tested their

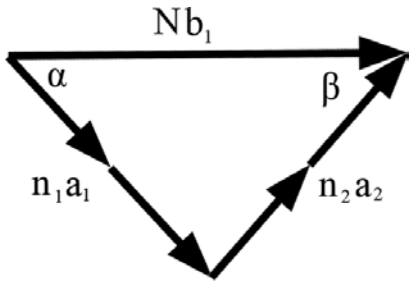

Figure 7.5 Visual of how the Pb unit vectors, $\vec{a_1}$ and $\vec{a_2}$ can be added together to match the length of the In $\sqrt{31}$ unit vector. The closer the two match the less strain the system will have and the more likely that alignment will be to manifest in the experiment.

n1	n2	N	Angle (α)	Strain	Angles in Si 10 frame	
6	0	0.98	0.00	2.1%	8.94*	-8.94*
4	3	0.99	25.28	0.7%	34.22	16.34
5	2	1.02	16.10	-1.9%	25.04*	7.16*
7	7	1.98	30.00	1.0%	38.94	21.06
11	2	1.98	8.21	1.0%	17.15	-0.73
8	6	1.99	25.28	0.7%	34.22	16.34
9	5	2.01	20.63	-0.3%	29.57	11.69
11	10	2.98	28.43	1.0%	37.37	19.49
12	9	2.99	25.28	0.7%	34.22	16.34

Table 7.2 Possible rotation angles for Pb on top of In $\sqrt{31}$. n_1 and n_2 represent the number of Pb unit vectors that are being added up to approximately equal N, the number of $\sqrt{31}$ unit vectors. Only N values of 3 or lower are shown with strain less than 2.5%. The angle, α, is in terms of the $\sqrt{31}$ unit cell so the right two columns show the conversion to the Si reference frame. The starred angles are ones that fit the data.

theory by writing down the Hamiltonian for the system and then trying to find the lowest energy. Using approximate potentials between a graphite substrate and rare gas atoms as well as potentials between the gas atoms and allowing lattice vibrations they found that Ne and Ar grown on graphite would have angles of 3.75° and 4.62° with respect to the substrate by minimizing the total energy of their Hamiltonian. The analysis done in this chapter will be simpler but it will follow the same basic idea. The system will arrange itself in the lowest energy configuration it can.

A coincident over-layer is always favorable to a non-coincident one because it takes less energy. Perhaps the 25° and 8.5° rotations are coincident just like the 0° rotation. Following Weitering et al.[8] and Bauer and van der Merwe[26], coincidence is achieved if:

$$N_i \overrightarrow{b_i} = \sum_{k=1}^{2} n_{ik} \overrightarrow{a_k} \tag{7.11}$$

In this case b_i are the unit vectors of the substrate, a_k are the unit vectors of the overlayer and N and n_k are both integers denoting the number of the vectors to be included. The definitions of b_i and a_k are the opposite of those given in Weitering et al.[8] because the In $\sqrt{31}$ unit cell is larger so it was easier to sum up the adsorbate unit cells rather than the substrate unit cells. However, unless the lattices coincide exactly, N will simply be close to an integer with its distance from the integer being an indication of strain. Since both substrate vectors have the same length only one of the above equations needs to be addressed for $N_1 + N_2 = 1$:

$$N \overrightarrow{b}_1 = n_1 \overrightarrow{a_1} + n_2 \overrightarrow{a_2} \tag{7.12}$$

The angles that satisfy the condition with N_1 and $N_2 = 1$ are not going to be addressed directly because those are less energetically favorable since they take longer to reach coincidence. However, they were investigated but dismissed since there were solutions to the above equation with $N_1 = N_2 = 1$, which have lower energy than higher values of N.

Using trigonometry it is relatively straight forward to derive the angle between the two lattices. See Figure 7.5, the hypotenuse is b_1 with the other two sides being composed of a number of either a_1's or a_2's. α is the angle between b_1 and a_1 and β is the angle between b_1 and a_2.

$$n_1 \sin\alpha = n_2 \sin\beta \tag{7.13}$$

$$n_1 \sin\alpha = n_2 \sin(\alpha - 60^\circ) \tag{7.14}$$

$$n_1 \sin\alpha = n_2 \left(\frac{\sqrt{3}}{2} \cos\alpha - \frac{1}{2} \sin(\alpha) \right) \tag{7.15}$$

$$\left(n_1 + \frac{n_2}{2} \right) \sin\alpha = n_2 \frac{\sqrt{3}}{2} \cos\alpha \tag{7.16}$$

$$\tan\alpha = \frac{\sqrt{3}}{2} \frac{n_2}{n_1 + \frac{n_2}{2}} \tag{7.17}$$

Treat that as a right triangle with α as one of the angles, and then the hypotenuse is:

$$hypotenuse = \sqrt{{n_1}^2 + n_1 n_2 + {n_2}^2} \tag{7.18}$$

The angle between $n_1$and the $\sqrt{31}$ vector is:

$$\sin\alpha \ = \frac{\sqrt{3}}{2}\frac{n_2}{\sqrt{{n_1}^2 + n_1 n_2 + {n_2}^2}} \tag{7.19}$$

Combining that with equation 7.12 it is possible to relate the angle and N. Inserting the Pb and the $\sqrt{31}$ vector values and letting the substrate rotate by angle α (it is easier to let the substrate rotate than forcing the two Pb vectors to rotate).

$$|b_1| = 3.84\sqrt{31}\ \mathring{\text{A}} \tag{7.20}$$

$$\overrightarrow{a_1} = 3.5\hat{x} \tag{7.21}$$

$$\overrightarrow{a_2} = 1.75\hat{x} + 3.5\frac{\sqrt{3}}{2}\hat{y} \tag{7.22}$$

$$3.85\sqrt{31}N\left(\cos\alpha\ \hat{x} + \sin\alpha\ \hat{y}\right) = 3.5n_1\hat{x} + n_2\left(1.75\hat{x} + 3.5\frac{\sqrt{3}}{2}\hat{y}\right) \tag{7.23}$$

Taking only the $\hat{y}$ direction:

$$3.85\sqrt{31}N\frac{\sqrt{3}}{2}\frac{n_2}{\sqrt{{n_1}^2 + n_1 n_2 + {n_2}^2}} = 3.5\frac{\sqrt{3}}{2}n_2 \tag{7.24}$$

$$N = 0.1637\sqrt{{n_1}^2 + n_1 n_2 + {n_2}^2} \tag{7.25}$$

There are a large number of solutions to equations 7.19 and 7.25 but they can be trimmed by applying two physics based rules: the fewer the unit cells it takes for the coincidence to occur the less energy the surface requires, and the smaller the strain the better. Limiting N to 3 or lower with strains of less than 2.5% and eliminating duplicate angles results in Table 7.2. 2.5% is stricter than the 3% used by Weitering et al.[8] but it was sufficiently large to describe our results. Note, the angle is the angle that the a_1 Pb vector makes with the In $\sqrt{31}$ vector, this defines the relative orientation of the two lattices. However, this is not the angle that is seen in the experiments because those angles are measured with respect to Si$[1\bar{1}0]$. Therefore 8.94° has to be added and subtracted to each of the angles to convert the angles to the Si reference frame the experimental data used and to take into account the two different $\sqrt{31}$ orientations.

See Figures 7.5 and 7.2 (a). The strain is how much the Pb lattice would have to adjust to match the underlying $\sqrt{31}$ lattice perfectly in this direction, it was calculated via $(b - b_0)/b_0$ where b is the length of the Pb vectors strained to make the lattices commensurate and b_0 is the length of the unstrained vectors. Therefore positive strains are stretching the Pb lattice.

Eliminating all N values greater than 1 leaves only three viable options. Two of which fit the data almost perfectly. The first row produces spots at $\pm 8.94°$ while the third row produces spots at 25°. That row also produces spots at 7.16° which may explain why the 8.5° spots are so broad. A closer look leaves the conclusion inconclusive but it is still worth mentioning. The 8.5° spots are, on average, 6.4% BZ long as measured from the base. The 25° spots are 3.6% BZ long and the 7.16° and 8.94° are 3.41% BZ apart. Even the 25° spot is not very sharp which makes it impossible to separate the 7.16° and 8.94° degree spots but their relative widths are in line with each other. Assume the 3.41% BZ separation and add 3.6% BZ for the width of the two non-overlapping sides and the result is 7.0% BZ.

This simple model leaves two problems. First, why are the most stable spots aligned along Si$[1\bar{1}0]$? Perhaps the Pb is sensitive to the underlying Si substrate despite resting on the In $\sqrt{31}$. Room temperature anneals reveal the first order In $\sqrt{31}$ spots which may indicate the Pb wetting layer recedes to the islands but does not prove the Pb islands rest directly on the Si. It does, however, show that the film itself is not completely destroyed. The second question is why are there no spots at 16.3° as suggested by the second row of Table 7.2. Of the three options it seems to be the best with only 0.7% expansion. The solution probably lies in the fact that this is a simple model and only takes into account the lattice vectors. There could be other atomic interactions that outweigh the seeming preference based on this model. Unfortunately, no physical arguments based on the arrangement of the atoms in the unit cell, like row matching, appear to shed any light on the situation. This simple model points in the general direction of why this system behaves this way but a more comprehensive model would be required to fill in the gaps.

Spots (° from Si [110])	Average total intensity/specular at 170 K	Average total intensity/specular at RT	% of Surface at 170 K	% of surface at 170K assuming the rotation model is correct	% of surface at RT
0	0.083	0.081	20.4	17.1	34.7
8.5	0.096	0.077	50.3	33.8	65.3
25 (7.2)	0.0	0	29.3	49.1	∼0.0

Table 7.3 The square root of the total intensity of the Pb spots along the different directions can be used to calculate the Pb aligned along each of those directions. This was done at 170 K and RT. At 170 K both 8.5° and 25° have more Pb aligned along them than 0°, this comparison was made by area. At RT there are essentially no spots along 25°, and 8.5° has about twice as much area covered by Pb along it than 0°. The rotation model is the possible alignment of the Pb displayed in Table 7.2. See Figure 7.3 (a) for an example of the kind of image this data was taken from.

7.4.4 Temperature dependence of preferred alignments

Another piece of the puzzle is to consider which orientations are preferred between 170 K and RT and by how much. 2D images were used to get the total intensity of the Pb spots. Using 2D scans is especially important in this case since some of these spots are elongated so extrapolating the total intensity based on a 1D scan could be difficult. To do this, the intensity of each pixel in a square box centered on the spots was summed, but only after the background was subtracted. The background in the vicinity was calculated by averaging all of the pixels on the perimeter. This method has been shown to be accurate in the past but does require intelligent choices for the edges of the box.[27] The reason for this is that it only takes the inclusion of one intense pixel to severely misrepresent the background. The intensity of a spot depends upon two things, the scattering factor and the area of the surface covered by the surface that creates the spot. Since all relevant spots are from Pb(111) crystals the scattering factor is the same. The area, which is the goal, is proportional to the square root of the intensity.

Table 7.3 was constructed by averaging the results from many different 2D scans, all had at least 3.5 ML of Pb on the surface. The data for the various spots were averaged together. For example all four 8.5° spots were averaged.

It was assumed that Pb islands that lead to the 0° spot could form on either of the $\sqrt{31}$

orientations but that spots at ±8.5° had to come from one orientation or the other but are equivalent. There are two different orientations so both must be included in the final calculations. To make up for this the ratio involving the 8.5° and 25° spots were doubled because they are caused by two different Pb island orientations.

At first glance it appears that the islands strongly prefer to align along 8.5° with 0° being the second preference. However, if the above model is correct then there are two spots around 8.5°, the 8.9° spot and the 7.2° spot. Assuming the 7.2° spot has the same intensity as the 25° makes it possible to calculate how intense the 8.9° spot is. The 7.2° and 25° spots have their origins in the same rotation with respect to the $\sqrt{31}$ lattice so it is reasonable to assume they have similar numbers of Pb islands aligned with them. The proximity to the other orientations that are acceptable and the different Si spots below the directions could both impact how favored aligning along 7.2° is. Despite that, when it is assumed that the ±7.2 and ±25° spots are all the same intensity the representative ratio above must be multiplied by a factor of four because they are really four separate Pb island orientations.

That results in the 2^{nd} column of Table 7.3. The area of Pb aligned along 8.5° is about twice that of the Pb islands aligned along 0°. The Pb could be more susceptible to growing along the $\sqrt{31}$ direction than the Si[1$\bar{1}$0] direction because the Pb grew on top of the $\sqrt{31}$. The actual interface below the Pb crystal is unknown but it should be noted that Pb crystals on In 4 x 1 went all of the way to the Si (111) substrate.[4] Most Pb islands align along 7.2° or 25°. Only 12.5 percent of the Pb island area is aligned along any one of the four directions. This is below the 17% of the island area that grew along each of the 8.5 and 0° directions.

Upon annealing to RT the spots along 25° almost completely disappear as was indicated before. The value in the table is listed as $\tilde{0}$ instead of exactly 0 because there were cases where there was some evidence a spot was there but they were so weak a value for the intensity could not be read above the background. 65.3% of the Pb grows along 8.5° with the remaining aligning with 0°. This is not quite the factor of two seen at 170 K but it is still close. Since there are no 25° spots at RT it was assumed that there are not any 7° spots either so the 8.5° spots should be narrower. However, this has not been quantitatively seen. Probably because, as mentioned above, the surface is not as ordered as it was at 170 K. The intensity of all the

spots is down and they are broader, making it harder to distinguish the spots and get accurate background values. The fact that the 8.5° spot is still roughly twice the area of the 0° spot is an indication that there was indeed a spot at 7.2° and that taking it into account when interpreting the 170 K data was the right thing to do.

7.4.5 Preferred island heights

Figure 5 (b) is a $G(S)$ curve, first introduced in Chapter 3, that shows that for a coverage of 3.0 ML of Pb at 170 K there is a preferred height of two layers. Data that is not shown shows that this configuration is preferred at 2.5 ML though 3.5 ML as well but the effect is weaker because more or less of the surface is covered in Pb islands. Figure 7.6 (c,f) shows two examples of in-phase and out-of-phase conditions which shows just how strong the effect is. Scanning Tunneling Microscopy (STM) data[28] is consistent with the $G(S)$ curve's height determination, Figure 7.6 (a). Figure 7.6 (d) shows a histogram of Figure 7.6 (a) which has approximately 1.6 ML of Pb on the surface that was deposited at 190 K. The Pb island peak is 0.614 nm above the In $\sqrt{31}$ substrate which works out to be about 2 layers of Pb(111). Higher coverage STM images show that the 2 layers of Pb forms a nearly complete film before the next layer starts to grow. This fits in well with the SPA-LEED data that shows that there are two layer tick films on the surface at 3 ML. This must consist of 2 complete layers of Pb and half of the surface covered in 2 layer thick islands.

The large peak at 0.205 nm in the histogram is the wetting layer, which looks like a lot of blobs in Figure 7.6 (a). Each blob is about 0.20 nm tall and less than 1 nm in diameter. Those traits stay roughly the same as Pb coverage increases but the density of the blobs increases even as the Pb islands grow larger. They do not exhibit any long range order according to inspection and a power spectrum done via Omicron's Scala Software. However, the power spectrum, or fourier transform, did reveal that the blobs tend to be about equally spaced from one another. Unfortunately a corresponding peak is not seen in SPA-LEED but that is not too surprising since the electrons do not interact with them strongly, the main spots of $\sqrt{31}$ pattern stay until well past 1 ML of coverage. Very similar blobs are seen when depositing In on Pb α-phase which makes it harder to just dismiss them as corrugation or groups of Pb atoms.[22]

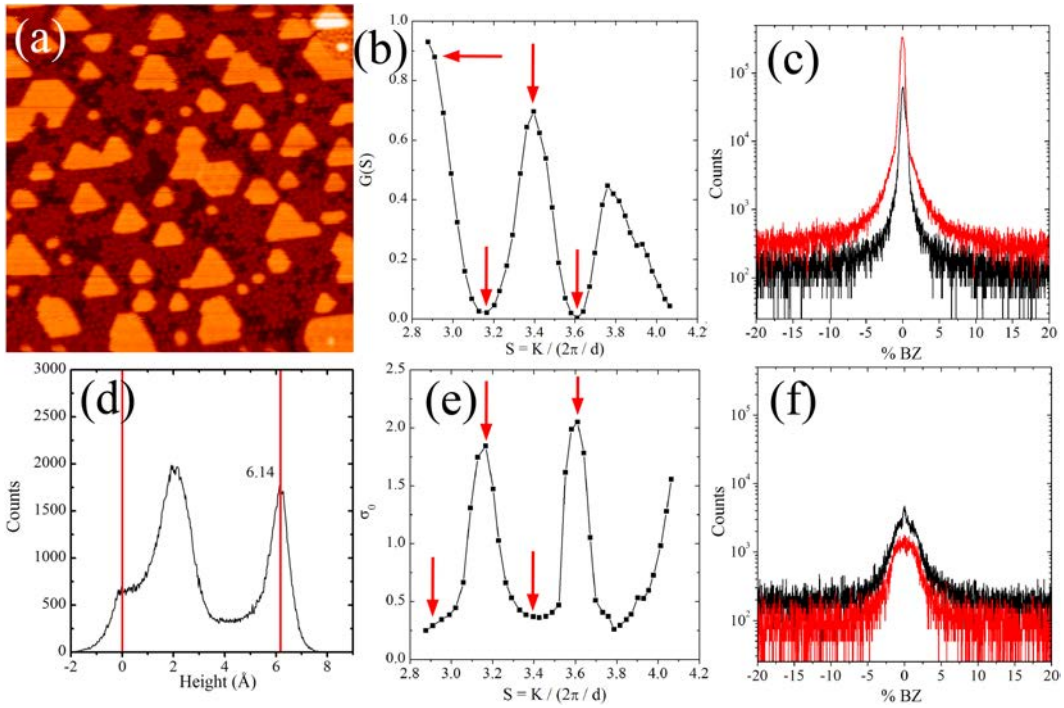

Figure 7.6 STM image take my Dr. Myron Hupalo. 1.6 ML of Pb deposited at 190 K on $\sqrt{31}$, 100 x 100 nm. (d) histogram of (a) which shows that the Pb islands are two layers high (b) $G(S)$ of a surface with 3.0 ML of Pb deposited at 170 K. The two strong oscillations indicate that the Pb islands are almost exclusively 2 layers tall (e) Profile of the specular as a function of S parallel corroborating (c) and (f) that the in and out of phase conditions were strong. The in and out of phase conditions are marked with red arrows in both (b) and (e) with the in phase conditions being the bottom two arrows in (e). The in phase energies in (c) are 39.0 (red/gray) and 53.0 eV (black). The out of phase energies in (d) are 46.1 (red/gray) and 60.0eV (black).

The location of the broad peaks about the specular in the out of phase conditions is an indication of island separation/island size. In this case those peaks are at ±1.08% BZ which means the average island separation is 35.6 nm and the island density is 0.001 islands/nm^2. In the STM data[28] the island density is about 0.006 islands/nm^2. However, as can be seen in Figure 7.6 (a) some of the islands are very small and many of the shapes are irregular, even at this relatively low coverage. Both of those things could contribute to the electrons in the SPA-LEED system reporting the islands are further apart than they are. For example, the smaller islands are definitely part of the system but do not contribute nearly as many reflected electrons as the much larger islands that have already started to merge.

$G(S)$ curves of 4 and 4.5 ML produce similar but very week single oscillations in σ_0 with some smaller extra oscillations producing unreliable $G(S)$ curves. This could be because the Pb had enough mobility that most of the islands it created with the additional coverage were too large to be detected by SPA-LEED or perhaps the differences in the various Pb orientations started to affect how the layers on top grew producing a variety of signals that cannot be deciphered. Even with knowing the coverage it is impossible to determine the various heights on this surface because the surface is not necessarily uniform which adds another variable making it even harder to come to conclusions.

The claim that the surfaces could grow differently past the first 4 ML because of different orientations on top of the substrate is a bold claim, especially since they grew similarly up until this coverage. Tang et al.[29] showed that increased interfacial energy could be offset by the adsorbate having a strong hybridization due to good electronic match which reduces the energy cost associated with QSE. In that paper this allowed an orientation of Pb(111) on Pb β-phase on Ge(111) be stable for low coverages even though there was a large lattice mismatch between the Pb and Pb β-phase in that orientation. In this chapter the argument goes the other way. Since the alignment of the Pb islands on top of the In $\sqrt{31}$, and therefore the underlying Si(111), is different for each angle it is likely that the electrons are interacting with the substrate differently and this could affect the strength of the confinement and thus change the conditions related to QSE. This could, in turn, affect the phase change of the electrons at the Si(111)/$\sqrt{31}$ and In $\sqrt{31}$/Pb(111) interfaces which would change the quantization conditions. It is possible that they are similar enough at lower heights to allow similar growth up to 4 ML and then switch above that. However, without spectroscopy data this remains a hypothesis.

7.4.6 Summary

Pb on In $\sqrt{31}$ has three orientations below 215 K and it has two orientations that are stable up to and including RT. This is relatively unique in the Pb, In, Si system – especially because it is stable to RT. There have been other experiments that deposited onto In $\sqrt{31}$, but none used Pb. Uchihashi et al.[30] deposited Ag at 100 K which, not surprisingly, did not have the same growth characteristics as the Pb but it is worth noting that they did not report anything about

the rotation of the Ag islands. He found discrete islands with heights with no strongly preferred heights but at a coverage of 2.7 ML there were no heights below 4 layers and the islands were nearly flat topped. Perhaps $\sqrt{31}$ only affects Pb this way. In has also been deposited onto In $\sqrt{31}$ at 170 K, depositions of In resulted in an In "1 x 1" pattern.[22] For low coverages of In, "nanodots" formed at RT.[11]

7.5 Pb on In $\sqrt{3}$

In $\sqrt{3}$ is a much more thoroughly studied surface with a much simpler and more widely known structure. The real space diagram can be seen in Figure 7.7 (a). The calculated and experimental reciprocal lattices are in Figure 7.7 (b) and (c), respectively. This is a very simple and straight forward pattern compared to In $\sqrt{31}$. A 1D scan along the direction of the $\sqrt{3}$ unit cell is in Figure 7.7 (d), Si[1$\bar{1}$0]. Correcting the 1D scans along this direction is complicated by the fact that there are relatively few Si spots along this direction so spots beyond about 90% BZ can be quite a bit off, however the discrepancy is consistent so direct comparisons can still be made. That is why the two spots that should be at 57.74% BZ are very close to that while the spots that should be at 115.47% BZ are off by more.

Depositing Pb on In $\sqrt{3}$ at 170 K produces one set of spots aligned along Si[1$\bar{1}$0], as seen in Figure 7.8 (b) which has 3.0 ML of Pb on it. This is also seen via the black line in Figure 7.8 (d) which shows the spots are at -111.8% BZ, and 109.8% BZ indicating that it is FCC Pb. In the Si[11$\bar{2}$] direction, the black line in Figure 7.8 (e) shows a clean In $\sqrt{3}$ surface. After deposition at 170 K all $\sqrt{3}$ spots disappear leaving just the Pb and Si peaks along the Si[1$\bar{1}$0] direction. During annealing the FCC Pb spots become much weaker while the $\sqrt{3}$ spots reappear and the Pb aligns along the $\sqrt{3}$ direction, this is seen in the two red lines in Figure 7.8 (d and e) which depict the surface after an overnight RT anneal. The specular is weaker but the background is also less intense. In the [11$\bar{2}$] direction there are now two peaks at around 60% BZ (this is less obvious at +60% than -60% but this merging was not a common occurrence in the data and using Origin Pro's fitting wizard the two constituent peaks showed very easily, centered at the two locations reported in the figure). Most of the Pb realignment is done by the time the sample is 265 K from its starting point of 170 K from natural warming after the cooling was

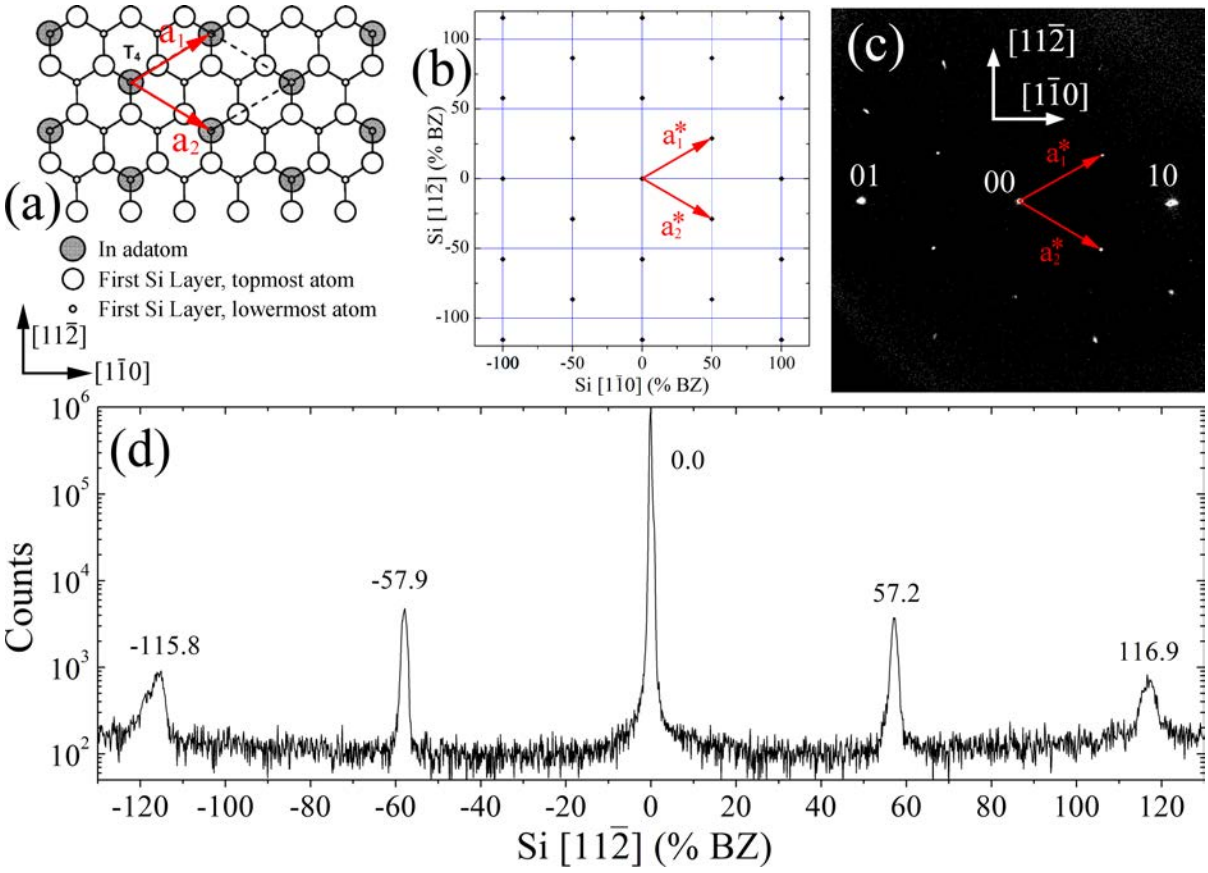

Figure 7.7 (a) Real space diagram of In $\sqrt{3}$ borrowed fromVlachos et al.[31]. The unit cell is marked with red arrows. (b,c) calculated and measured reciprocal space images of In $\sqrt{3}$ with the reciprocal lattice vectors marked by red arrows. (d) 1D scan along the Si [11$\bar{2}$] direction to show that the pattern is indeed $\sqrt{3}$. It was taken with 38.0 eV electrons and the spot locations were determined with a Gaussian fit. See text for details.

turned off. However, the spots at 60% evolve quite a bit during the overnight wait.

The Pb is undergoing a large change between 170 K and room temperature with most of it realigning along $\sqrt{3}$ instead of Si[1$\bar{1}$0]. The In $\sqrt{3}$ spots reappearing is an indication that the Pb wetting layer must retreat to the islands or form a $\sqrt{3}$ structure of their own. Since annealing Pb on top of the In $\sqrt{31}$ phase revealed the In $\sqrt{31}$ spots and Pb is not known to create a $\sqrt{31}$ phase it was concluded that the Pb was moving off of the In $\sqrt{31}$. It is likely that the Pb did the same thing on top of the $\sqrt{3}$ despite being capable of creating a $\sqrt{3}$ phase of its own on Si(111) 7 x 7. The extra spot at 59.9% BZ are similar to the spots seen in the Devil's

Staircase[3] but there is no record of seeing Devil's Staircase in In. It also would not explain why the 114% BZ spots are not split and the fact that the spacing between these two spots are the same in every experiment. The Devil's Staircase phases are very sensitive to coverage, it seems unlikely that the system would form the exact same phase every time.

Depositions near and above 215 K result in Pb islands forming along the Si[11$\bar{2}$] direction producing the same pattern seen after annealing the cooler depositions mentioned above to RT. This is further proof that the alignment along Si[1$\bar{1}$0] is less stable than alignment along Si[11$\bar{2}$]. However, at RT, as mentioned above, the Pb still shows up along Si[11$\bar{2}$] but it has much weaker intensity suggesting that the bulk of the Pb is not being seen by the SPA-LEED as described above.

This behavior is different than when depositing In on top of In $\sqrt{3}$ at low temperature. In that system the surface first transforms into In "1 x 1" as is the case with In on In $\sqrt{31}$. Pb deposition on top of Pb β-phase (which is analogous to the In $\sqrt{3}$ phase being discussed) on Ge(111) had a very similar reaction but there are differences.[29] In that system the Pb formed its normal Pb(111) structure on top of the beta phase despite the fact that it is not coincident. This is a common occurrence and happens on Si(111) as well as for Ag on Ge(111).[32] However, in the Pb on Pb β- phase case the islands start to rotate to align with the beta phase starting above 2 ML of coverage (above and beyond the coverage associated with the β-phase). In this chapter the rotations are more strongly affected by temperature than coverage, depositing up to 4 ML had no effect on the growth of the Pb along the Si[1$\bar{1}$0] direction but slowly annealing to 265 K via lack of cooling caused most of the Pb to align along the $\sqrt{3}$ direction. Further annealing overnight had relatively little effect on the Pb orientation with just 10 percentage points more moving.

7.6 Pb on In $\sqrt{3}$, In $\sqrt{31}$, and In 4 x 1

As mentioned in the beginning of this chapter it is relatively difficult to create a surface with just In $\sqrt{31}$ on the surface so there were quite a few experiments done with more than one phase. These results were not actively studied on their own but some of the trends show strong agreement with the results from the surfaces with only one phase on them so they will

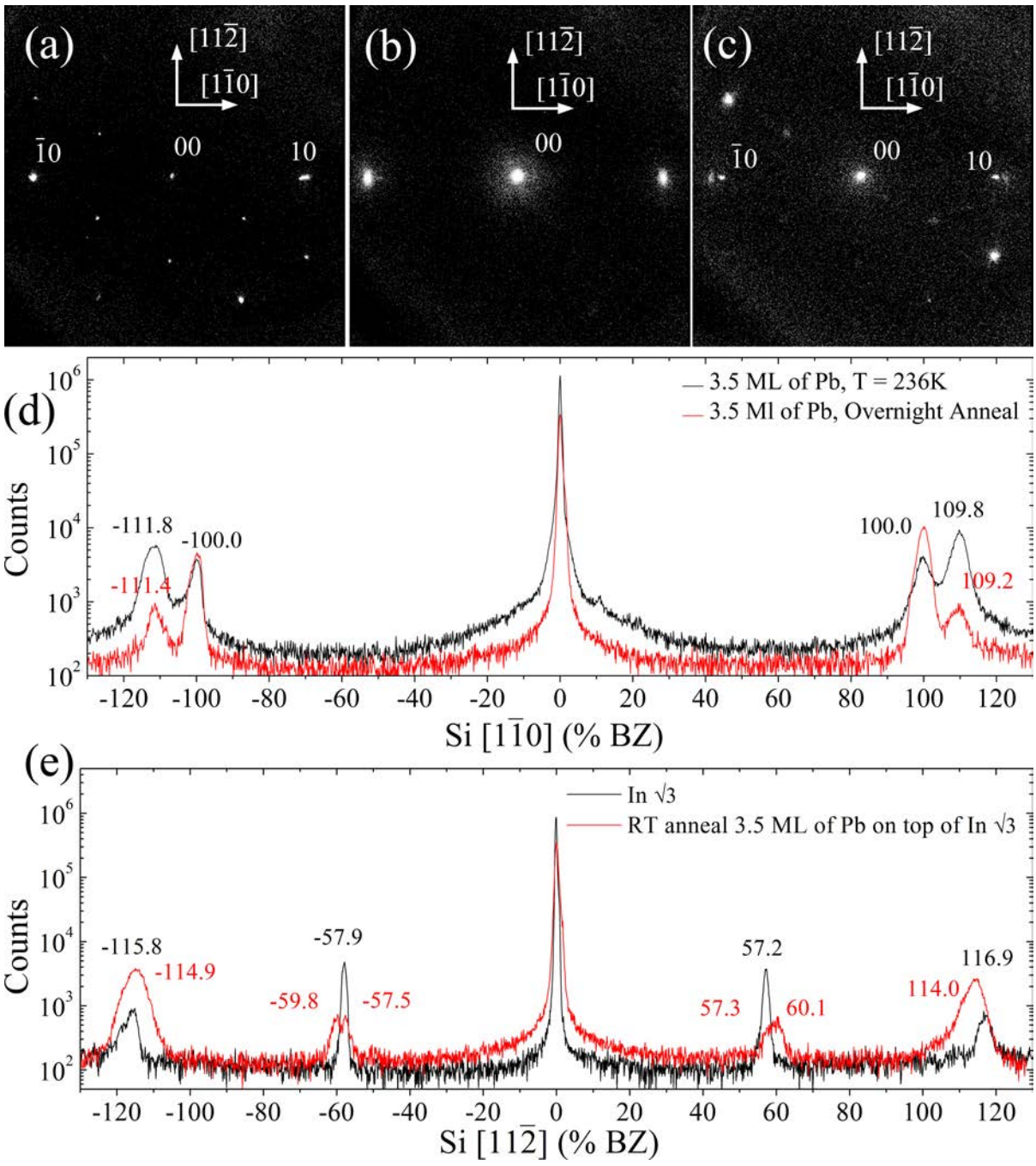

Figure 7.8 (a) Clean In $\sqrt{3}$. (b) 3.0 ML of Pb deposited at 170 K, as you can see the Pb aligned itself along the Si[1$\bar{1}$0] direction. All traces of the $\sqrt{3}$ are gone leaving just the FCC Pb and Si 1 x 1 spots which can also be seen in the black line of (d). (c) Overnight RT anneal showing that the Pb FCC islands were not completely stable up to RT and that the $\sqrt{3}$ pattern came back, this is best seen in the red line of (e).

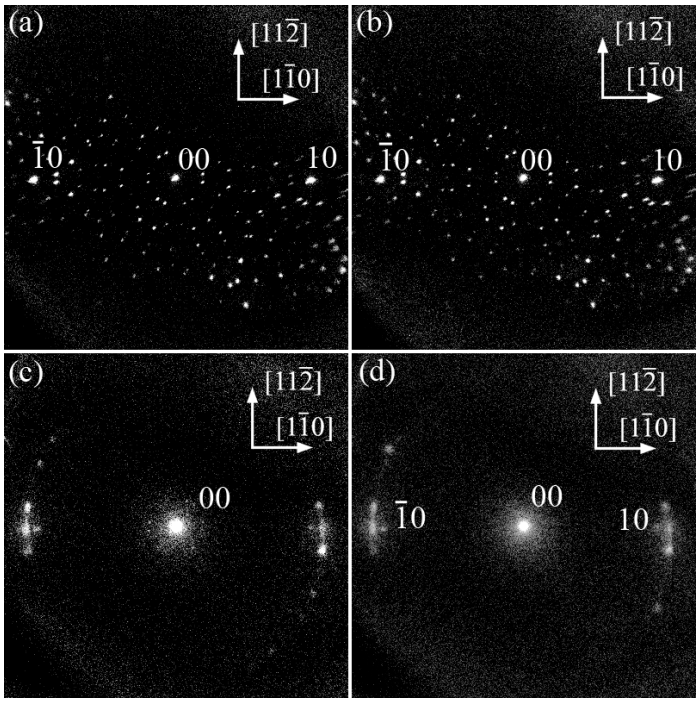

Figure 7.9 Pb depositions onto surfaces with significant amounts (>30%) of both In $\sqrt{3}$ and In $\sqrt{31}$. (c) 3.0 ML of Pb deposited at 195 K on top of (a) shows that as expected Pb spots appear at 0°, 8.5°, and 25° while the Pb spots associated with growth on In $\sqrt{3}$ spots do not appear (d) 3.50 ML of Pb deposited at 215 K on top of (b) also resulted in spots as expected from the pure surfaces. Very weak 25° spots at this high of a temperature but the Pb spots associated with growth on In $\sqrt{3}$ spots are able to form setting 205 K to 215 K as the transition temperature between the two growth phases.

be mentioned briefly. Note: this paper does not cover Pb depositions onto In 4 x 1 because that was done extensively by Yakes et al.[4] found that the Pb diffusion on In 4 x 1 is anisotropic with the Pb preferring to go along the Si[1$\bar{1}$0] direction which resulted in very long Pb nanowires. This made the specular of the SPA-LEED data into a 6 pronged star due to the fact that the islands along the [1$\bar{1}$0] direction were so long and separated while the distance between the islands in the [11$\bar{2}$] direction was shorter. Pb islands grown on In 4 x 1 are stable up to RT, this is not seen on any of the other In phases, including the ones discussed in this dissertation.

When there is In $\sqrt{31}$ and In 4 x 1 on the surface at the same time the Pb grows as if there was no 4 x 1 on the surface at all. The 4 x 1 domains constituted as much as 40 percent of the surface (assuming that the scattering factor for the two surfaces is the same. The percentages

were calculated based on the intensity of the spots and the fact that intensity goes like the area squared. Not once did the star pattern centered at the specular form like the patterns seen in Yakes et al.[4] despite a similar temperature and coverage. At 170 K the arms are not expected to show up strongly but they should be visible during the annealing experiments and during the higher temperature deposition experiments – none are seen. However, instead of seeing arms after RT anneals, the 4 x 1 spots reappear. This means that at least some of the Pb moves off of the 4 x 1 but probably not all of it because the 4 x 1 spot intensity is not all that high. Affects due to small domains and large boundaries have been reported before by Xu et al.[11] who deposited In onto a surface composed of In 4 x 1 and In $\sqrt{31}$. In that system In wires only grow on 4 x 1 at RT when there is $\sqrt{31}$ present, the reason given was that diffusion is just too fast on pure 4 x 1. In the Pb on 4 x 1 and $\sqrt{31}$ case the opposite appears to be true, at least to an extent. That was qualified because STM images of a surface that is roughly half $\sqrt{31}$ and half 4 x 1 show wires grow on the 4 x 1 and the coverage on both the $\sqrt{31}$ and the 4 x 1 sections is similar at 190 K.

Pb deposited onto a surface with both $\sqrt{31}$ and $\sqrt{3}$ is much more straight forward because it acts exactly as expected based on the pure phase experiments. Figure 7.9 (a) shows the results of depositing 3.0 ML of Pb at 195 K on a surface that is approximately 35% $\sqrt{3}$, once again assuming that the scattering factors of the two phases are similar. The temperature is below 215 K so the 25° spot shows up and the 30° spot does not, both as expected. The spots at 0 and 8.5° are there as well. Figure 7.9 (b) is 3.5 ML of Pb on top of a surface with 40% $\sqrt{3}$ and 60% $\sqrt{31}$. The Pb was deposited at 215 K which is the temperature at which the 25° spots no longer show up, though there is a faint hint of them in this case. 215 K appears to be warm enough for the $\sqrt{3}$ spots to show up but they are faint yet. Once again, the 0 and 8.5° spots are there. Annealing above 215 K results in stronger spots at 30° and the 25° spots disappearing. The most interesting thing about this is that the temperature range around 215 K is important to the Pb alignment in both the $\sqrt{31}$ and $\sqrt{3}$ surfaces though it is probably just a coincidence.

7.7 Pb on In "1 x 1"

Pb on In "1 x 1" As stated earlier, the exact structure of In "1 x 1" is under debate which limits the conclusions that can be drawn. However, that does not prevent experiments to see what happens. Unlike the other In phases, when Pb is deposited onto "1 x 1" it behaves very similarly to that of In.[22] Figure 7.10 (a) shows the initial "1 x 1" surface. The starting surface can also be seen in Figure 7.10 (e), it is the black line with peaks around 103.85% BZ.[20] Using Bauer's result the coverage should be 1.08 ML. Shortly after 2.0 ML the "10x10" unit cell spots start to show up, at 170K they reach their maximum intensity around 3.0 ML and are essentially gone by 4.5 ML. This structure is called "10x10" because the spots appear around 10.5% BZ, therefore they are not exactly 10x10 or 9x9. However, the vectors that describe the pattern are 60° apart which matches the underlying Si(111) structure. Lastly, these spots are seen at a large range of coverages, 2 to 4.5 ML, indicating that it is most likely not a 2D phase. At 170 K the spots are broad but annealing to 205 K is enough to make the spots quite a bit sharper as in fFigure 7.10 (b). At this temperature $\sqrt{3}$ spots are already showing up, they can be easily seen in the red line in Figure 7.10 (e) with peaks around 57.8%. The 18.0% spots are the "10x10" spots, if the spots were exactly 10x10 they would be at 17.3% instead of 18% which is why the 10x10 is in quotes. Though, if the spots were commensurate with the In "1 x 1" lattice with a period of 10x10 they would be at 17.6% BZ which is quite a bit closer to the measured value. In depositions onto In "1 x 1" also had 10x10 spots. However, Pb's is generally worse because it has broader spots and only a few second order spots.

Pb FCC spots show up after 1.0 ML of coverage and by 3.0 ML they are very well defined as seen in Figure 7.10 (d). The black line in that figure shows the still weak "10x10" spots and the Pb spots at 109.2% BZ. Annealing to 250 K does not change the surface too much except that the "10x10" spots are more intense and have shifted inward slightly, 0.5% BZ. However, after an overnight anneal to RT the surface changes drastically. In the Si[$1\bar{1}0$] direction the FCC Pb spots as well as the "10x10" spots are completely gone, leaving only the Si peak. In the [$11\bar{2}$] direction the $\sqrt{3}$ peaks are now the dominant feature with no other spots showing up. This is another case where the Pb spots disappear suggesting that the Pb had a lot of

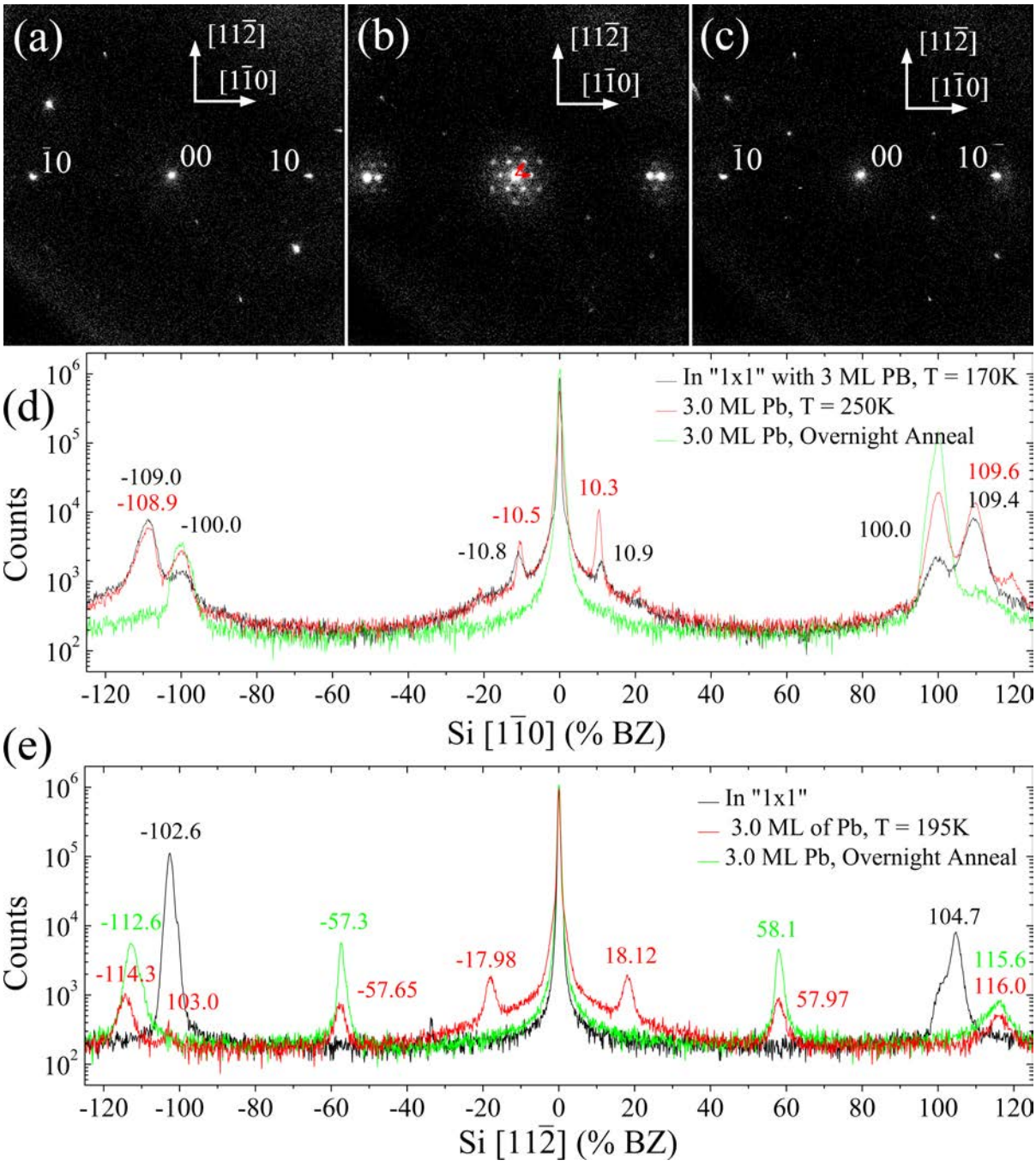

Figure 7.10 (a) clean In "1 x 1". (b) 3.0 ML of Pb deposited at 170K and then annealed to 205 K produces the sharpest "10x10" spots. The unit cell is marked with red arrows. The FCC Pb spots can still be seen positions are so different (c) After an overnight anneal to RT a $\sqrt{3}$ pattern emerges and there are no Pb spots. (d and e) scans from before the deposition to after the overnight anneal along the two relevant directions, Si [1$\bar{1}$0] and Si [11$\bar{2}$].

mobility and formed large islands which cannot be seen by SPA-LEED. Somehow the In "1 x 1" is either covered by Pb $\sqrt{3}$ (which occurs on Si(111)) or it is converted into $\sqrt{3}$ on which Pb moves very quickly at RT and creates islands that are large and do not readily show up in SPA-LEED. There are two differences though, this $\sqrt{3}$ pattern is much better than that seen after depositing Pb onto In $\sqrt{3}$ itself. Also, the first order spots are only one peak. Also, the first order spots are comparable to the second order spots. Surprisingly enough this is where the similarities to In on "1 x 1" ends because after a RT anneal In on "1 x 1" results in plain old "1 x 1" again.[22] The In coverages are different in the two experiments since In $\sqrt{3}$ only has 1/3 of a ML while In "1 x 1" has at least 1 ML. However, the Pb coverages are the same with experiments with 3 and 3.5 ML of coverage.

7.8 Summary

The Pb on In submonolayer and Si system has many interesting features and the growth of Pb on In phases continued this trend. Table 7.4 includes a rundown of some of the basic traits of Pb deposition on In phases. Specifically, Pb islands grown on $\sqrt{31}$ and $\sqrt{3}$ grow along directions other than Si[$1\bar{1}0$] which is a relatively rare occurrence when it comes to Pb and Si. Two of those rotations are even stable at RT, 8.94° on $\sqrt{31}$ and 30° for $\sqrt{3}$which has not been reported before. However, this is also seen in the Pb on Pb β-phase on Ge(111) system where all islands 2 layers or shorter were aligned along the Si[$1\bar{1}0$] direction but at thicknesses over 2 ML preferred alignment along Si[$11\bar{2}$].

Finding orientations that make the $\sqrt{31}$ and Pb island lattices commensurate is enough to suggest the reasons behind the locations of the Pb spots but it does miss a couple important facts so a more thorough theoretical model will need to be applied. Depositions onto the other In phases is a bit less conclusive, especially after RT anneals. The locations of initial Pb spots on $\sqrt{3}$ and "1 x 1" are as expected but after RT anneals the Pb seems to disappear on the "1 x 1" leaving a $\sqrt{3}$ pattern. Part of this could be caused by the Pb having a lot of mobility and forming very large Pb islands. However, turning "1 x 1" into $\sqrt{3}$ involves a new phase of In $\sqrt{3}$, a Pb In mixture, or mass transport of In as well as Pb.

Understanding rotations and why they are preferable is an important step in understanding

Surface	Preferred Height (layers)	Wetting Layer (ML)	Preferred Orientation
Si 7 x 7	7	1	Along Si[1$\bar{1}$0] and 6° off
In $\sqrt{3}$	Below 210 K: no preferred height. Above ∼215 K: 4. RT: Islands are too large.	larger than 1	170-215 K: Along Si [1$\bar{1}$0]. Above 215K: Along [11$\bar{2}$]. RT: unknown.
In $\sqrt{31}$	170-215K: 2, then 4. Above 215K: no preferred height.	1.2 ML	Rotated +/-8.9° from Si[110] direction and along Si [110], below 215K it also aligns along +/-7.2° and +/-25°
In 4 x 1*	2, then 4.	2 ML at 185 K	Along Si[1$\bar{1}$0]
In "1 x 1"	Islands form but the $G(S)$ curves do not indicate a preferred height.	larger than 1	170-230K: Si [1$\bar{1}$0]. RT: unknown

Table 7.4 Summary of results for Pb depositions onto various In phases. *data about Pb on In 4 x 1 comes from Yakes et al.[4].

thin film growth and, as seen,[29] can have an effect on QSE. This means that growing films at different orientations is one more way to manipulate QSE allowing even more opportunities to create specific structures. This adds to the list of known ways to control atomistic processes, including changing the height as covered in previous chapters of this dissertation.

References

[1] M. Hupalo, S. Kremmer, V. Yeh, L. Berbil-Bautista, E. Abram, and M. C. Tringides, Surf. Sci. **493**, 526 (2001), ISSN 0039-6028, URL http://www.sciencedirect.com/science/article/pii/S0039602801012626. 7.2

[2] S. H. Chang, W. B. Su, W. B. Jian, C. S. Chang, L. J. Chen, and T. T. Tsong, Phys. Rev. B **65**, 245401 (2002). 7.2

[3] M. Yakes, V. Yeh, M. Hupalo, and M. C. Tringides, Phys. Rev. B **69**, 224103 (2004). 7.2, 7.5

[4] M. Yakes, J. Chen, M. Hupalo, and M. C. Tringides, Applied Physics Letters **90**, 163117

(pages 3) (2007), URL http://link.aip.org/link/?APL/90/163117/1. (document), 7.2, 7.4.4, 7.6, 7.6, 7.4

[5] J. Kraft, M. G. Ramsey, and F. P. Netzer, Phys. Rev. B **55**, 5384 (1997). (document), 7.2, 7.2, 7.1, 7.4.1

[6] A. A. Saranin, A. V. Zotov, A. N. Tovpik, M. A. Cherevik, E. N. Chukurov, V. G. Lifshits, M. Katayama, and K. Oura, Surf. Sci. **450**, 34 (2000), ISSN 0039-6028, URL http://www.sciencedirect.com/science/article/pii/S0039602899012364. (document), 7.2, 7.2, 7.4.1, 7.4.1, 7.2

[7] A. D. Novaco and J. P. McTague, Phys. Rev. Lett. **38**, 1286 (1977). 7.2, 7.4.3

[8] H. H. Weitering, D. R. Heslinga, and T. Hibma, Phys. Rev. B **45**, 5991 (1992). 7.2, 7.4.3, 7.4.3, 7.4.3, 7.4.3

[9] L. Vitali, M. Ramsey, and F. Netzer, Applied Surface Science **175176**, 146 (2001), ISSN 0169-4332, ¡ce:title¿10th International Conference on Solid Films and Surfaces¡/ce:title¿.

[10] J. Zegenhagen, T.-L. Lee, Y. Gunder, F. U. Renner, and B. O. Fimland, Z. Phys. Chem, **221**, 1273 (2007). 7.2

[11] M. Xu, A. Okada, S. Yoshida, and H. Shigekawa, Applied Physics Letters **94**, 073109 (pages 3) (2009), URL http://link.aip.org/link/?APL/94/073109/1. 7.2, 7.4.6, 7.6

[12] Z. Wei, H. Lim, and G. Lee, Applied Surf. Sci. **256**, 1152 (2009), ISSN 0169-4332, vASSCAA-4 - Proceedings of the Session on Surf. Sci. of the 4th Vacuum and Surf. Sci.s Conference of Asia and Australia, URL http://www.sciencedirect.com/science/article/pii/S0169433209007521. 7.2, 7.4.1

[13] A. A. Saranin, A. V. Zotov, V. G. Lifshits, J. T. Ryu, O. Kubo, H. Tani, T. Harada, M. Katayama, and K. Oura, Phys. Rev. B **60**, 14372 (1999). 7.2

[14] J. L. Stevens, M. S. Worthington, and I. S. T. Tsong, Phys. Rev. B **47**, 1453 (1993). 7.2

[15] N. Nakamura, K. Anno, and S. Kono, Surface Science **256**, 129 (1991), ISSN 0039-6028. 7.2

[16] O. Bunk, G. Falkenberg, J. H. Zeysing, L. Lottermoser, R. L. Johnson, M. Nielsen, F. Berg-Rasmussen, J. Baker, and R. Feidenhans'l, Phys. Rev. B **59**, 12228 (1999). 7.2

[17] S. Mizuno, Y. O. Mizuno, and H. Tochihara, Phys. Rev. B **67**, 195410 (2003). 7.2

[18] C. Collazo-Davila, L. D. Marks, K. Nishii, and Y. Tanishiro, Surface Review Letters **4**, 65 (1997). 7.2

[19] J. Kraft, S. Surnev, and F. Netzer, Surface Science **340**, 36 (1995), ISSN 0039-6028. 7.2

[20] A. Pavlovska, E. Bauer, and M. Giessen, in *Journal of Vacuum Science and Technology* (AVS, 2002), vol. 20, pp. 2478–2491, URL http://link.aip.org/link/?JVB/20/2478/1. 7.2, 7.3, 7.7

[21] H. Ofner, S. L. Surnev, Y. Shapira, and F. P. Netzer, Phys. Rev. B **48**, 10940 (1993), URL http://link.aps.org/doi/10.1103/PhysRevB.48.10940. 7.2

[22] J. Chen, Ph.D. thesis, Iowa State University (2009). 7.3, 7.4.5, 7.4.6, 7.7, 7.7

[23] M. H. von Hoegen, Zeitschrift fr Kristallographie **214**, 591 (1999). 7.3

[24] S. Stepanovskyy, V. Yeh, M. Hupalo, and M. Tringides, Surface Science **515**, 187 (2002), ISSN 0039-6028. 7.4.3

[25] M. Hupalo, V. Yeh, T. L. Chan, C. Z. Wang, K. M. Ho, and M. C. Tringides, Phys. Rev. B **71**, 193408 (2005). 7.4.3

[26] E. Bauer and J. H. van der Merwe, Phys. Rev. B **33**, 3657 (1986). 7.4.3

[27] R. Roucka, J. Jiruse, and T. Sikola, Vacuum **65**, 121 (2002), ISSN 0042-207X, URL http://www.sciencedirect.com/science/article/pii/S0042207X01003608. 7.4.4

[28] M. Hupalo, data. 7.4.5, 7.4.5

[29] S.-J. Tang, C.-Y. Lee, C.-C. Huang, T.-R. Chang, C.-M. Cheng, K.-D. Tsuei, H.-T. Jeng, V. Yeh, and T.-C. Chiang, Phys. Rev. Lett. **107**, 066802 (2011). 7.4.5, 7.5, 7.8

[30] T. Uchihashi, T. Nakayama, and M. Aono, Japanese Journal of Applied Physics **46**, 5975 (2007), URL http://jjap.jsap.jp/link?JJAP/46/5975/. 7.4.6

[31] D. Vlachos, M. Kamaratos, S. D. Foulias, F. Bondino, E. Magnano, and M. Malvestuto, The Journal of Physical Chemistry C **114**, 17693 (2010), URL http://pubs.acs.org/doi/abs/10.1021/jp105278r. (document), 7.7

[32] K. Budde, E. Abram, V. Yeh, and M. C. Tringides, Phys. Rev. B **61**, R10602 (2000). 7.5

CHAPTER 8. Conclusions

Even though an element may have been well characterized in bulk, many avenues of investigation remain open due to its wildly different properties on the atomic scale. These quantum size effects (QSE) have been shown to affect many properties of the material, including thin film heights, electron density, electrical resistivity, work function, nucleation properties, and chemical reactivity. The properties relating to catalysis are of particular interest due to their far-reaching applications in the energy and chemical industries.

To build on the required knowledge base, this dissertation addressed the ability of QSE to affect diffusion and nucleation on top of Pb films. The single layer height difference between 4- and 5-layer Pb films has been shown to cause the Pb island density on the 4-layer film to be as much as 60 times that of the 5-layer film at 40 K and a 0.1 ML/min flux rate. This is attributed to the effect of QSE on the critical island size, the number of atoms it takes to create a stable island. The effect is a purely vertical one, so the cause is decoupled from the lateral direction. The fast diffusion and fractal-like geometry of the grown islands also explains the previously shown layer-by-layer growth of Pb at temperatures between 18 and 70 K.

In depositions on top of Pb films showed that even at 110 K and in a heteroepitaxial system, QSE still causes the island density to differ by a factor of 2 between 4- and 5-layer Pb films. Once again, the 5-layer films had fewer islands on them, but this time the difference in island density is caused by diffusion on the 5-layer film being faster than on the 4-layer film. The 2^{nd} layer of In was much less likely to nucleate, especially on the 5+1-layer films, and is caused by a very high diffusion rate, which lead to the In to fall off of the predominantly Pb islands and grow along the sides of the Pb islands, slowly encasing them in In.

In addition to QSE, this dissertation explored lattice rotations as a way to affect the energy of thin films. Pb depositions on top of three different In phases produced a myriad of different

Pb crystal orientations with strong temperature dependence. At temperatures below about 215 K, there are four orientations of Pb crystals on In $\sqrt{31}$, aligned along Si[$1\bar{1}0$], and clockwise and counter-clockwise to Si[$1\bar{1}0$] by 7.2°, 8.9°, and 25°. The Pb aligned along Si[$1\bar{1}0$] and clockwise and counter-clockwise to Si[$1\bar{1}0$] by 8.9° are stable at temperatures above about 215 K. A similar effect is seen for Pb on In $\sqrt{3}$, with alignment along Si[$1\bar{1}0$] being preferred at temperatures below about 215 K and alignment along Si[$11\bar{2}$] being preferred above about 215 K.